I give permission for public access to my thesis and for copying to be done at the discretion of the archives' librarian and/or the College library.

Signature Date

THE ROLE OF INHIBITOR OF APOPTOSIS (*DIAP1*) IN FAT BODY REMODELING IN *DROSOPHILA MELANOGASTER*

by

Yoana Y. Gendzhova

A Paper Presented to the

Faculty of Mount Holyoke College in

Partial Fulfillment of the Requirements for

the Degree of Bachelor of Arts with

Honor

Department of Biological Sciences

South Hadley, MA 01075

May, 2011

This paper was prepared
under the direction of
Professor Craig Woodard
for eight credits.

To the one most dear to me, my mother

ACKNOWLEDGMENTS

I would like to sincerely thank my advisor, Professor Craig Woodard, for being an invaluable mentor and allowing me to grow from a research student into a scientist. His passion for research, critical insight and admirable personality has been an inspiration for me throughout my time in his lab. I thank Professors Jeff Knight and Darren Hamilton for honoring me by joining my thesis committee. I want to express my gratitude to Professor Knight for encouraging me to challenge myself and hypothesize independently. I am indebted to Professor Hamilton for taking the time to read and evaluate my work. My appreciation to Professor Wei Chen for being my role model for a female scientist and supporting me in writing a thesis even outside of my major.

I would like to acknowledge Dr. Nichole Bond, Kathryn Gorski and Professor Sharon Stranford's lab members for their assistance with Real Time qPCR. I appreciate Marian Rice's help with microscopy, which was indispensable for this project. I am grateful to the Biology Department at Mount Holyoke College for supporting my research.

I thank my friends and lab-mates for their faith in me and all the laughs we had together. Last but not least, I cannot thank my family enough for giving me inspiration and strength to carry on.

TABLE OF CONTENTS

LIST OF FIGURES

LIST OF TABLES

ABSTRACT

The metamorphosis of *Drosophila melanogaster* results in destruction of many larval tissues by programmed cell death (PCD). PCD is regulated by the steroid hormone 20-hydroxyecdysone (ecdysone) (Yin et al., 2007). PCD is initiated by down-regulation of the antiapoptotic gene *Inhibitor of Apoptosis* (*diap1*). DIAP1 regulates PCD by inactivating caspases. Proapoptotic genes suppress *diap1* to initiate histolysis of most larval tissues. A unique exception is the fat body, which instead of PCD undergoes remodeling from an organized tissue to a loose association of individual cells (Nelliot et al., 2006).

The timing of fat body remodeling is ecdysone-dependent, but its genetic regulation still needs to be elucidated. I hypothesize that the fat tissue is refractory to PCD due to upregulation of *diap1*. To test this hypothesis, I constructed a temporal profile of *diap1* expression in fat body via quantitative Real Time PCR (qPCR). Additionally, I investigated if *diap1* is necessary for fat body remodeling by studying fat body development in tissue specific loss-of-function *diap1* animals. Here, I demonstrate that *diap1* is upregulated throughout prepupal and early pupal development. While *diap1* is not essential for fat body survival, *diap1* appears essential for normal timing of fat body remodeling and pupal viability.

INTRODUCTION

Programmed Cell Death (PCD)

The precise regulation of programmed cell death (PCD) is critical for homeostasis and development (Thummel, 2007). The term PCD was established to distinguish physiological or genetically controlled cell death from necrotic cell death, caused by disease or injury (Lockshin and Zakeri, 1991). In development, PCD is an integral component of limb formation and nervous system remodeling (Robinow et al., 1993). Cell death is also involved in removal of abnormal cells during development, as well as the ones that form during tumorigenesis (Thompson, 1995).

Physiologically controlled cell death has three distinct modes. These modes have been determined from the results of morphological studies of developing vertebrate embryos (Schweichel and Merker, 1973). The first mode, *apoptosis*, is found in isolated dying cells, which exhibit nuclear and cytoplasmic condensation. Macromolecular synthesis decreases, cellular DNA is cleaved at internucleosomal sites, resulting in fragmentation in multiples of approximately 180 bp (Schwartzman and Cidlowski, 1993). Then, the DNA is released in membrane-bound vesicles, which are eliminated in vivo by phagocytosis (Kerr et al., 1972). The second mode, *autophagy*, is observed when groups of associated cells or entire tissues are dying. These cells contain cytoplasmic vacuoles, which function in the degeneration of their

components (Lee and Baehrecke, 2001). The third mode of PCD, *non-lysosomal cell death*, is least common. It is characterized by swelling of membrane-bound cavities and subsequent degeneration without lysosomal formation. While autophagy fulfills the definition of programmed cell death, given above, and occurs during development of various organisms (Clarke, 1990), little is known about the molecular genetic mechanisms undergoing this type of cell death (Lee and Baehrecke, 2001) .

Because programmed cell death plays such a critical role in both normal and abnormal development, extensive studies have focused on its regulation. These have identified hormonally regulated genes that function at different levels in the PCD pathway, to either induce or prevent PCD. Complementary studies in the nematode *Caernohabitis elegans*, *Drosophila melanogaster* and mammalian cell culture have revealed that many of these critical regulators have been conserved through evolution (Steller, 1995; Jacobson et al., 1997). Specifically, the genes *ced-3*, *ced-4* and *ced-9* encode proteins that are homologous to mammalian caspases (cysteine proteases, which function as apoptosis effectors) (Lee et al., 2000). While CED-3 is homologous to the mammalian caspase family, CED-4 is homologous to Apaf-1, which activates caspases in the presence of steroid-triggered programmed cell death responses of cytochrome **c** and dATP (Li et al., 1997; Zou et al., 1997). CED-9 is from the Bcl-2 family of cell death regulators and is

known to impact Apaf-1 activity (Vaux et al., 1992; Hengartner and Horvitz, 1994).

Steroid Regulation of PCD in Development

Steroid hormones have been recognized as important regulators of programmed cell death. Steroids are lipophilic hormones, i.e. they can pass through the cell membrane and interact with their receptors (Rahman, 2008). Pioneering studies of programmed cell death analyzed intersegmental muscle degeneration in insects, specifically tobacco hornworms, *Manduca sexta* (Lockshin and Williams, 1964, 1965). At the onset of metamorphosis, degeneration occurs in response to a pulse of the steroid hormone 20-hydroxyecdysone (hereafter referred to as ecdysone). Simultaneously, larval motor neurons and labial glands also degenerate (Weeks and Truman, 1985). At the end of metamorphosis, in response to a decrease of the ecdysone titer, abdominal interneurons and intersegmental muscles die (Finlayson, 1956; Schwartz and Truman, 1982).

Induction of apoptosis by addition or withdrawal of steroid hormones from responsive tissues has been documented in murine lymphoid cells (Evans-Storms and Cidlowski, 1995). Thymus cell lines have served as a model to study steroid-mediated apoptosis since they are extremely sensitive to induction of apoptosis by glucocorticoids. In vivo glucocorticoid treatment of rats' thymuses leads to the activation of calmodulin, an 18 kDa protein

with endonuclease activity (Shipston and Antoni, 1992). Calmodulin inhibits the activity of kinases such as caseine kinase 2, which leads to a decrease in phosphorylation. The imbalance between phosphorylation and dephosphorylation leads to apoptosis of the murine thymocites (Uckun et al., 1992).

Another example of steroid control of developmental PCD is the hormonal regulation of the human reproductive system. Removal of androgens causes prostate regression via apoptosis of ventral prostate epithelial cells. Similarly, withdrawal of progestins results in apoptotic regression of lactating breast tissue (Tenniswood et al., 1992). Estrogens inhibit and androgens enhance ovarian granulosa cell apoptosis, while progesterone suppresses apoptosis in uterine epithelial cells (Billig et al., 1993).

Further research has shown that ecdysone-controlled programmed cell death is an integral component in the development of other organisms, such as *Drosophila*. Eye differentiation, removal of excess cells between ommatidia, as well as development of the central nervous system is ecdysone-dependent. *Drosophila* eye differentiation depends on the ordered elimination of extra cells between the ommatidia via PCD (Cagan and Ready, 1989; Wolff and Ready, 1991). In a similar manner, a set of approximately 300 neurons in the central nervous system undergoes programmed cell death following adult eclosion (Taylor and Truman, 1992). These cells

selectively express the EcR-A isoform of the ecdysone receptor and their death is dependent on a decrease in ecdysone titer, implicating the hormone as a primary signal for this response (Robinow et al., 1993; Talbot et al., 1993).

Steroid-controlled PCD during *Drosophila* metamorphosis is a particularly interesting phenomenon to study, since the larval salivary glands undergo autophagy, directed by genes that are part of a conserved apoptotic pathway (Jiang et al., 1997; Lee et al., 2000). Specifically, two components of the core apoptotic machinery, the caspase *dronc* and homolog of *ced4/Apaf-1 ark*, are expressed immediately before salivary gland death (Lee et al., 2000). In contrast, ecdysone triggers a classic apoptotic response in the larval midgut (Jiang et al., 1997). Understanding of the relationship between these cell death mechanisms necessitates an overview of the hormonal and genetic regulation of PCD in *Drosophila* metamorphosis.

Steroid Control of *Drosophila melanogaster* Metamorphosis

Drosophila melanogaster undergoes holometabolous, or complete metamorphosis, which includes embryonic, larval, pupal and adult stage. During metamorphosis, many larval tissues are destroyed by PCD, whereas the adult progenitor cells (histoblasts and imaginal discs), differentiate and proliferate (Yin and Thummel, 2004). The histolysis, or breakdown and dissolution of larval organs, as well as their replacement by adult tissues, is tightly controlled by ecdysone. Ecdysone, prothoracicotropic hormone

(PTTH) and juvenile hormone (JH) are the major hormonal controls of *Drosophila* development. Molting is mediated by PTTH, which is secreted by the CNS to evoke ecdysteroid biosynthesis and release from the prothoracic gland (Zhou et al., 2004). Once the critical larval weight for metamorphosis is reached, there is a decline in JH levels from the corpora allata (Fig.1). The prothoracic glands, which secrete ecdysone (Kiriishi et al., 1990), are part of the ring gland, which also contains the corpora allata and the corpus cardiacum (a neurohemal organ).

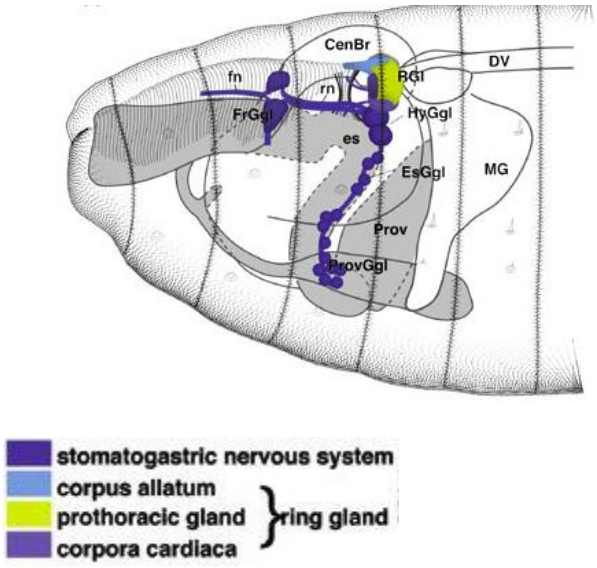

Figure 1. *Drosophila melanogaster* ring gland structure and function(modified from Hartenstein, 1993). The ring gland is a part of the neuroendocrine system. The ecdysteroid molting hormone (ecdysone) is secreted from the prothoracic glands, and the sesquiterpenoid juvenile hormone (JH) is secreted from the corpus allatum. Ecdysone levels determine the timing of molting from one instar to the next, whereas JH levels determine whether the animal molts to larval, pupal, or adult form (Harvie et al., 1998).

Titers in PTTH induce successive titers in α-ecdysone, released as a prohormone in the haemolymph. Once α-ecdysone reaches its target organs, such as the fat body, it is converted into its functional form, β-ecdysone (20-hydroxyecdysone) by the enzyme 20-monooxygenase (Fig.2).

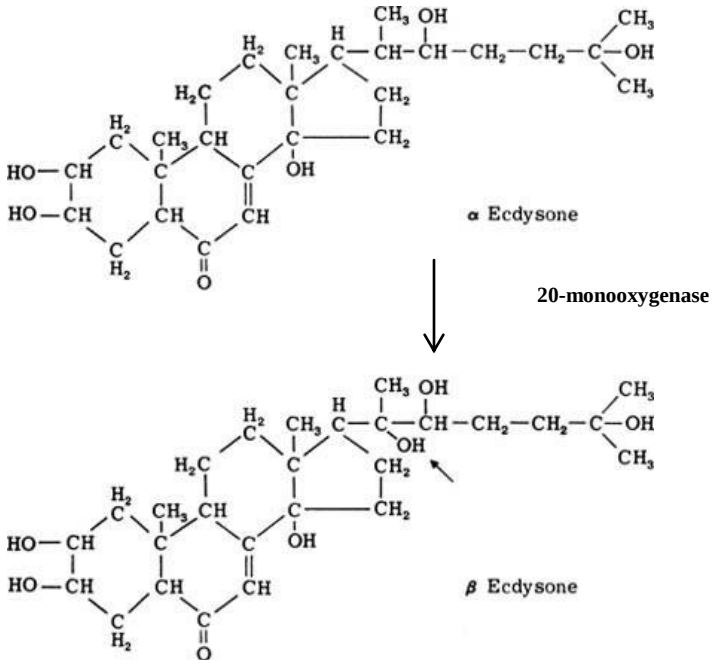

Figure 2. Conversion of the prohormone α-ecdysone into functional β-ecdysone (20-hydroxyecdysone). Ecdysone is converted into its active form, 20-hydroxyecdysone, once it reaches target organs such as the fat body, imaginal discs and epidermis (Riddiford, 1993). The enzyme that catalyzes the above reaction, 20-monoxygenase, belongs to the oxidoreductase family, and hydroxylates α-ecdysone at C-20 (Johnson and Rees, 1977). Ecdysone has a carbon skeleton with four fused rings, characteristic of the steroid family, along with glucocorticoids, retionoids, thyroids and sex hormones.

In *Drosophila*, ecdysone is activated by binding a ligand to a heterodimeric nuclear-receptor complex of Ecdysone Receptor (EcR) and

Ultraspiracle(USP) (Riddiford et al., 2000). Nuclear receptors are ligand-regulated transcription factors, to which small lipophilic molecules, such as steroids, bind (King-Jones and Thummel, 2005). As a member of the nuclear receptor superfamily, USP/EcR is characterized by the presence of a highly-conserved DNA binding domain (DBD) and a less conserved C-terminal ligand-binding and dimerization domain (LBD) (Fig. 3).

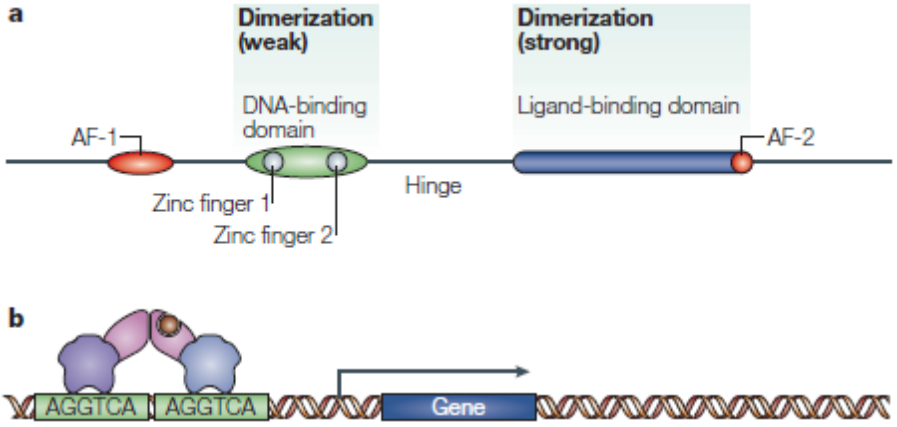

Figure 3. Structure of nuclear receptors.
a) The common features of nuclear receptors are a highly conserved DNA-binding domain (DBD) and a less conserved ligand-binding domain (LBD), connected by a hinge region. The DBD contains two zinc fingers: the first one provides DNA-binding specificity and the second one allows the DBD to dimerize in the presence of a target DNA molecule. The LBD constitutes the principal dimerization interface of the nuclear receptor superfamily. It consists of α-helices that form a hydrophobic pocket, which allows for binding of lipophilic molecules, such as ecdysone. There are two activation function (AF) domains, AF-1 and AF-2, which are ligand-dependent and are located at the N- and C-terminus, respectively.
b) Each nuclear receptors binds to a half-site derived from, or identical to, the archetypal AGGTCA sequence. Some receptors function as monomers, others as homodimers or heterodimers (such as EcR/USP). Receptors without known ligands are referred as orphan nuclear receptors (King-Jones and Thummel, 2005).

The EcR and USP receptors are orthologs of the vertebrate farsenoid X receptor (FXR) and retinoid X receptor (RXR), respectively (King-Jones and Thummel, 2005). *EcR* produces three protein isoforms: A, B1 and B2, whereas *usp* encodes only one isoform (Riddiford et al., 2000). EcR-A and EcR-B1 are expressed during the onset of metamorphosis and their distribution contributes to the spatial specificity of 20E responses (Li and Bender, 2000). USP is required for the allosteric effects of EcR, facilitating its DNA- and ligand-binding activity (Hu et al., 2003).

The effects of ecdysone are regulated through the transcription factor function of the EcR/USP receptor, thus coordinating downstream gene expression. The targets of the ecdysone-EcR-USP complex are also members of the nuclear receptor superfamily. There are six nuclear-receptor genes, which are transcriptionally regulated by 20E and show changes in mRNA levels in synchrony with 20E pulses during development: *Drosophila* hormone receptor 3 (*DHR3* or Hr46), *DHR4* (Hr4), *DHR39* (Hr39), *E75*, *E78*, and *fishu tarazu* transcription factor 1 (*ftz*-f1) (King-Jones and Thummel, 2005). The EcR-USP targets are essential for embryogenesis and metamorphosis.

There are high ecdysone titers during mid-embryogenesis, indicating an embryonic role for the ecdysone-EcR-USP complex (Riddiford, 1993) (Fig.4). However, these are difficult to study, due to maternal contribution to EcR mRNA and EcR protein. After embryogenesis, *Drosophila* progresses

through three larval instars, to enter metamorphosis and finally emerge as an adult fly. Each of the transitions between these stages is triggered by ecdysone, which leads to a complete transformation in body plan (Fig.4). There are two major ecdysone pulses that trigger the larval-prepupal and the prepupal-pupal transition by means of a strictly orchestrated genetic regulatory hierarchy (Buszczak and Segraves, 2000). The first pulse in late third-instar larvae induces puparium formation, marking the onset of prepupal development (Woodard et al., 1994). The second pulse, 10-12 hours later, triggers head eversion, defining the prepupal-pupal transition. Ecdysone activates adult structure morphogenesis, as well as stage- and tissue-specific programmed cell death of the larval tissues.

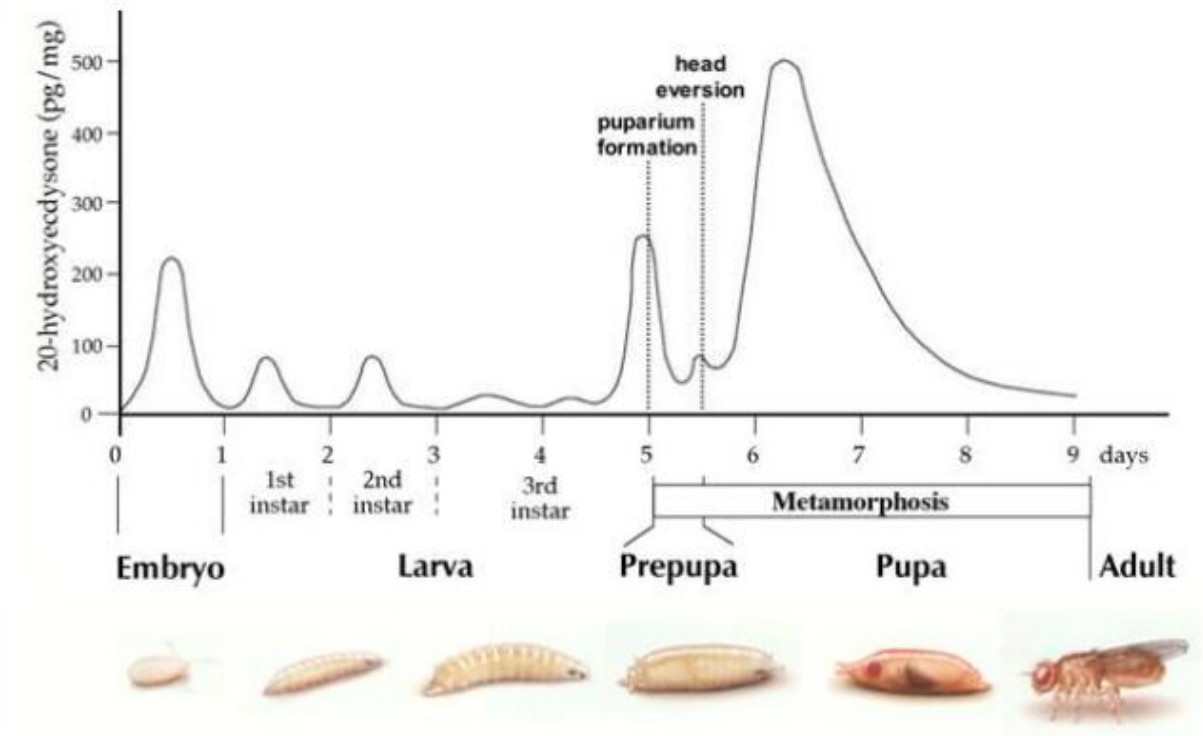

Figure 4. Ecdysone titer profile during *Drosophila* development (Riddiford, 1993). The concentration of ecdysone is plotted as a function of metamorphic development. Major changes associated with the two titers at 0 hr APF and 12 hr APF are marked by dotted lines. The 20E titer profile is expressed as ecdysone equivalents in whole body homogenates (Ayerh, 2008).

The destruction of larval tissues occurs in a precisely regulated stage- and tissue-specific manner following each ecdysone pulse (Jiang et al., 1997). The anterior larval muscles and larval midgut degenerate during the first half of prepupal development, while the larval salivary glands and some abdominal muscles undergo histolysis immediately after pupation. The larval midgut consists of polyploid epithelial cells, which lie on an external base membrane. Adjacent to the base membrane are diploid progenitor cells, which proliferate into a new cell layer during prepupal development. This

layer gives rise to the adult midgut, while the larval cells are discharged shortly after eclosion. In contrast, the larval salivary gland degenerates very rapidly by ~15 hr after pupation. A ring of diploid imaginal cells in its anterior serves as a source of cells to form the adult salivary gland (Jiang et al., 1997).

The adult *Drosophila* structures originate from imaginal discs that differentiate in response to the high ecdysone titers described above. The imaginal discs are epithelial sheets, which serve as primordia for adult appendages, wings, antennae and eyes (McClure and Schubiger, 2005). They are derived from the blastoderm and their cell fate is determined during embryogenesis. The adult exoskeleton and sensory organs differentiate by expressing tissue-specific genes (Fristrom and Fristrom, 1993). The adult abdomen develops from a subset of imaginal discs, called histoblasts. The histoblasts remain undifferentiated during the three larval instars. Instead, they divide rapidly and migrate to secrete the pupal cuticle, and then form the adult abdomen (15 hours after puparium formation). The larval abdominal structures are removed by hemocytes through phagocytosis.

Genetic Regulation of PCD During Metamorphosis

Drosophila larval salivary gland histolysis provides an ideal opportunity to understand the steroid regulation of programmed cell death. Salivary gland histolysis is ecdysone-dependent and is almost synchronous in

all cells that constitute this tissue (Bodenstein, 1943). An ecdysone-triggered genetic regulatory hierarchy, which precedes salivary gland death, has been identified (Woodard et al., 1994; Baehrecke and Thummel, 1995; White et al., 1997). This two-step regulatory hierarchy is composed of *early* and *late* genes, identified by the puffing patterns of the salivary gland polytene chromosomes (Ashburner et al., 1974). The *early* genes are induced directly by the EcR/USP complex and act as transcription factors that induce *late* gene expression (Russell and Ashburner, 1996; Thummel, 1996). The *late* genes, in turn, appear to play a more direct role in salivary gland development and function.

The *early* genes, induced at the larval-prepupal transition, are *Broad Complex* (*BR-C*), *E74* and *E75* (Buszczak and Segraves, 2000). A drop in ecdysone titer during mid-prepupal development is associated with an increase in the expression of *βftz-f1*, an orphan nuclear receptor from the nuclear receptor superfamily. βftz-f1 provides early genes with the competence to respond to the prepupal ecdysone pulse (Woodard et al., 1994). The subsequent late prepupal titer leads to the re-induction of *BR-C*, *E74* and *E75.* The stage-specific induction of *E93* during the late ecdysone pulse is directed by *βFTZ-F1.* Also in response to *βFTZ-F1,* the antiapoptotic genes *Inhibitors of Apoptosis (diap1 and diap2)* are upregulated at the mid-prepupal stage (Hay et al., 1995). Ecdysone-directed *diap* suppression

together with upregualtion of two proapoptotic genes, *head involution defective* (*hid*) and *reaper* (*rpr*), results in salivary gland histolysis (Fig.5)

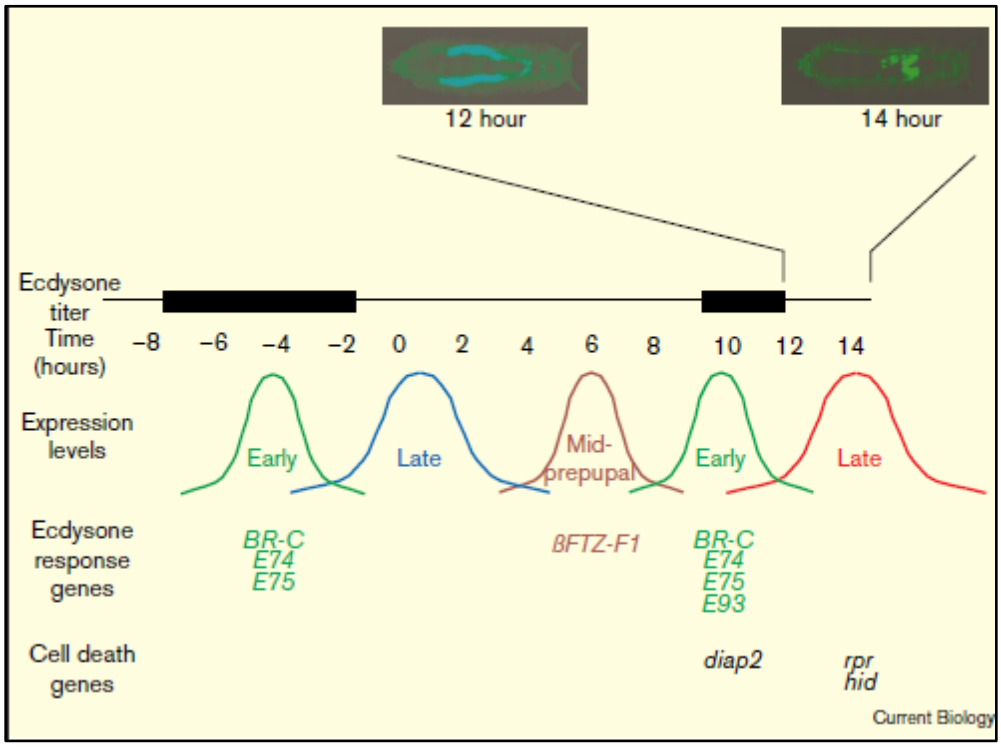

Figure 5. Genetic regulation of the ecdysone-triggered salivary gland histolysis.
This two-step regulatory hierarchy directs larval salivary gland death via ecdysone-inducible transcription factors. In third-instar larvae (L3), expression of the early genes *BR-C*, *E74* and *E75* is induced and then followed by mid-prepupal *βftz-f1* expression. The early genes are reinduced in late prepupae, together with the stage-specific *E93*. At this stage, *diap* genes are downregulated and cell death genes are upregulated to effect salivary gland destruction.

A similar regulatory hierarchy is triggered by ecdysone in the larval midgut. Markers of PCD including acridine orange staining and DNA fragmentation indicate that the larval midguts undergo histolysis at the early prepupal stage (Jiang et al., 1997). Only midguts isolated from ecdysone-

injected animals show uniform acridine staining, indicative of ecdysone-controlled PCD. Animals injected with control solution exhibit developmental arrest without any midgut histolysis (Fig.6). Elucidation of the specifics of the larval midgut's response to ecdysone is hampered by the midgut's unviability in culture. The larval midguts are complex organs, composed of several tissues including epithelial, muscle and tracheal. In contrast, larval salivary glands are ideal to study steroid control of PCD in development due to their simple structure and longevity in culture.

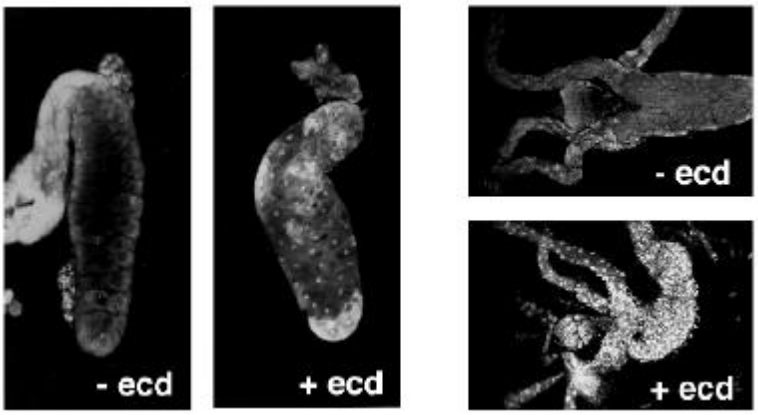

a)Salivary glands **b)Midguts**

Figure 6. Ecdysone triggers programmed cell death in larval salivary glands and midguts. a) Salivary glands dissected from 8 hour prepupae cultured in the absence (-ecd) or presence (+ecd) of 5 x 10^{-6} of ecdysone for 5 hours and tested for viability by incubation with acridine orange. Only salivary glands cultured in presence of ecdysone undergo cell death as indicated by nuclear staining. Mid third-instar larvae were injected with ecdysone(+ecd) or solution lacking ecdysone(-ecd), dissected after 8-10 hours, and tested for viability by incubation with acridine orange. b) Midguts were dissected 10 hours later and midguts from ecdysone injected larvae began cell death as indicated by nuclear staining (Jiang et al., 1997).

The mechanism of steroid signaling during histolysis of the salivary glands has been studied via polytene chromosomes, which form ecdysone induced puffs, reflecting the transcriptional regulatory hierarchy described above (Ashburner, 1974). The late genes are thought to have a more direct role in controlling the organismal response to ecdysone than the early regulatory genes (Lee et al., 2000). While *βftz-f1* has an indirect role as a competence factor, EcR, USP, BR-C, and E74A play a more direct role in triggering salivary gland cell death through the coordinate induction of *rpr* and *hid* transcription. However, they are not sufficient for PCD, as they do not direct this response to the first ecdysone pulse at puparium formation. The critical regulator of midgut and salivary gland PCD is *E93*, whose transcription increases immediately before these organs' histolysis and is coordinately induced with *rpr* and *hid* (Baehrecke and Thummel, 1995).

E93 encodes a novel nuclear protein that is expressed in larval cells prior to steroid-induced cell death and binds to specific sites in the polytene chromosomes. *E93* mutants fail to undergo salivary gland PCD and die during metamorphosis. Ectopic expression of *E93* rescues salivary gland death (Lee et al., 2000). E93 protein binds to sites in the salivary gland that contain both steroid regulated genes and cell death genes. Mutations in *E93* result in decreased transcription levels of *rpr*, *hid*, *ark*, *dronc*, and *crq*, which are all genes of the cell death machinery (Figure 7) (Lee et al., 2000; Lee et al., 2002).

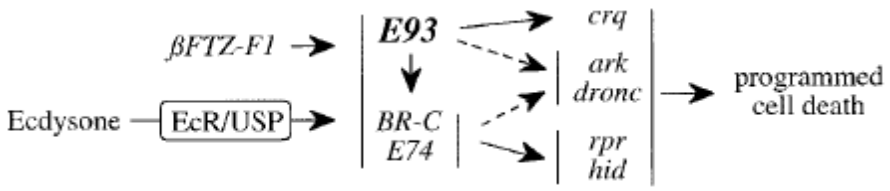

Figure 7. Role of E93 in regulation of larval salivary gland PCD during the prepupal-pupal transition. The competence factor *βftz-f1* facilitates ecdysone induction of the *BR-C, E74, E75* and *E93* early genes. E93 is essential for the proper transcription of the *BR-C, E74, E75* genes as well as the cell death regulators, *rpr, hid, arc, crq* and *dronc* (Lee et al., 2000; Lee et al., 2002).

The destruction of the larval salivary glands is triggered by ecdysone in a transcriptional cascade that converges on *reaper (rpr)* and *head involution defective (hid)* (Yin et al., 2007). There are ecdysone pulses preceding salivary gland histolysis, some of which induce *BR-C* and *E74A* expression. Yet, *rpr* and *hid* are only expressed in response to the prepupal pulse of ecdysone (Fig.8). The temporal specificity of *rpr* and *hid* expression, and hence, the appropriate timing of steroid-triggered cell death, are determined by Fork head (Fkh), the defining member of the Fork head family of transcription factors (Friedman and Kaestner, 2006).

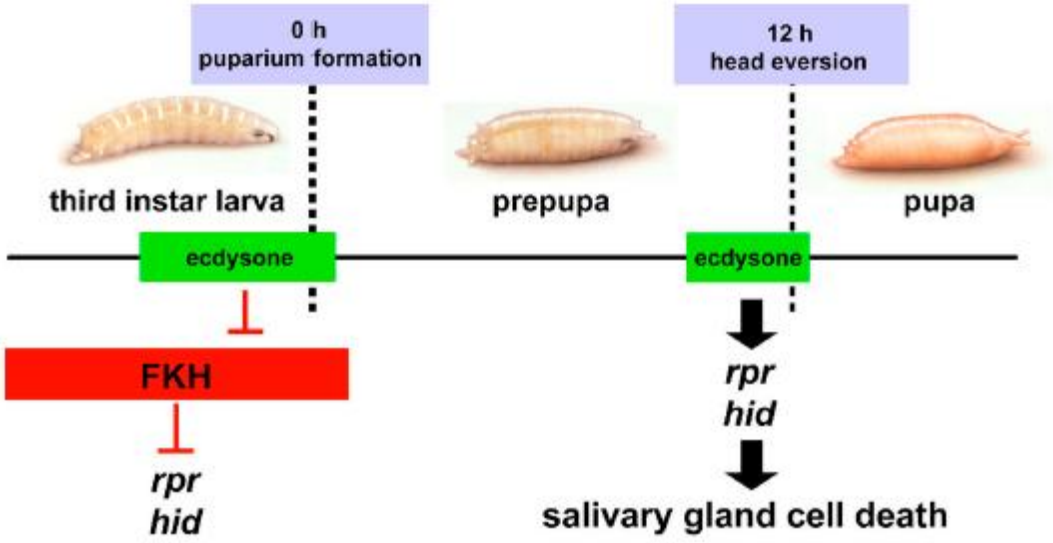

Figure 8. **A model for the temporal specification of salivary gland cell death by Fkh**. The Fkh transcription factor is expressed throughout larval stages in the salivary glands, effectively blocking *rpr* and *hid* death activator expression. Only after puparium formation, apparently in response to the late-larval ecdysone pulse, that Fkh is down-regulated. In the absence of Fkh, the prepupal ecdysone pulse can induce *rpr* and *hid*, triggering salivary gland cell death (Thummel 2007).

Fkh is normally expressed in the salivary glands throughout the larval stages, and then down-regulated at puparium formation, in synchrony with the late-larval ecdysone pulse (Renault et al., 2001), (Fig. 8). Down-regulation of *fkh* provides competence for salivary gland cell death, allowing the death cascade to be triggered by the subsequent prepupal pulse of hormone. Cao et al. (2007) show that this down-regulation of *fkh* is essential for the proper timing of cell death. Ectopic *fkh* expression in mid-prepupae results in a complete block in salivary gland cell death 6 h after the wild-type glands are destroyed. Microarray analysis demonstrates that ectopic *fkh* down-regulates other cell death genes including *Jafrac2*, *dark*, and *dronc*,

demonstrating widespread effects on the death pathway (Thummel, 2007). Thus, *Fork head* not only maintains salivary gland function during larval stage, but also blocks its destruction. In this way, Fkh acts as a survival factor and ensures that the salivary glands can provide their normal functions for the larva.

Drosophila Programmed Cell Death Machinery

The apoptosis of larval tissues in Drosophila is dependent on caspases, which activate proteolytic cascades and act as cell death effectors (Leulier et al., 2006). Initiator caspases cleave and activate downstream effector caspases, amplifying the proteolytic activity required for cell destruction. Caspases consist of an N-terminal regulatory prodomain, followed by a large subunit containing the catalytically active cysteine (p20), and a C-terminal small subunit (p10). Initiator caspases carry an extensive prodomain (more than 90 amino acids) that contains a homotypic protein interaction motif in the form of either a caspase recruitment domain (CARD) or a death effector domain (DED). In contrast, effector caspases harbour only a relatively short pro-peptide (20–30 amino acids) with no apparent motif (Orme and Meier, 2009).

Apoptosis in Drosophila requires the action of seven caspases: Dronc, drICE, DCP-1, Dredd/DCP-2, Strica/Dream, Decay and Damm (Salvesen and Abrams, 2004). From these, Dronc and Dredd/DCP-2 are intiatior (apical)

caspases, while the remaining ones are effector caspases. Dronc is essential for many forms of PCD, for instance, apoptosis triggered by cytotoxic agents. It is homologous to mammalian caspase-9 and requires the cell death regulator complex Dark/Hac-1/dApaf1 for activation and transduction of proteolyic activity (Zhou et al., 1999). In contrast, the other initiator caspase Dredd, homologous to mammalian caspase-8, is not essential for PCD. Instead, Dredd, together with its activator dFadd, is required for antibacterial immune response (Leulier et al., 2000).

Systematic *in vivo* RNA interference (RNAi) studies have identified which effector caspases are required for apoptotic cell death in *Drosophila*. This method allows for selective knockdown of the seven caspases and their adaptors (Dark/Hac-1/dApaf1 and dFadd). In the larval salivary glands, apoptosis is accompanied by autophagy, regulated by noncaspase proteases (MMP2) and yeast autophagy homologs (*apg*-related genes)(Baehrecke, 2003). Thus, additional studies of salivary gland death have been done using baculovirus P35 overexpression, which prevents apoptosis (Hay et al., 1994). P35 merely delays but does not block salivary glands death (Fig.9), suggesting that this tissue is indeed removed by autophagy and not apoptosis. A similar delay in salivary glands removal is observed in RNAi animals after knockout of *Strica*, *Dronc*, *Dark* and *Drice* (Leulier et al., 2006). Therefore, these rate-limiting caspases and autophagy function together function in the efficient removal of larval tissues during metamorphosis. In

contrast, RNAi-mediated depletion of dFadd, Dredd, DCP-1, Damm and Decay has no apparent effect, suggesting these caspases have little or no role in salivary glands histolysis.

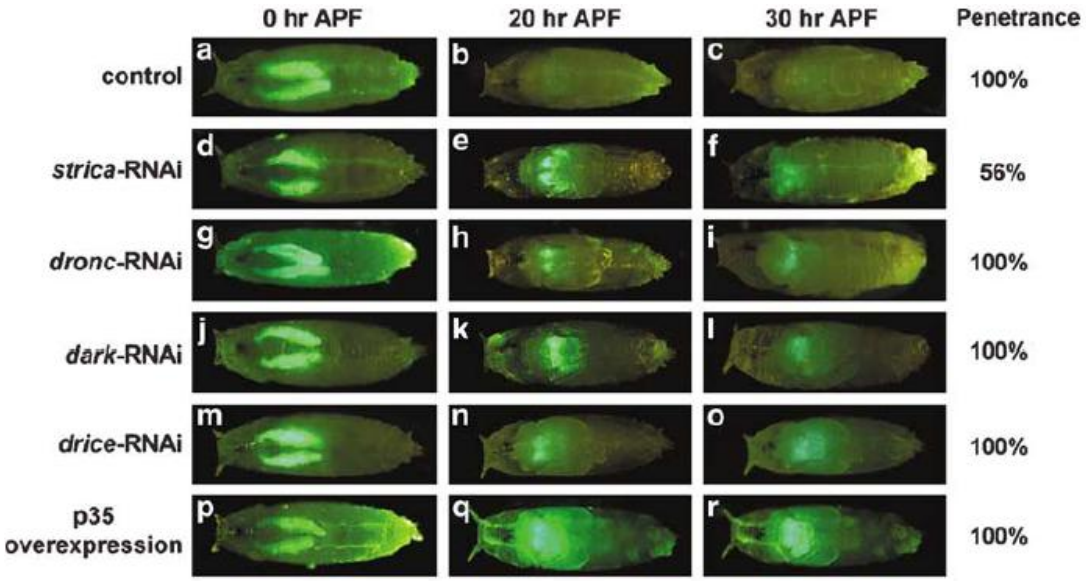

Figure 9. The caspases Strica, Dark, Dronc and drICE are required for the timely removal of larval salivary glands during *Drosophila* metamorphosis. The salivary glands (SGs) are marked with green fluorescent protein (GFP). Their PCD is triggered at 14.5 hr after puparium formation (APF). By 20 hr APF, histolysis is complete and no GFP is detectable in wild-type animals (a–c). In contrast, RNAi-mediated depletion of Strica- (d–f), Dronc- (g–i), Dark- (j–l) and drICE- (m–o) like overexpression of p35 (p–r) severely delayed the removal of GFP-positive SGs. Here, persistent GFP fluorescence is apparent up to 30 hr APF. While the delay in SG removal is fully penetrant in *dronc*-, *dark*- and *drice*-RNAi-treated SG, *strica*-RNAi was only 56% penetrant (Leulier et al., 2006).

The Proapoptotic Genes: *rpr, hid* and *grim*

In cells destined to die, cell death is induced by the proapoptotic genes *reaper* (*rpr*), *grim*, hid (*head involution defective*), *sickle* and *jafrac2* (Salvesen and Abrams, 2004). The most important regulators of *Drosophila* apoptosis are *rpr* , *hid* and *grim*. The genes encoding these regulatory proteins are clustered together within the 75C1, 2 region on the third chromosome that is uncovered by the small deletion H99 (Orme and Meier, 2009). Embryos that are homozygous for this deletion are almost completely deficient in apoptosis, and fail to hatch. Overexpression of any of the aforementioned proapoptotic genes in *Drosophila*, or in tissue culture cells, triggers ectopic cell death.

Although in *Drosophila,* over-expression of *rpr*, *grim*, *hid* or *jafrac2* is sufficient to induce apoptosis in a wide variety of cell types, genetic analyses of *rpr*, *grim* and *hid* argue that these IAP-antagonists are not redundant but must act in combination with each other to induce apoptosis (Wing et al., 1998). Studies of embryonic central nervous system and midline development with deletions that remove various combinations of *rpr*, *grim* and *hid* indicate that these genes do not induce PCD alone, but act synergistically. Nevertheless, the proapoptotic activity of *grim* is regulated differently from *rpr* and *hid*. While the antiapoptotic regulatory protein *Inhibitor of Apoptosis 2* (*diap2*) blocks *rpr* and *hid* expression (Hay et al., 1995; Vucic et al., 1997), it fails to block *grim*-induced PCD. In

metamorphosis, there is no *grim* transcription in larval salivary glands and midguts, suggesting that this gene does not function in prepupal and pupal development (Jiang et al., 1997).

The Antiapoptotic Genes: *Inhibitors of Apoptosis (diap1* and *diap2)*

For salivary gland histolysis to occur, induction of *rpr* and *hid* must overcome the inhibitory effect of the antiapoptotic genes *Inhibitors of Apoptosis* (*IAP*s). IAPs are a family of cell death inhibitors, originally identified in baculoviruses. IAP homologs have been identified in other viruses, *Drosophila melanogaster*, *Caenorhabditis elegans* and mammals (Uren et al., 1998). IAPs protect cells from apoptosis by regulating caspase-induced proteolysis. IAPs are defined by the presence of the Baculovirus IAP Repeat (BIR) domain that is homologous to the BIR identified in the viral protein OpIAP (Orme and Meier, 2009). The BIR domain consists of one or more repeats of a ~70-amino acid motif. IAPs also contain a C-terminal Really Interesting New Gene (RING) E3 ubiquitin ligase domain that can target bound proteins, as well as the IAP itself, for ubiquitination and in some cases degradation (Huh et al., 2006).

The *Drosophila* genome encodes two BIR and RING domain-containing IAP family members, DIAP1 and DIAP2, and ectopic expression of either protein inhibits apoptosis (Hay et al., 1995). While DIAP1 carries two IAP-defining BIR domains, the second Drosophila IAP, DIAP2, harbors three such

domains (Fig. 10a). The BIR domain functions as protein interaction module that, for DIAP1, mediates binding to DRONC, drICE and DCP-1. Importantly, different caspases bind to distinct BIRs: while the BIR1 region of DIAP1 is essential for binding to the effector caspases drICE and DCP-1, the BIR2 region directly associates with the initiator caspase DRONC. As a consequence of this differential binding, one molecule of DIAP1 can bind simultaneously to DRONC and drICE or DCP-1. Physical association between DIAP1and effector caspases is essential for cell survival. Embryos homozygous for *diap*1 loss-of-function mutations that completely abrogate binding to effector or initiator caspases, die during embryogenesis due to inappropriate cell death (Zacharinou et al., 2003).

DIAP1 is activated via proteolytic cleavage, which removes its inhibitory N-region and exposes a ubiquitination site for UBR-containing E3 ligases (Fig. 10b). Recruitment of N-end UBR E3 ligases, together with DIAP1's RING domain, promotes ubiquitination and inactivation of drICE and DCP-1. DIAP2 is activated by mechanism, very similar to that used by the viral caspase inhibitor P35. DIAP2 functions as a pseudo-substrate to drICE, which binds to DIAP2 and cleaves it at D100. A covalent bond forms and restricts the catalytic activity of drICE, which is completely ubiquitinated after DIAP2 cleavage (Orme and Meier, 2009).

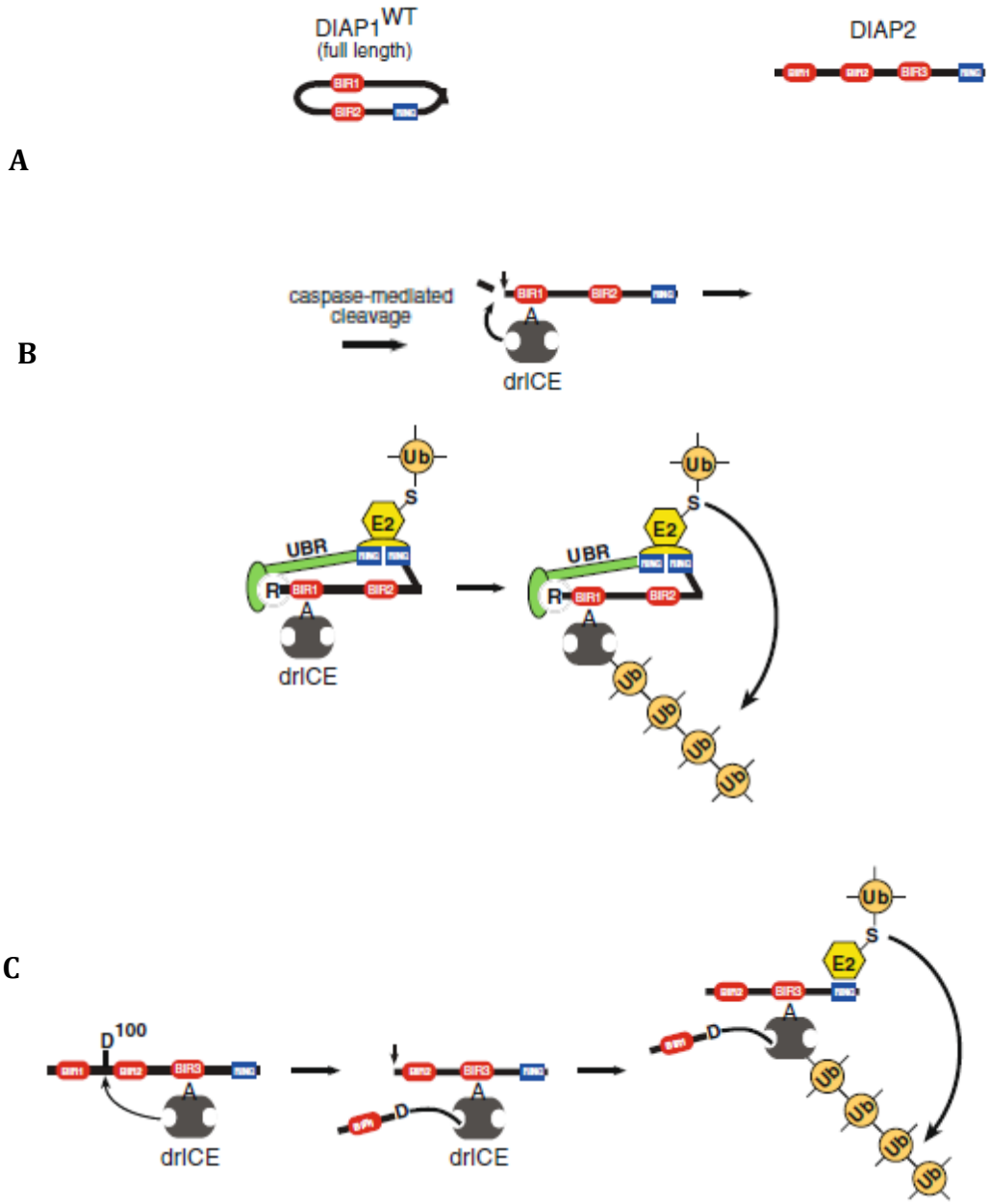

Figure 10 a) Structure of DIAP1 and DIAP2; b) Mechanism of drICE inactivation by DIAP1 c) and DIAP2 . Adapted from Orme and Meier (2009)**.**

To investigate if DIAP1 or DIAP2 have an essential role in cell survival, the viability of loss-of-function *diap1* and *diap2* mutants has been assayed. Wang et al. (1999) report that DIAP1 is indispensable for cell survival, since removal of zygotic DIAP1 leads to morphogenetic arrest. Homozygous *diap1* mutant embryos exhibit a severe lethal phenotype and do not form a cuticle. Additionally, loss of DIAP1 results in disproportionate caspase activity, which is inhibited after addition of purified DIAP1. Furthermore, Yin and Thummel (2004) demonstrate that DIAP1 is required for third-instar larval viability. Heat-induced *diap1* dsRNA expression *in hs-diap1-RNAi* third-instar larvae causes premature cell death by necrosis and organismal death before head eversion. Reducing *diap1* function via RNAi in larval salivary glands and midguts results in premature destruction of these tissues (Fig.11).

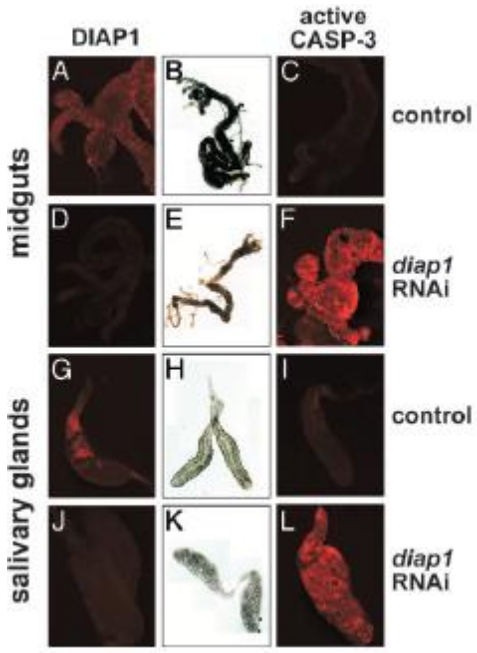

Figure 11. Expression of *diap1* dsRNA leads to premature larval midgut and salivary gland cell death. Control w^{1118} and *hs-diap1-RNAi-11* mid-third-instar larvae are subjected to heat treatment and allowed to recover for 6 hr. Larval midguts and salivary glands were then dissected from these animals and examined by light microscopy (B, E,H, and K), immunostaining to detect DIAP1 (A, D, G, and J), or immunostaining to detect active caspase-3 (C, F, I, and L). Physical signs of cell death (E and K) and caspase activation (F and L) are only seen when DIAP1 levels are reduced by RNAi (D and J) (Yin and Thummel, 2004).

Unlike DIAP1, DIAP2 is dispensable for cell survival. As seen in Figure 5, there is a brief burst of *diap2* transcription, preceding *rpr* and *hid* induction in doomed salivary glands. As *diap2* expression parallels that of *diap1* during late larval and prepupal development, similar heat shock-induced RNAi experiments have been performed. No effects on viability have been observed in *hs-diap2-RNAi-p35* animals at any developmental stage (Yin and Thummel, 2004). Instead, DIAP2 is required in immune resistance to Gram-negative bacteria (Huh et al., 2006). DIAP2 functions as a E3 ligase in

the IMD-mediated humoral response to Gram-negative bacteria. The role of DIAP2 is to promote cleavage and nuclear translocation of the NF-κB transcription factor Relish in response to immune challenge.

Therefore, it is *diap1* that must be downregulated to induce larval salivary gland histolysis. During most of larval development, DIAP1 cannot be overcome by death activator expression in larval salivary glands. This is due to high levels of DIAP1 in this tissue at early stages, substantially higher than are present at the onset of metamorphosis. This switch in DIAP1 levels occurs in the mid-third instar and depends on EcR and a CREB binding protein (CBP) (Yin et al., 2007). CBP is necessary and sufficient to first reduce DIAP1 levels, providing salivary glands with the competence to die. Then*, rpr* and *hid* eliminate residual DIAP1 and trigger histolysis (Fig. 12).

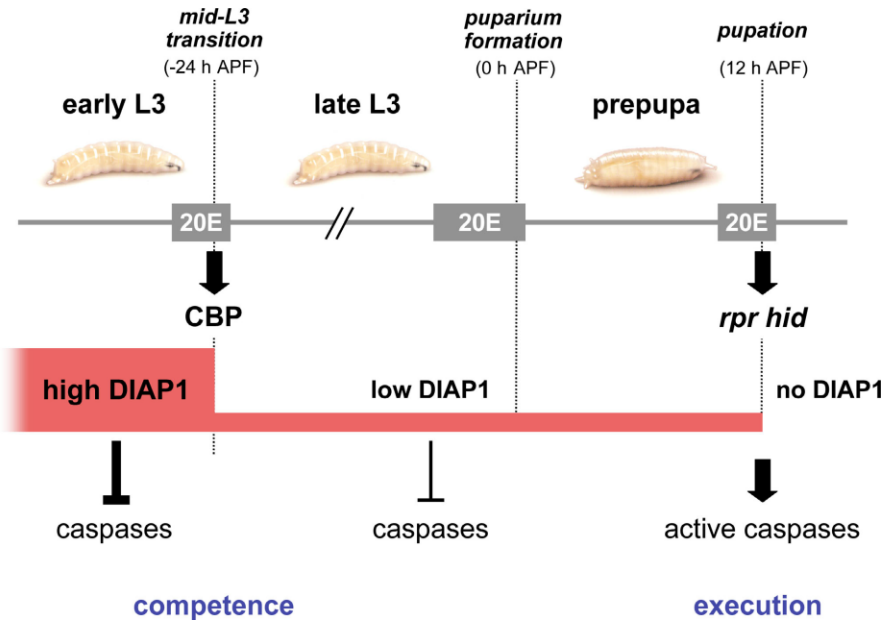

Figure 12. Down-regulation of DIAP1 provides competence for ecdysone-induced PCD. Ecdysone (labeled 20E) induces CBP expression at the mid-L3 transition and directs down-regulation of DIAP1 in larval salivary glands to a critical threshold level, establishing competence for cell death. Later, ecdysone-induced *rpr* and *hid* expression at pupation (12 hr APF) eliminates the remaining DIAP1, allowing caspase activation and salivary gland destruction (Yin et al., 2007).

Drosophila melanogaster Fat Body Development

While most larval tissues undergo ecdysone-directed PCD through the two-step regulatory hierarchy, described above, the larval fat body is an exception, as it undergoes ecdysone-regulated remodeling. Fat body remodeling is essential for completion of pupal development (Cherbas et al., 2003). Remodeling occurs be undergoing tissue dissociation, resulting in redistribution of individual fat cells throughout the body of the pupa (Nelliot et al., 2006). Eventually, the fat body is destroyed in the young adult by autophagy (Rusten et al., 2004). To understand the developmental fate of the

fat body and the impact of its remodeling on its physiological role in the pupa and the young adult, we need to first understand its development.

The embryonic mesoderm is divided into somatopleura and splachnopleura (Hoshizaki, 1994). The somatopleura gives rise to the embryonic fat body at stage 10/11 and it forms a morphologically distinct structure, composed of lateral fat body, ventral commissure and dorsal projections (Fig. 13). The lateral fat body forms a bilateral ribbon located between the somatic body-wall muscle and the gut. The ventral commissure extends from the anterior of the lateral fat body and spans the ventral midline. The dorsal projections extend from the posterior of the lateral fat body and flank the heart (Hartenstein and Jan, 1992).

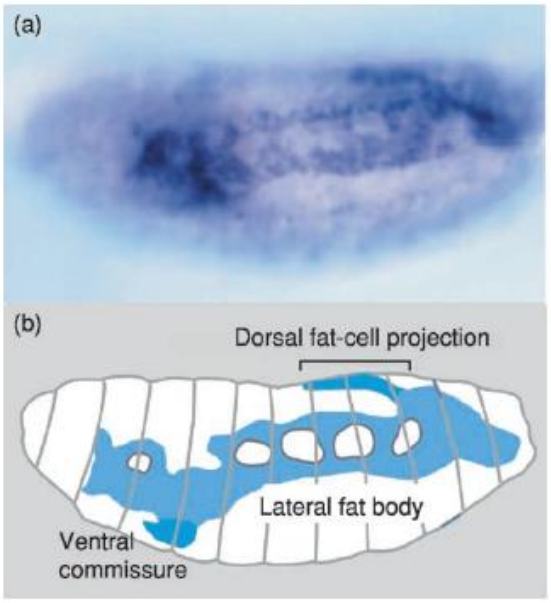

Figure 13. Embryonic Fat Body Morphology: a) Lateral view of a whole-mount stage-16 embryo stained for Serpent (Srp) protein, used to identify cell lineage b) Corresponding schematic indicating the three morphological domains of the fat body: lateral, ventral and dorsal (Miller at el., 2002).

The stages of fat cell development (determination, differentiation, and terminal differentiation) have been identified based on the temporal expression of the genes *Adh* (alcohol dehydrogenase encoding gene), *DCg1 (Drosophila collagen IV)*, and *svp (seven-up)* Additionally, differentiation has been visualized via P-element enhancer trap lines P[29D], P[J3-76a], and [PX8-157a]. These enhancer lines contain a *lacZ* reporter gene from the promoter region of *serpent* (*srp*). The reporter of P[lacZ] elements is a b-galactosidase fusion protein that is targeted to the cell nucleus (O'Kane and Gehring, 1987). Expression of svp marks the beginning of differentiation in early fat precursor cells. Expression of *Adh* and *DCg1* designates the onset of late fat precursor cell differentiation. Finally, the enhancer trap lines P [J3-

76a], and [PX8-157a] are active during late terminal differentiation (Fig. 14) (Hoshizaki et al., 2005).

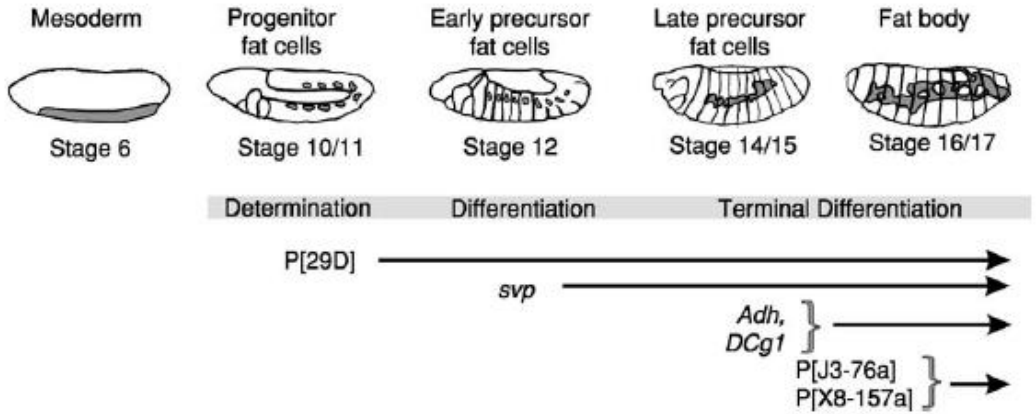

Figure 14. Fat-cell lineage of the lateral fat body and stages of fat-cell development. The mesoderm arises from the ventral region of the embryo at stage 6. The nine bilateral clusters of cells (stage-10, 11 embryo) expand to form the dorsal fat body (stage-12 embryos). The *svp* gene is first detected at stage 12 in the nine bilateral cells (marked by P [29D]) and then acts as.a fat-cell-specific regulator of *Adh* and *DCg1* expression. *Svp* expresson indicates the onset of fat-cell differentiation (stage-12 embryo). *Adh* and *DCg1*, which are involved in cell metabolism, are expressed at the beginning of terminal fat-cell differentiation. The enhancer trap lines P [J3-76a] and [PX8-157a] are active late in stage 15 (Hoshizaki et al., 1994).

The mature lateral fat body originates from nine bilateral mesodermal cell clusters located in parasegement (PS) 4-12. There are two other groups of cells, which also contribute to the mature fat body: the lateral and ventral secondary fat-cell clusters. These have been identified based on expression of *A-Box binding factor gene* (*Abf*), also known as *serpent* (*srp*). Examination of *srp* has allowed to identify the primary fat-cell clusters in PS 4–9, the lateral

and ventral secondary fat cells in PS 4–12 and PS 3–11, respectively, and the dorsal fat-cell cluster in PS 13/14 (Figure 15) (Riechmann et al., 1998).

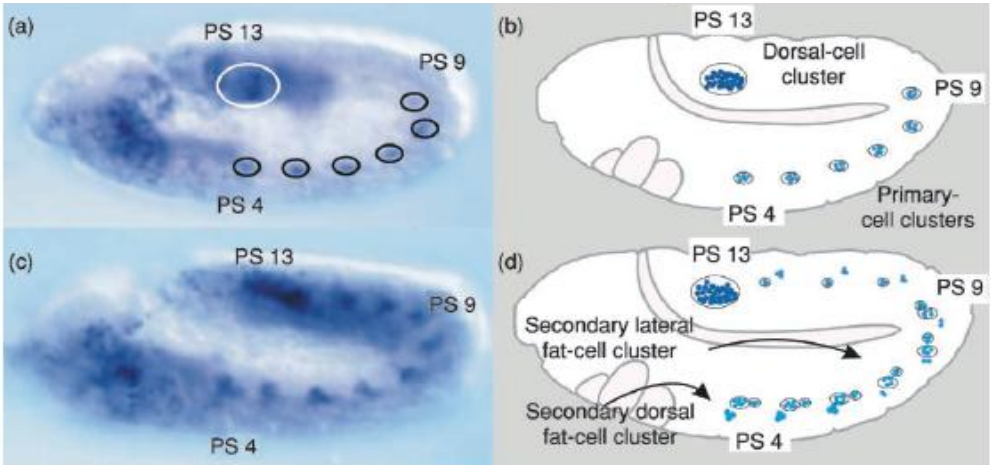

Figure 15. Precursor cells of the fat body domains. **(a, c)** Lateral view of a whole-mount embryo stained for Srp. **(b, d)** Schematic drawings highlighting precursor fat-cell clusters
(a, b) Stage-10 embryo. The dorsal fat-cell cluster is located in the in the dorsal mesoderm of PS 13/14 and the primary fat-cell clusters are located in the lateral mesoderm of PS 4–9.
(c, d) Stage-11/12 embryo. The secondary ventral fat-cell clusters are located in the ventral mesoderm of PS 3–11, ventral to the primary fat-cell clusters A second group of subsidiary precursor fat cells are located posterior to the primary cell clusters in PS 4–9 and in the equivalent position in PS 10–12.

Finally, the origin of the adult fat body is distinct from that of the larval fat body. During embryogenesis, presumptive imaginal cells, which give rise to the adult epidermis, are segregated from the larval cells. These imaginal cells reside in the larva either as discs of ectodermal cells surrounded by peripodial membrane or as clusters of cells known as histoblasts, which do not have a peripodial membrane. Based on analysis of

two independent enhancer trap lines, X8-157a and 3-76a, the putative imaginal fat cells were identified as a subset of histoblast cells associated with the body wall of the larva, and as a subset of adepithelial cells associated with specific imaginal discs (Hoshizaki et al., 1994). The *lacZ* reporter gene associated with these two enhancer-trap lines exhibits activity in embryonic, larval, and adult fat cells and appears to mark all fat-cell lineages.

Fat Body Function

The *Drosophila* fat body has a central role in larval development by fueling its rapid growth through its participation in the intermediary metabolism. The larval fat body also plays an active role in coordinating larval growth by monitoring the nutritional status of the animal and altering the feeding and other behavioral responses according to need (Hoshizaki, 2005). Furthermore, the larval fat body produces mitogenic growth factors, which control imaginal cell proliferation.

The fat body is an endocrine organ and has a critical role in development as it produces growth factors. Martin et al. (2000) report that the gene *minidiscs* (*mnd*) is expressed in the fat body and is responsible for a secreted factor necessary for imaginal disc proliferation. Mutations in minidiscs result in smaller imaginal discs and brain lobes, the fat body

appears to be depleted of lipids, and these mutant animals die late in larval development.

Bryant and co-workers (Kawamura et al., 1999; Zurovec et al., 2002) have identified two classes of growth factors, produced by the fat body: imaginal disc growth factors (IDGFs) and adenosine-deaminease-related growth factors (ADGFs). Recombinant forms of IDGF1 and IDGF2 promote cell proliferation in the imaginal disc cell line C1.8 and promote cell growth and formation of pseudopodia in the presence of insulin (Kawamura et al., 1999). The cooperation between IDGFs and insulin in stimulating imaginal disc cell growth suggests that the IDGFs might function as cofactors to insulin and insulin-like peptides (Stocker and Hafen, 2000). The ADGFs stimulate imaginal disc proliferation and one of them, ADGF-D, is expressed primarily in the fat body and brain.

Besides its role in growth factor synthesis, the fat body also maintains energy homeostasis through altering feeding and other behavioral responses. Zinke et al. (1999) have identified the gene *pumpless* (*ppl*), which is expressed specifically in the fat body and codes for a glycine cleavage system subunit, which has high homology to the vertebrate protein H subunit of the glycine cleavage system. This vertebrate enzyme complex is involved in the catabolism of glycine into ammonia, carbon dioxide, and other one-carbon molecules (Hoshizaki, 2005). Thus, the *ppl* gene is likely to be also involved in amino acid metabolism through the catabolism of glycine and the

generation of one-carbon molecules. The *ppl* behavioral mutants have a drastic reduction in growth and eventually die as small larvae, as they suppress food intake in response to amino acids (Zinke et al., 1999). It is possible that *ppl* coordinates the nutritional status the animal (or the fat body) with the first ecdysone pulse during metamorphosis.

Fat Body Remodeling

During the last larval instar, at the onset of metamorphosis, the fat body undergoes extensive structural reorganization as its function changes and the animal undergoes the transition from larval to adult life (Hoshizaki, 2005). The fat body switches from the production and secretion of storage proteins, which serve as a source of polypeptides and amino acids for the re-architecture of the animal into the adult form (Haunerland, 1996), to the re-adsorption of these proteins from the hemolymph. The storage proteins are subsequently sequestered into large proteinaceous storage granules. During metamorphosis, these proteins are used in the transformation of the fat body from an organized tissue to a loose association of individual cells (Dean et al., 1985). This morphological change is associated with loss of adhesion whereby mitochondria, microbodies and rough endoplasmic reticulum are sequestered in organelle-specific autophagic vacuoles and destroyed by hydrolytic enzymes (Locke and Collins, 1968).

The chronology of morphological changes during fat body remodeling has been correlated to the relative ecdysone titer that directs metamorphosis. This has been accomplished using the GAL4 driver/UAS promoter system to restrict expression of Green Fluorescent Protein (GFP) only to the fat body (Fig. 16).

Prior to metamorphosis, at the third larval instar stage, the fat body consists of monolayer sheets of white, translucent cells floating between the body wall and the midgut (Fig. 16b(1); 17a). Following the first ecdysone pulse during metamorphosis, the larva becomes stationary and transforms into a white prepupa (Fig. 16b(2); 17b) At this time point, referred to 0 hr after puparium formation (APF), the fat body morphology remains extended, with the fat cells tightly associated. Over the next ~4 hr, the puparium cuticle (pupal case) forms, followed by apolysis, or the separation of the larval epidermis from the cuticle (Fig. 16). Apolytic fat cells assume a rounded appearance (Fig.17d). Completion of apolysis at 6 hr APF marks the onset of prepupal development.

Duirng prepupal development, the fat cells lose adhesion to each other, a process, referred to as disaggregation (Fig. 17d). The second ecdysone pulse occurs at 12 hr APF and triggers head eversion (Fig. 16b (7)). At this point, anterior fat cells become spherical and physically detach from each other (Fig. 17e). They are propelled in the head region by abdominal

contractions and by 14 hr APF, fat cells are freely packed in the pupa's interior.

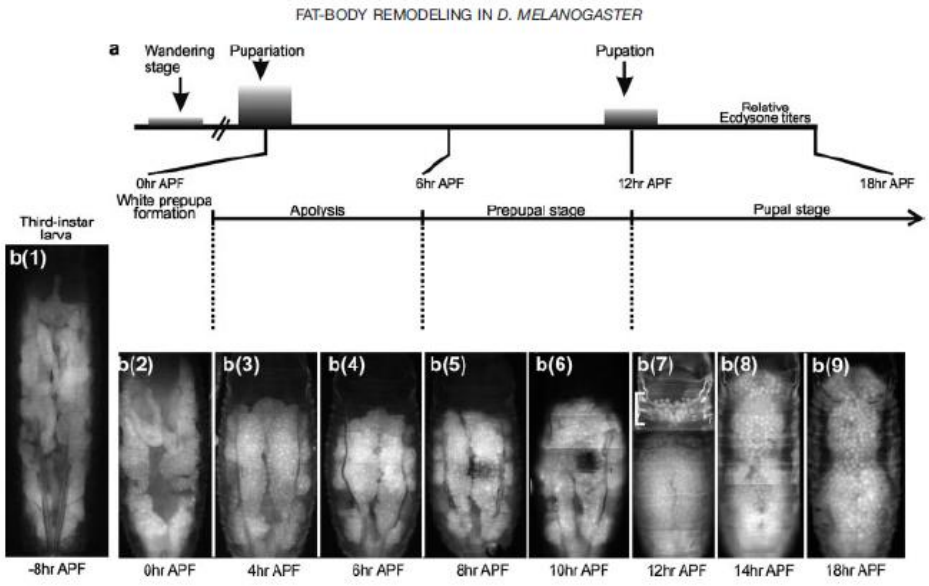

Figure 16. Stages in fat body remodeling and corresponding relative ecdysone titer in whole animals. Ecdysone induces fat body remodeling characterized by four major steps: 1) tissue extension prior to pupariation → 2) retraction from the anterior region at 0 hr APF →3) disaggregation at 6 hr APF → 4) dispersal throughout the head region by muscular contractions at 12 hr APF (Nelliot et al., 2006).

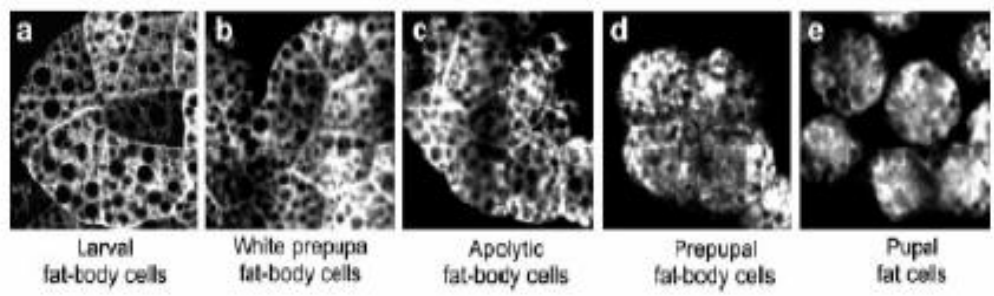

Figure 17. Changes in fat cell morphology during fat body remodeling. The sheets larval flat polygonal cells are remodeled into individual spherical cells as the animal metamorphoses from larva into pupa. The process is associated with a loss of cell-to-cell adhesion and is ecdysone-regulated (Nelliot et al., 2006).

Newly eclosed adult *Drosophila* contains dissociated larval fat body cells, which persist as a nutritional resource during the early, non-feeding stage of adulthood. These larval fat cells increase starvation resistance in the adult until the adult fat body forms from imaginal discs (Hoshizaki, 1995). Then, 3-4 days post-eclosion, the larval fat body is removed by caspase-

dependent autophagy (Aguila et al., 2007). Experimental blockage of larval fat cell death via ectopic expression of *p35* and *diap1* through the GAL4/UAS system further increases adult starvation resistance from 58 hr to 72 hr. Therefore, the final destruction of larval fat body is inhibited by expression of *p35* and *diap1.* Nevertheless, the inhibition of PCD by *p35* and *diap1* does not change the number of larval fat cells recovered from the newly eclosed adult. The genetic regulation of the larval fat PCD in transgenic *p35* and *diap1* animals is unclear, specifically the mechanism of antiapoptotic gene suppression.

The developmental fate of the fat body represents a conundrum as it undergoes dissociation but not cell death like the other ecdysone-regulated larval tissues. Alternative hypotheses suggest that programmed autophagy of the fat body begins as early as the third instar stage (Butterworth and Forrest, 1984). Rusten et al. (2004) propose that the fat body undergoes ecdysone-directed autophagy via downregulation of the class I phosphoinositide (PI) 3-kinase (PI3K) pathway. Normally, activation of the PI3K way by the cytokine interleukin-13 suppresses autophagy (Petiot et al., 2000). Scott et al. (2004) suggest that starvation induces fat body autophagy, which in turn can be suppressed by the Target of Rapamycin (TOR) pathway. These findings necessitate further research to elucidate the timing and nature of fat body remodeling and autophagy .

Project Aim

The timing and morphological specificity of fat body remodeling have been clearly identified. Changes in ecdysone titer during metamorphosis result in subsequent changes in fat body organization from a monolayer of polygonal cells to individual spherical cells. However, the genetic regulation of fat body dissociation and reorganization still needs to be elucidated. Based on research by Aguila et al. (2007), *diap1* has been identified as a suppressor of larval fat autophagy in newly eclosed adult *Drosophila*. My project examines the role of endogenous and ectopic *diap1* expression in the fat body during metamorphosis. I hypothesize that, while larval salivary glands undergo PCD at 12 hr APF, the neighboring fat tissue is resistant to PDC due to upregulation of *diap1*.

To test this hypothesis, I used quantitative Real Time PCR to determine tissue-specific *diap1* expression at different time-points during metamorphosis (L3, 0 hr APF, 6 hr APF, 12 hr APF and 14 hr APF). Additionally, I visualized fat body development in transgenic animals in which *diap1* is knocked down specifically from the fat body. I employed RNA interference to selectively knock down *diap1* from the fat body and Green Fluorescent Protein (GFP) to fluorescently tag this tissue. The bipartite GAL4/UAS diver-responder system was used to restrict GFP expression to the fat body. The resulting transgenic animals were examined for changes in fat body fate and viability.

MATERIALS AND METHODS

Drosophila husbandry and maintenance

For the purpose of this study, four different genotypes of fruit flies were maintained on standard yeast medium supplemented with yeast at 25°C. The *Canton S* stock was used in molecular characterization of wildtype *diap1* expression in fat body. To visualize fat body remodeling a *UAS-GFPgap; Lsp2-Gal4* (referred in the text as *Lsp2-Gal4*) stock was generated. The *UAS-GFPgap* stock was provided by the *Drosophila* Stock Center, Bloomington IN. To examine the effect of *diap1* gene knockdown on the remodeling process, we created a *Lsp2-gal4; diap1-RNAi* strain (Fig. 18). The diap1-*RNAi* line was generously provided by L. Holderbaum (Harvard Transgenic RNAi Project). In microscopy experiments, both control *Lsp2-gal4* and tissue-specific *diap1* knockouts expressed Green Fluorescent Protein (GFP) in the fat body. Virgin flies were collected to generate the *Lsp2-gal4; diap1-RNAi* progeny. Stock bottles were cleared and newly eclosed flies were collected after 8 hours of storage at 25°C or 18 hours of storage at 18°C. To delay aging, virgins were stored at 18°C, while crosses were kept at 25°C to ensure successful mating.

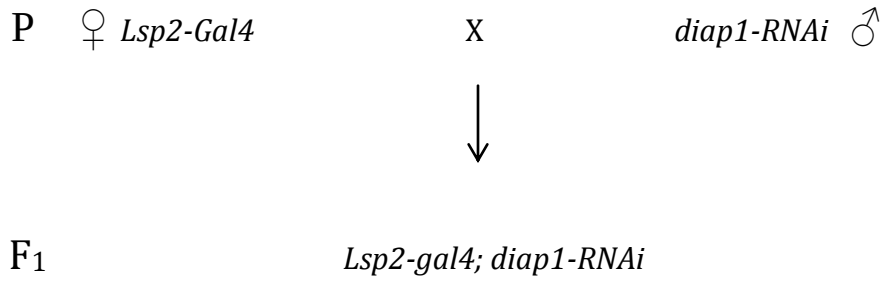

Figure 18. Experimental cross to generate the *Lsp2-gal4; diap1-RNAi* strain.

The GAL4-UAS system

Expression of Green Fluorescent Protein is localized specifically in the fat body using the GAL4-UAS system for targeted gene expression. GAL4 is a galactose-inducible gene regulator in the yeast, *Saccharomyces cerevisiae* (Duffy, 2002). GAL4 regulates the transcription of the divergently transcribed GAL10 and GAL1 genes by directly binding to four related 17 bp sites located between these loci (Giniger et al., 1985). These sites define an Upstream Activating Sequences (UAS) element, analogous to an enhancer element defined in multicellular eukaryotes, which is essential for the transcriptional activation of these GAL4-regulated genes. GAL4 expression is capable of stimulating transcription of a reporter gene under UAS control in *Drosophila* without deleterious phenotypic effects. In this project, we use the

bipartite approach for directing GFP expression. GFP, termed the *responder*, is controlled by the presence of the UAS element, which includes optimized GAL4 binding sites. To activate transcription in the *UAS-GFPgap* responder lines, flies from these lines are mated to flies expressing GAL4, termed the driver, in a specific cell type. The GAL4 driver-UAS responder system allows targeting gene expression in a time- and tissue-specific manner.

RNA interference mechanism

In this study, the *UAS-diap1-RNAi* genotype is capable of selectively silencing *diap1* expression in the fat body by introducing double-stranded *diap1* RNA (dsRNA). This conserved biological response to dsRNA activation is known as RNA interference or post-transcriptional gene silencing (Hannon, 2002). RNA interference is initiated by an enzyme from the RNase III class, called Dicer. Dicer cleaves double-stranded RNA into ~22 nucleotide long small interfering RNAs (siRNAs). Dicer functions as a dimeric enzyme, with four compound catalytic sites, two of which are defective. siRNA fragment length is dependent on the spacing between the active sites. The siRNAs are incorporated into a multicomponent nuclease, RNA-induced silencing complex (RISC). RISC is an RNA-protein effector complex that recognizes and destroys target mRNAs. Latent RISC, containing a double-stranded siRNA, is activated by siRNA unwinding. RISC binds to unwound

siRNA and uses it to recognize complementary mRNA. RISC degrades mRNAs, reducing translation and effectively silencing gene expression (Fig. 19).

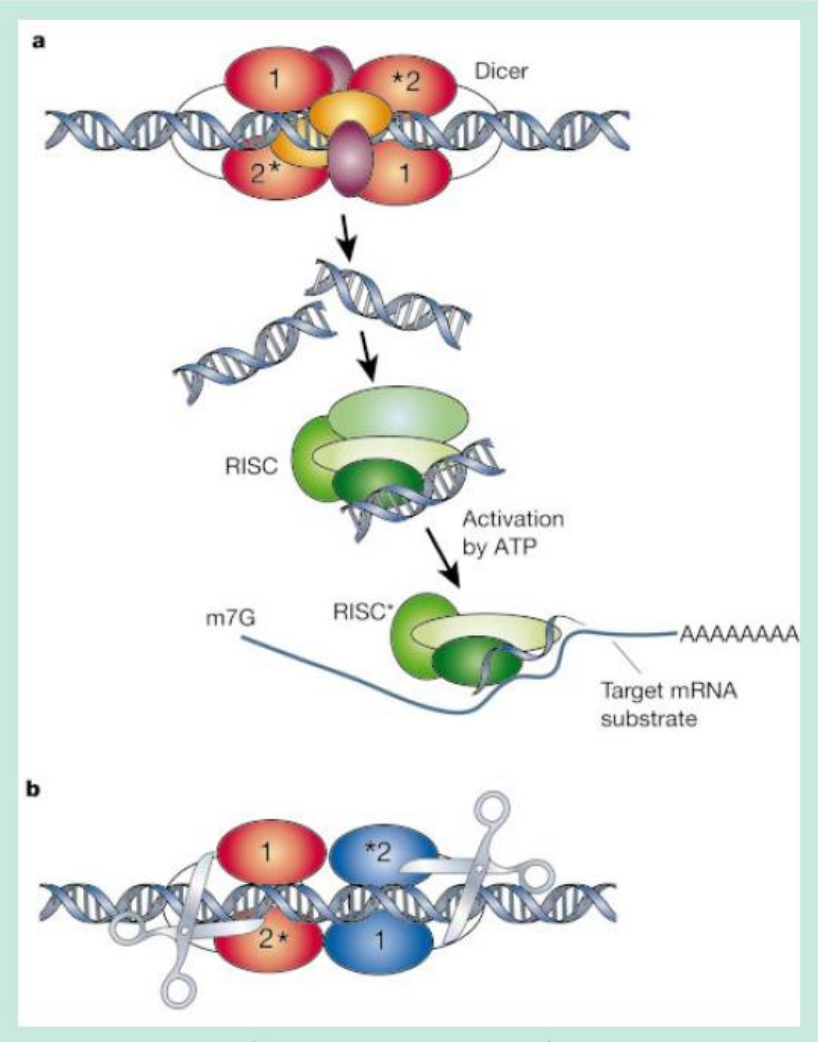

Figure 19. Mechanism of RNA interference: a) Dicer cleaves dsRNA and RISC binds to the 22bp long duplexes. RISC is activated in ATP-dependent manner and unwinds ds fragments to form ss siRNA. The single stranded si RNA is used as a guide to degrade complementary mRNA, silencing the specific gene. **b)** Diagram representing dsRNA cleavage by Dicer. In the two separate Dicer molecules shown, only the catalytic sites numbered **1** are active (Hannon, 2002).

Fluorescence Microscopy

The course of fat body tissue reorganization was followed in control *Lsp2-gal4* and knockout *diap1-RNAi* via fluorescence microscopy. Flies were collected at the white prepupal (0 h APF stage) and aged to multiple time points: 6, 12, 14, 20, 22 and 24 h APF. The white prepupal stage is easily identifiable by their untanned cuticle, everted spiracles and immobility. These prepupae were aged on moistened filter paper in a humidity chamber for the appropriate time period and immediately imaged. Images were captured with a Zeiss Axiocam 2 epifluorescence compound microscope. The pupae were positioned in a moist chamber with their dorsal side facing the objective lens. Each specimen was visualized under the 4X objective via the imaging software MetaVue. The brightness and contrast of the images presented in this paper were adjusted with Adobe Photoshop CS3.

diap1 gene expression

In order to qualitatively determine *diap1* expression in wildtype (*Canton S*) fat body, we used the Reverse Transcriptase Polymerase Chain Reaction (RT-PCR). PCR is a molecular biological technique, used to amplify a specific DNA sequence (target sequence). Short DNA fragments, complementary to the 3' ends of the sense and antisense DNA strands, called

primers, are used to enable selective and repeated amplification. The target sequence is amplified via cycles of repeated heating and cooling (thermal cycling). After each cycle, the DNA template is exponentially amplified in a continuous chain reaction. Template replication is enabled by the heat-resistant *Taq* DNA polymerase, isolated from the bacterium *Thermus aquaticus*. This enzyme uses oligonucleotides to generate new copies of the target DNA.

During thermal cycling, the reaction is first heated to 90°C in order to separate the single strands of the target DNA via denaturation. Then, the reaction is cooled to 50-65°C, so that the primers can anneal to their complementary DNA strands, bracketing the region of interest. Next, the reaction is heated to 72°C, which allows *Taq* polymerase to attach to each priming site and to synthesize a new DNA strand (Fig. 20). This cycle is repeated 40 times, generating sufficient PCR product to detect the expression of the gene of interest (*diap1*) by gel electrophoresis.

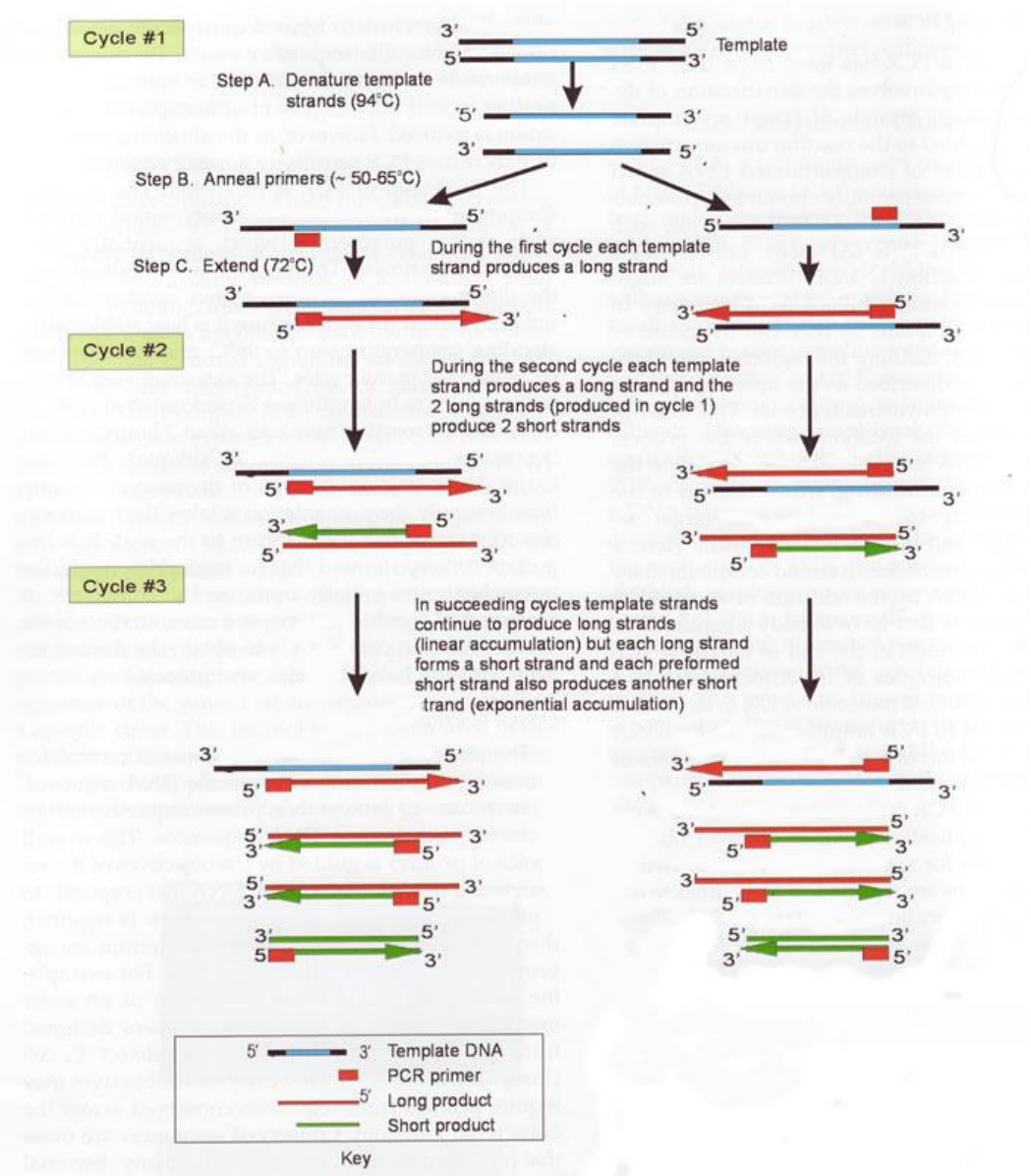

Figure 20. PCR amplification of a target DNA sequence. To amplify a DNA region of interest by PCR, the reaction is first heated so the DNA denatures. Next, the enzyme *Taq* polymerase synthesizes two new strands of DNA, using the original strands as templates. Then each of the new strands can be used to create two new copies. The cycle of denaturing and synthesizing new DNA is repeated as many as 30 or 40 times, leading to more than one billion exact copies of the original DNA segment (National Human Genome Research Institute, http://www.genome.gov/10000207).

RNA Isolation from Fat Body Tissue

Wildtype *Canton S* flies were aged to several time-points: L3, 0 h APF, 6 h APF, 12 h APF and 14 APF and dissected under a dissection microscope. Fat bodies were collected from 7-10 flies in individual 1.5 mL microfuge tubes in 30 μL 1X Robb buffer. The samples were promptly homogenized and lysed with 300 μL TRIzol reagent (Invitrogen). TRIzol-treated samples were stored at -80°C until RNA isolation.

Fat body RNA was isolated by the chloroform-isopropanol method. 2 mL RNAse-free Phase Lock Gel Heavy Eppendorf tubes were pre-spun for one minute at 12,000 rpm. Samples were incubated at room temperature and transferred to the Phase Lock microfuge tubes in 60 μL chloroform. The samples were shaken vigorously and centrifuged for 10 minutes at 12,000 rpm at 4°C. The aqueous phase was quantitatively transferred to a new RNas-free 1.5 mL microfuge tube and 160 μL isopropanol were added to each sample. The tubes were vortexed and stored at -20°C to precipitate overnight.

After precipitation, the samples were centrifuged for 30 min at 13,400 rpm at 4°C. The supernatant was removed and the pellet was suspended in 500 μL freshly prepared RNAse-free 75% ethanol. The samples were spun for 10 min at 13,400 rpm at room temperature. The supernatant was

removed . The pellet was air-dried for one minute, redissolved in 11 μL RNase-free water and vortexed to facilitate mixing.

The isolated RNA was quantified on a ThermoScientific NanoDrop 2000c spectrophotometer. 1-2 μL undiluted RNA were used to determine concentration. Sample quality was evaluated based on optical density $(OD)_{260\text{-}280}$ nm absorption ratio, absorbance curve and concentration. The absorption ratio is a measure of nucleic acid purity and accounts for the presence of protein, phenol and other organic compounds. A pure RNA sample has an OD_{260}/OD_{280} value of 1.95-2.00.

DNase Treatment to Remove Genomic DNA

Contaminating genomic DNA was removed from the isolated RNA with the Ambion DNA-free DNase kit. To each 10 μL of RNA, 1 μL 10X DNase buffer and 1 μL r-DNAse-I were added. Samples were incubated at 37°C for 25 to 30 min. After incubation, 2 μL of pre-vortexed DNase Inactivation Reagent were added to each sample, followed by incubation at room temperature for two minutes. Samples were then spun at 10,000 g for 90 s and the clear, supernatant RNA was transferred to a new, RNase-free tube.

The DNase treatment was repeated with 1.5 μL 10X DNase buffer instead of 1 μL, the rest of the protocol was otherwise identical. The DNase-treated RNA was quantified and quality was determined based on the

parameters used before DNA removal. After DNase treatment, all RNA samples had 260/280 values greater than 1.9, indicating high purity.

Reverse Transcription

In order to generate a stable form of the labile RNA template, reverse transcription was carried out to synthesize stable single-stranded complementary DNA (cDNA). cDNA synthesis is performed using reverse transcriptase (RT), an RNA-dependent DNA polymerase. Like all DNA polymerases, RT cannot initiate synthesis *de novo* but depends on the presence of a primer. Two types of frequently used primers of DNA synthesis are oligo-dT and random hexamers. Additionally, the enzyme RNase H is required to produce single-stranded nicks in the RNA, which RT uses as synthesis initiation sites (Wagner, 1997). Once RNA is converted to cDNA, the cDNA can be used for RT-PCR, as a probe for expression analysis.

Reverse transcription was performed using the Invitrogen First-Strand SuperScript® Reverse Transcriptase Synthesis Kit for RT-PCR. For each synthesis, no more than 250 ng of DNase-treated RNA were used. For each standard cDNA reaction, a no reverse trancriptase (no RT) control was prepared. To each 1 μL RNA sample, the following reagents were added in the specified order: 1 μL 10 mM dNTPs, 1 μL 0.5 μg μL^{-1} $oligo(dT)_{12\text{-}18}$ and 7 μL DEPC-treated water for a final volume of 10 μL. After mixing, the reactions were incubated at 65°C for 5 minutes.

A master mix was prepared for n+1 reactions, containing 2 μL 10X RT buffer, 4 μL 25 mM $MgCl_2$, 2 μL 0.1 M DTT and 1 μL RNase OUT per reaction. 9 μL of the master mix were added to each of the cDNA syntheses and they were incubated for two minutes at 42°C. To each reaction, 1 μL SuperScript II Reverse Transcriptase was added. To each no RT control, 1 μL DEPC-treated water was added. The samples were incubated for fifty minutes at 42°C. The cDNA synthesis was then terminated for fifteen minutes at 70°C. Then, the samples were picofuged and chilled on ice prior to RNase H treatment. To eliminate the RNA template, 1 μL RNase H was added to the syntheses and they were incubated for twenty minutes at 37°C. The resulting cDNA was stored at -20°C.

Primer Design

PCR primers were designed with Primer3Plus (Untergasser et al., 2007) and produced by Integrated DNA Technologies (IDT), using sequences from FlyBase (Tweedie et al., 2009). Primers were designed over exon-intron boundaries to ensure that gene transcript sequences are amplified rather than any remaining genomic DNA. cDNA sequences were obtained from NCBI's website using the BLAST tool. The experimental primers in Table 1 include *diap1* and *diap2* primers, since this project studied *diap2* expression, prior to elucidating *diap2*'s secondary role in PCD regulation. The *diap1* primers were designed within exon 1 of the gene, while *diap2* primers were

designed within exon 1 and 2. The expected product sizes were 147 bp and 116 bp, respectively. The β-actin primers were pre-designed within the sequence of the *actin 5C* gene with expected product size 158 bp. In this experiment, *β-actin* (hereafter referred as *actin 5C*), was used as an endogenous standard, since it is a non-regulated, housekeeping gene. Housekeeping genes are present in all nucleated cell types because they are necessary for cell survival (Pfaffl, 2001).

Table 1. Primer sequences for target genes and endogenous controls.

Gene	Primer ID	Sequence
actin 5C	forward	5'-TCT ACG AGG GTT ATG CCC TT-3'
	reverse	5'-GCA CAG CTT CTC CTT GAT GT-3'
diap1	forward	5'-CGG TTT ATC CAT TGC TCG AT-3'
	reverse	5'-TCT GGC TCC TTT CCT CTG AA-3'
diap2	forward	5'-TGG TAA CTT TCA AGG ACT GGC CGA-3'
	reverse	5'-TCC GTT GCA CCA AAC ACA CTT CAC -3'

Primers were hydrated with nuclease-free water to a stock concentration of 500 μM. Stock solutions were diluted to 10 μM for RT-PCR and 1-5 μM for quantitative real time PCR.

Reverse Transcriptase Polymerase Chain Reaction (RT-PCR)

PCR reactions were prepared with the First Strand SuperScript® Reverse Transcriptase System kit for RT-PCR on Techgene or Progene thermocyclers by Techgene. The reagents were combined according to the general pipetting scheme outlined in Table 2 to prepare a master mix for n+1 50 µL reactions. *Taq* polymerase was added last. The basic RT-PCR thermocycler profile is shown in Table 3, with the following annealing temperatures: 60.2°C for *actin 5C* and *diap2*, 55.4°C for *diap1*.

Table 2. Pipetting scheme for RT-PCR.

Reagent	Amount per reaction	Final concentration
10X RT Buffer-$MgCl_2$	5 µL	-
50 µM $MgCl_2$	3 µL	3 mM
10 mM dNTPs	1 µL	200 µM
10 µM forward primer	2 µL	400 µM
10 µM reverse primer	2 µL	400 µM
cDNA	2 µL	-
Nuclease-free water	34.6 µL	-
Taq Polymerase 0.4 µl	0.4 µL	2 units

Table 3. General thermocycler profile for RT-PCR.

Stage	Temperature	Duration	Cycle count
Denaturation	94°C	30 sec	35 cycles
Annealing	Primer-specific	30 sec	
Extension	72°C	30 sec	
Final extension	72°C	5 min	1 cycle
Final hold	4°C		

Agarose Electrophoresis

PCR products were visualized on 1.6% gels prepared with agarose from Sigma and 1X TAE buffer. Each 20 µL PCR product was treated with 2 µL Gel Loading Dye (6x) from New England BioLabs®. This is a pre-mixed loading buffer containing bromophenol blue, a standard tracking dye for electrophoresis. Ethidium bromide (EtBr) was used as a fluorescent tag to image DNA samples under UV light. Small (10-well) gels were stained with 7 µL EtBr and run for 20 minutes at 150 V. Large (32-well) gels were stained with 10 µL EtBr and run for 35 minutes at 150 V. An Axygen Biosciences 100 bp Ladder was used to determine amplicon size. The gels were imaged on the Fujifilm LAS-3000 Luminescence Image Analyzer.

Quantitative Real Time PCR (qPCR)

While traditional RT-PCR detects PCR amplification at its final phase or end-point, Quantitative Real Time PCR (qPCR) measures amplification in the early phase of the reaction (Applied Biosystems, 2011). End-point detection is only a qualitative method as results are not numeric and based on fragment size determination, which is not very precise. Additionally, RT-PCR does not account for changes in gene expression and the gels do not reflect variability in reaction yield.

To understand the limitations of end-point PCR, it is important to know the stages of a PCR reaction:

1. Exponential: Exact doubling of product is accumulating at every cycle (assuming 100% reaction efficiency). The reaction is very specific and precise.

2. Linear (High Variability): The reaction components are being consumed, the reaction is slowing, and products are starting to degrade.

3. Plateau (End-Point): The reaction has stopped, no more products are being made and if left long enough, the PCR products will begin to degrade.

Figure 20 illustrates the increasing variability in reaction yield during the course of a PCR reaction. Thus, RT-PCR, which begins to measure DNA quantity during the plateau phase, gives a less precise estimation of DNA amount than qPCR, which quantifies PCR products during the exponential amplification phase.

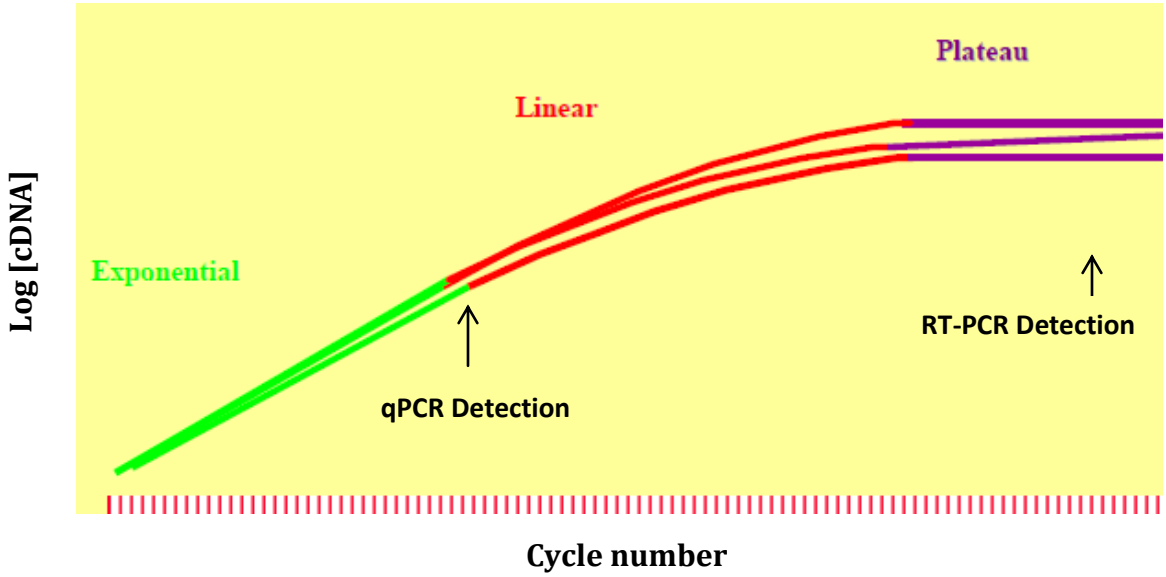

Figure 21. Phases of PCR amplification. The three replicates depicted above have the same initial quantity. During the exponential phase, all reagents are readily available and the reaction kinetics favors doubling of the amplicon. The gradual depletion of reagents occurs at a different rate for each reaction. Due to varying reaction kinetics, each sample will plateau at a different time-point and DNA concentration. Therefore, early [cDNA] measurements give a more adequate representation of relative amplicon amounts (Applied Biosystems, 2011).

Theoretically, there is a quantitative relationship between amount of starting target sample and amount of newly synthesized PCR product at any given cycle number. There are two detection techniques for newly synthesized PCR products: using a TaqMan® oligonucleotide probe or SYBR Green I fluorescence dye (Applied Biosystems, 2011).

TaqMan® detection is dependent on the 5'-exonuclease activity of AmpliTaq Gold DNA Polymerase. TaqMan® and DNA polymerase function together in the 5' nuclease assay. The TaqMan® probe is designed to anneal to a *specific target sequence* of template between the forward and reverse primers. The probe sits in the path of the polymerase as it starts to copy DNA or cDNA. When the enzyme reaches the annealed probe the 5'-exonuclease activity of the enzyme cleaves the probe. Cleavage of the probe leads to fluorescence energy transfer to a dye, termed the Reporter dye. The energy transfer increases the Reporter signal. The amount of reporter signal increase, detected by the qPCR software, is proportional to the amount of product being produced for a given sample.

In this project, I used the alternative detection method, SYBR Green chemistry, which was used in this project due to its simplicity and affordability. The major distinction between TaqMan® and SYBR Green is that SYBR binds to the minor groove of *any* double-stranded DNA. During qPCR, following the denaturation step, SYBR molecules are unbound. Then the primers anneal to the template and the newly synthesized single strand is extended. When DNA polymerization is complete, SYBR binds to the double stranded DNA and fluoresces. As more double stranded amplicons are produced, the SYBR Green dye signal will increase (Applied Biosystems, 2011).

Thus, the *amplification plot* is the plot of fluorescence signal versus cycle number. The *threshold* line is the level of detection or the point at which a reaction reaches a fluorescent intensity above background. The threshold line is set in the exponential phase of the amplification for the most accurate reading. The cycle at which the sample reaches this level is called the *cycle threshold*; C_t. Quantification of the amount of a target gene in an unknown sample is achieved by relating fluorescence intensity to C_t values. A smaller C_t means that there is a greater amount of template present, as the reaction entered the phase of exponential amplification earlier (Yuan et al., 2006).

The qPCR experiments presented in this paper were performed with the Quanta Biosciences Perfecta® SYBR Green Supermix with ROX. The reactions were run on a Applied Biosciences 7300 Real Time PCR System and analyzed via 7300 Bioanalyzer software.

Primer Concentration Optimization

To ensure optimal amplification efficiency, forward and reverse primer concentrations for *actin 5C* and *diap1* were optimized at the melting temperatures, specified by IDT (55.3°C and 55.4°C, respectively). The primers were tested at 500 nM, 300 nM and 100 nM final concentrations, for a total of nine combinations. The optimal combination of concentrations was selected based on lowest C_t value and the absence of primer dimer, evaluated

by the melting temperature of the DNA present in the final reaction. The temperature profiles for *diap1* and *actin 5C*, used in these and subsequent qPCR reactions are shown in Table 4.

Table 4. Thermocycler settings for qPCR experiments with *diap1*.

Stage	Temperature	Duration	Cycle count
Taq activation	95 °C	2 min	1
Denaturation	95 °C	15 sec	40
Annealing	55.4°C	30 sec	
Extension	72 °C	30 sec	
Dissociation	95 °C → 60 °C → 95 °C → 60°C	15 sec → 1 min →15 sec → 15 sec	1

A master mix for n + 2 reactions was prepared for *diap1* and *actin 5C* , with the components listed in Table 5. The cDNA was added to each reaction individually and was the final component of each for a total volume of 25 μL. An example layout for primer optimization is shown in Table I of the Appendix .

Table 5. Pipetting scheme for qPCR.

Reagent	Amount per reaction	Final concentration
2X Perfecta®SYBR Green Supermix with ROX	12.5 μL	1X
Forward primer	2.5 μL	100-500 nM
Reverse primer	2.5 μL	100-500 nM
cDNA	2.5 μL	-
Nuclease-free wanter	5 μL	-

Amplification Efficiency

Real time PCR amplification efficiency is determined by producing a standard curve. PCR reactions were performed on five twofold dilutions of cDNA from whole12 hr APF animals. Each reaction was performed in duplicates. The standard curve plots averaged C_t values against the log of cDNA dilutions. The slope of the standard curve indicates the amplification efficiency. A slope of -3.32 indicates 100% efficiency. A slope that is more negative than -3.32 indicates lower efficiency and can usually be corrected via primer optimization. A slope significantly greater than -3.32 reflects sample quality or possible pipetting error. The amplification efficiency is determined by the formula:

$$\text{Efficiency} = 10^{\frac{-1}{slope}} - 1$$

Efficiency values should preferentially lie between 95-105%, but a broader range is acceptable, depending on the analysis method selected. For the purpose of this experiment, amplification efficiencies of 80%-120% were considered acceptable.

Experimental qPCR Setup

The expression of *diap1* at each of the developmental time-points in this experiment was evaluated by relative quantification. Four types of qPCR reactions were needed for this estimation: standard curves, experimental reactions, no RT controls and no template controls. Two sets of these

reaction types were performed: one for the target gene (*diap1*) and one for the endogenous control (*actin 5C*). Experimental reactions were run in triplicate, while standard curve dilutions and controls were run in duplicate. As above, master mixes for n+2 reactions were prepared, using the optimized primer concentrations. The cDNA concentration in experimental wells was equivalent to 50 ng/μL of the original RNA. The same concentration was defined as 2^0 in constructing standard curves. Thus, the following samples were prepared via serial dilution: 2^{-1} (25 ng/μL), 2^{-2} (12.5 ng/μL), 2^{-3} (6.25 ng/μL) and 2^{-4} (3.125 ng/μL). A sample 96-well plate layout for a qPCR experiment is shown in Table II of the Appendix.

Relative Quantification Analysis: Pfaffl Model vs. Delta-delta Method

Relative quantification determines the change in expression of the target gene (*diap1*) relative to the reference gene (*actin 5C*), which has a constant expression level. There are several methods for relative quantification analysis. Previous research in this lab employed the delta-delta ($\Delta\Delta C_t$) method, presented by Applied Biosystems. The relative change in expression (RE) ratio is calculated by the equation:

$$RE = 2^{-\Delta\Delta Ct}$$

Where $\Delta\Delta C_t = \Delta C_t\ (experimental) - \Delta C_t (control)$. The expression of the target gene in experimental and control samples is measured by the ΔC_t value, obtained by the equation:

$$\Delta C_t = C_{t\,(target)} - C_{t\,(endogenous)}$$

For the delta-delta calculation to be valid, the amplification efficiencies must be nearly equal or optimally, identical.

This project employed an alternative mathematical model, referred to as the Pfaffl normalization method. The Pfaffl model presents a more reliable and exact estimation of relative gene expression than $\Delta\Delta C_t$. This model accounts for the fact that the reproducibility of reverse transcription (RT) varies greatly between tissues, the RT isolation technology and the RT enzymes. Under identical reaction conditions, the RT efficiency is also dependent on cDNA input concentrations (Pfaffl, 2001). Thus, the $\Delta\Delta C_t$ method is only applicable for a quick RE estimation.

The Pfaffl method calculates the relative target gene expression ratio by the equation:

$$RE = \frac{(E_{target})^{\Delta C_{t\,(control-experimental)}}}{(E_{ref})^{\Delta C_{t\,(control-experimental)}}}$$

Where E_{target} and E_{ref} the amplification efficiencies of the target and the reference gene transcript, respectively, calculated by$E = 10^{\frac{-1}{slope}}$. ΔC_t is the difference between averaged $C_{t(control)}$ and $C_{t(experimental)}$ values. The relative expression ratio of the target gene is normalized with the expression of the unregulated reference gene to compensate for inter-PCR variations

between runs. Pfaffl reports the model is highly accurate and has only <2.5% relative error for qPCR reactions with varying efficiencies (± 20%). In this project, the Pfaffl method was selected over the delta-delta method, as it standardizes each reaction run over a range of amplification efficiencies. Real time qPCR runs are standardized with respect to RNA integrity, sample loading and inter-assay variations.

RESULTS

Fluorescence Microscopy

Figures 22-27 illustrate that early *diap1-RNAi* knockout prepupae undergo fat body remodeling in sync with wildtype prepupae. Due to the intensity of GPF fluorescence, individual fat cells could not be resolved in imaging prepupal development. Nevertheless, the gross morphology of control and transgenic animals clearly remodeled in wildtype fashion. At 0 hr APF, all animals had contracted into white prepupae. The fat body was extended throughout the body cavity and filled the space between the body wall and the gut. By 6 hr APF, the fat tissue began to shrink and retract from the animal's anterior. Thus, the retraction phase had identical duration in both experimental groups.

At 6 hr APF, apolysis, the separation of the larval epidermis from the tanned puparium cuticle marked the onset of prepupal development. The next phase in fat body remodeling, disaggregation occurred between 6 and 14 hr APF in both the *Lsp2-Gal4* and the *diap1 RNAi* strains. In well-resolved images such as Figure 26 and 27, individual fat cells became visible, which is evidence of gradual loss of cell-to-cell adhesion. The images collected between 10 and 12 hr APF indicated the gas bubble was dislocated from the central to the anterior region, as a result of abdominal contractions.

The control animals underwent pupation by 14 hr APF, marked by the eversion of the head capsule. Fat cells were propelled into the head capsule in response to the muscular contractions. Figure 28 demonstrates the fat cells became spherical and clearly separated from each other. However, these changes were not observed in *diap1-RNAi* animals at 14 hr APF. In Figure 29, the fat body retained prepupal morphology and failed to disaggregate completely. As the cells did not entirely dissociate, they remained in the thoracic and abdominal region.

Between 20 hr and 24 hr APF, the fat cells in the control group were freely packed throughout the interior of the pupa. The ones in the head capsule were dispersed uniformly to support the development of the central nervous system. The masses of fat cells formed three clearly distinct domains: anterior, thoracic and abdominal (Figures 30 and 32). At 20 hr APF, the transgenic group continued to exhibit a delay in fat body remodeling. Figure 31 shows that although the heads of the *diap1 RNAi* animals are clearly everted, no fat cells are released into them. The bulk of the fat body appears tightly associated into an intact tissue. No morphological changes occurred by 24 hr APF, suggesting a developmental arrest in the transgenic group.

It must be noted that the aforementioned differences in remodeling were observed in 50%-75% of the loss-of-function *diap1* mutants. The

discrepancies between the control and the experimental group became more pronounced in older animals. During stock maintenance, I observed a decrease in mutant viability. At 36 hr APF and later, half of the *diap1 RNAi* pupae failed to eclose. Upon inspection, the animals appeared fully developed inside their pupal cases, yet died before the end of metamorphosis. No such lethality was observed in the control group.

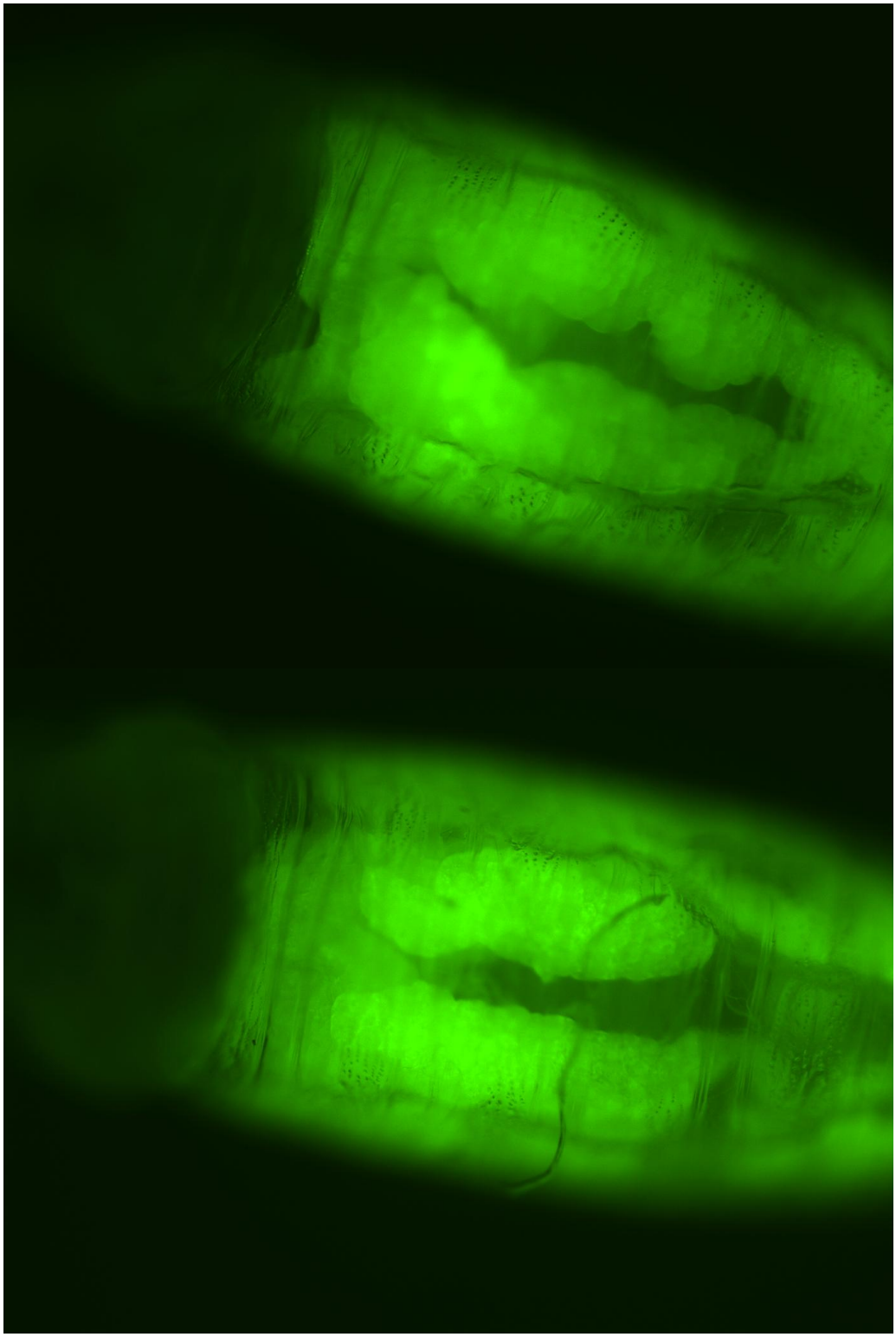

Figure 22. Fat body structure in *Lsp2-Gal4* animals at 0 hr APF.

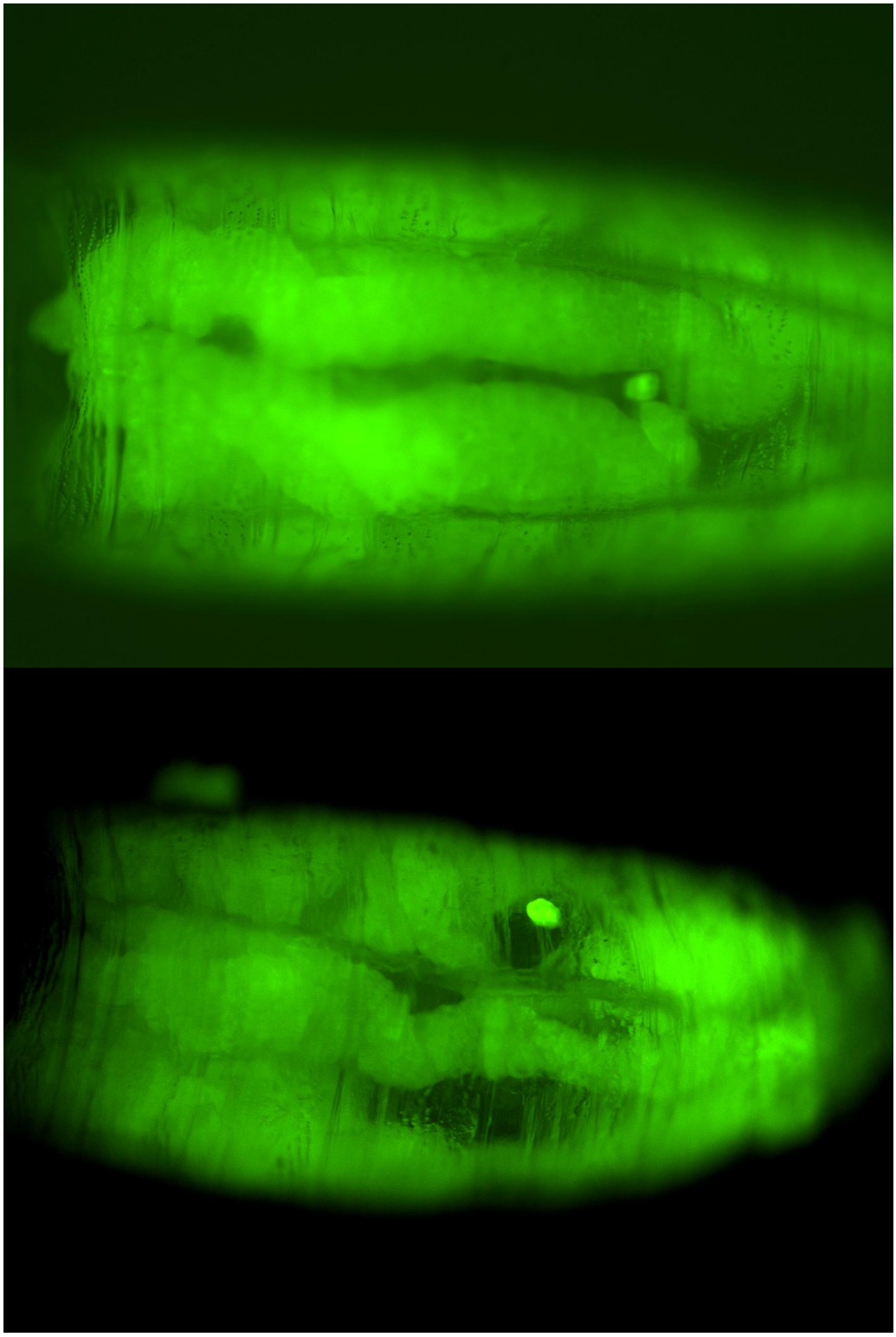

Figure 23. Fat body structure in *diap1 RNAi* animals at 0 hr APF.

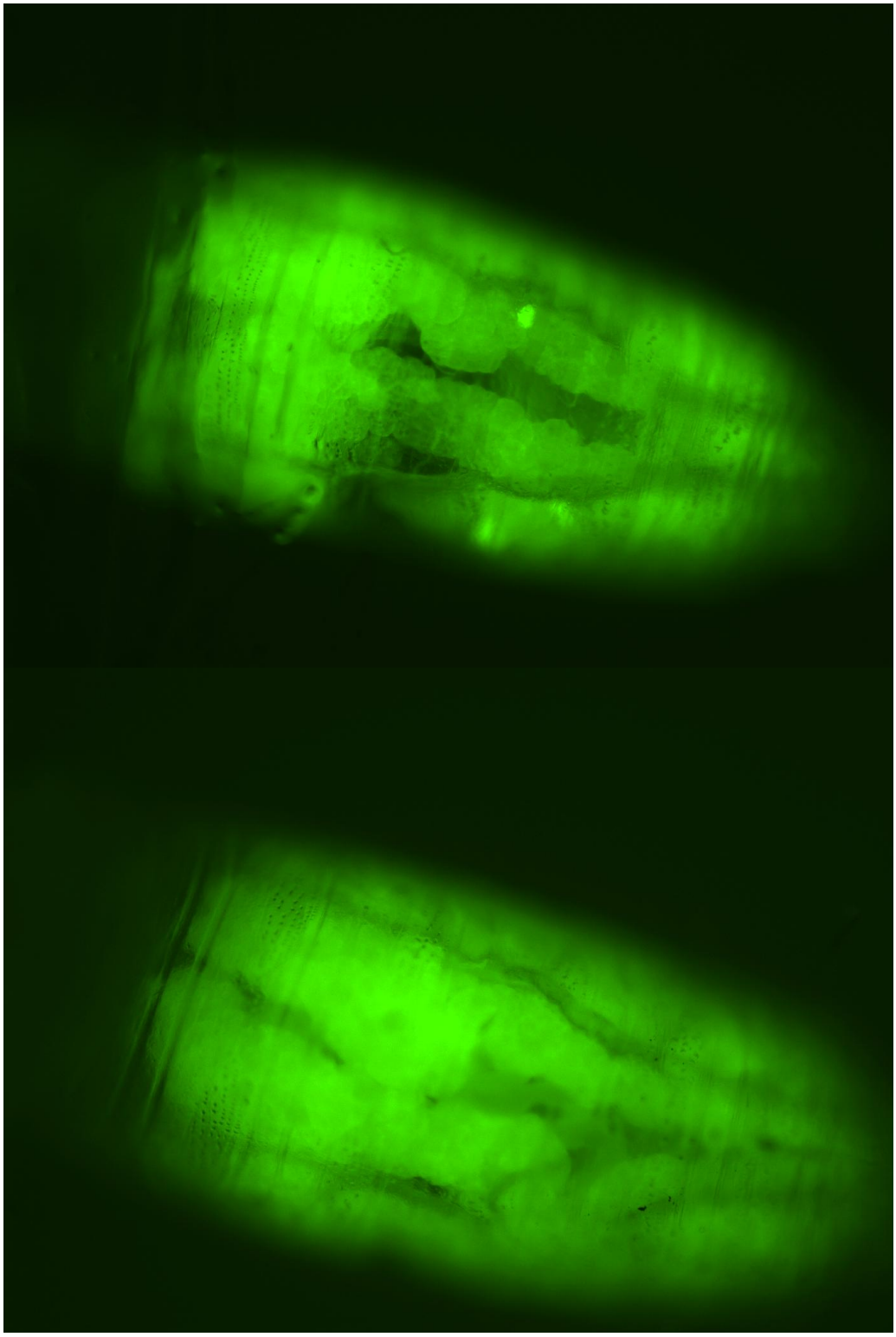

Figure 24. Fat body structure in *Lsp2-Gal4* animals at 6 hr APF.

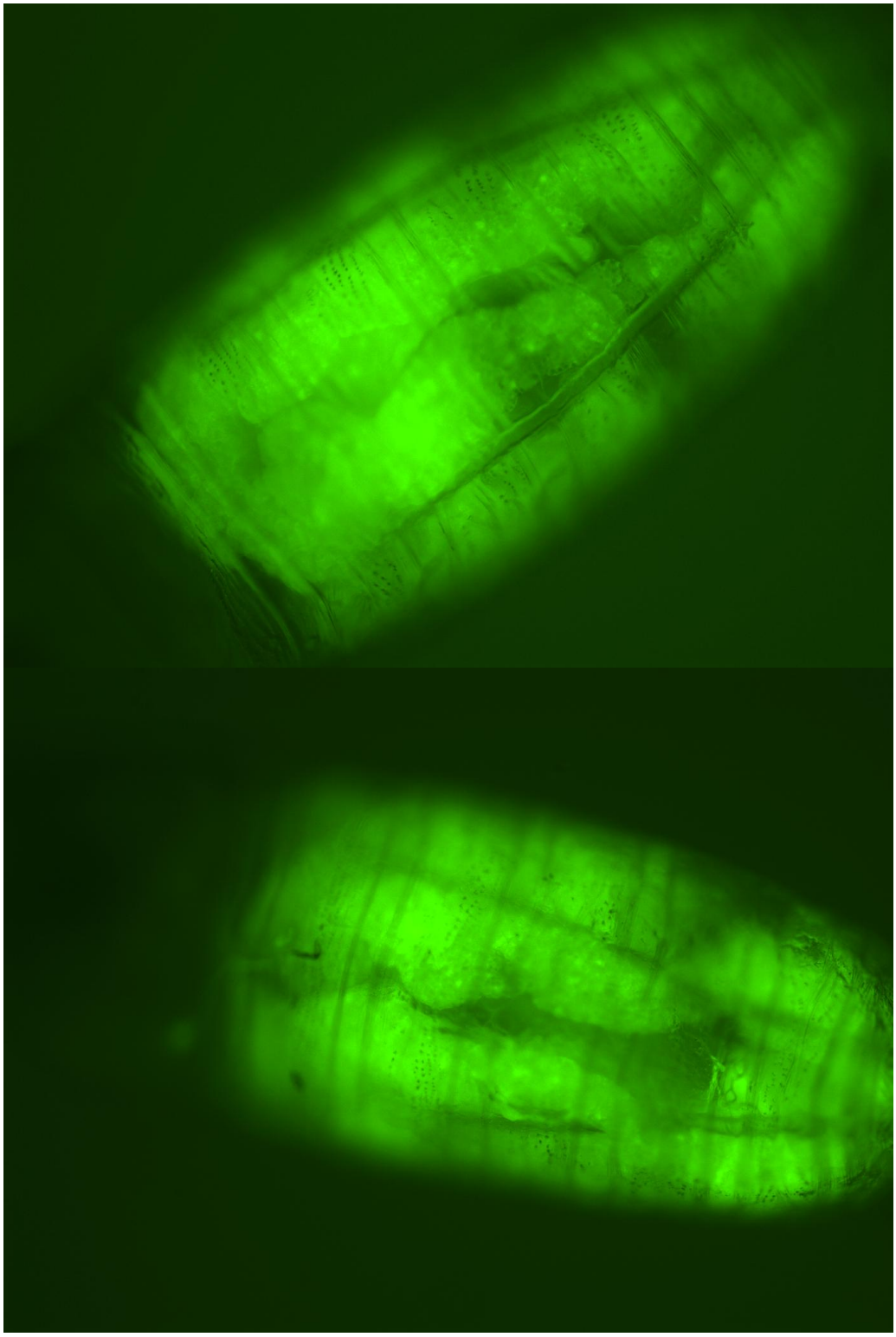

Figure 25. Fat body structure in *diap1 RNAi* animals at 6 hr APF.

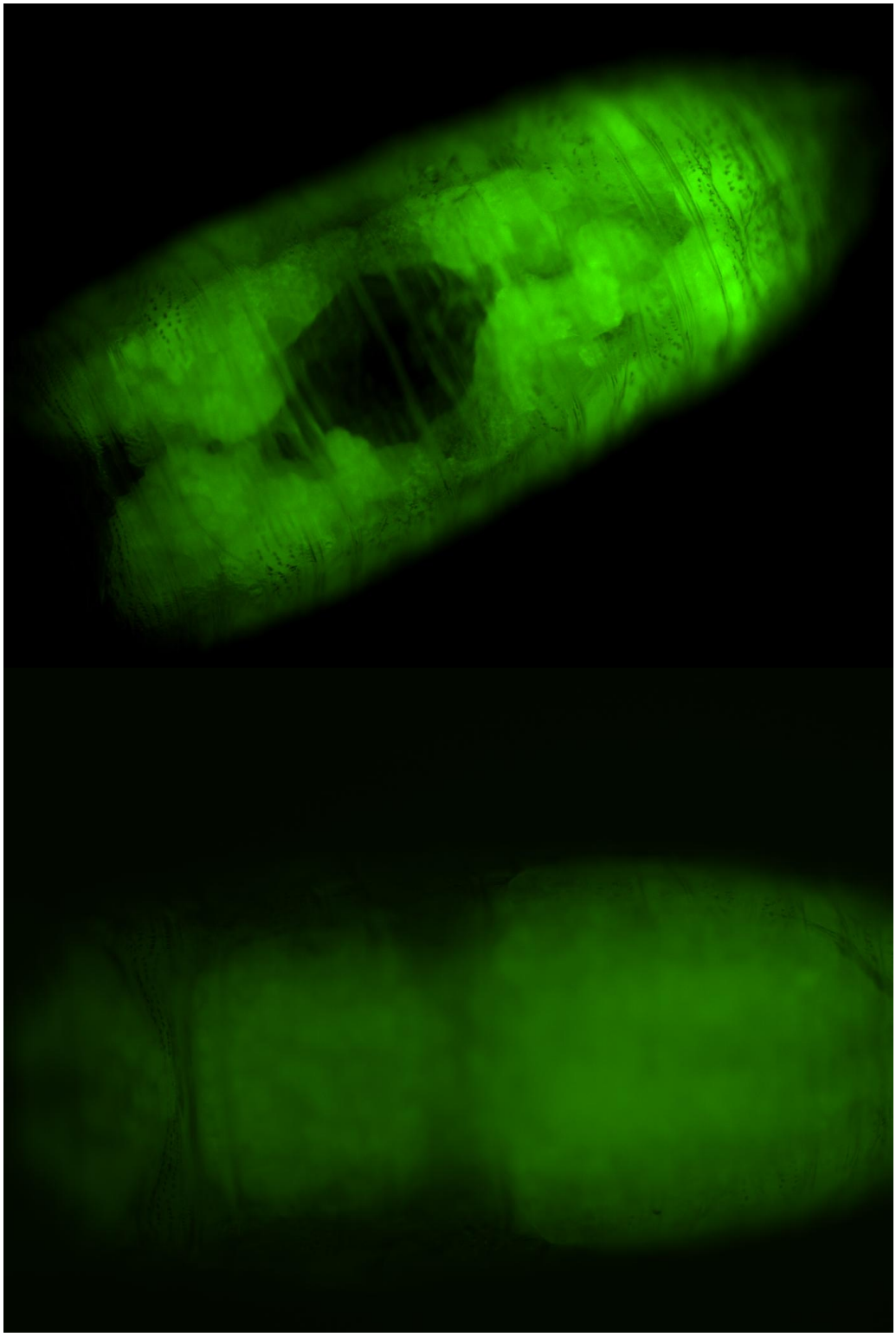

Figure 26. Fat body structure in *Lsp2-Gal4* animals at 12 hr APF.

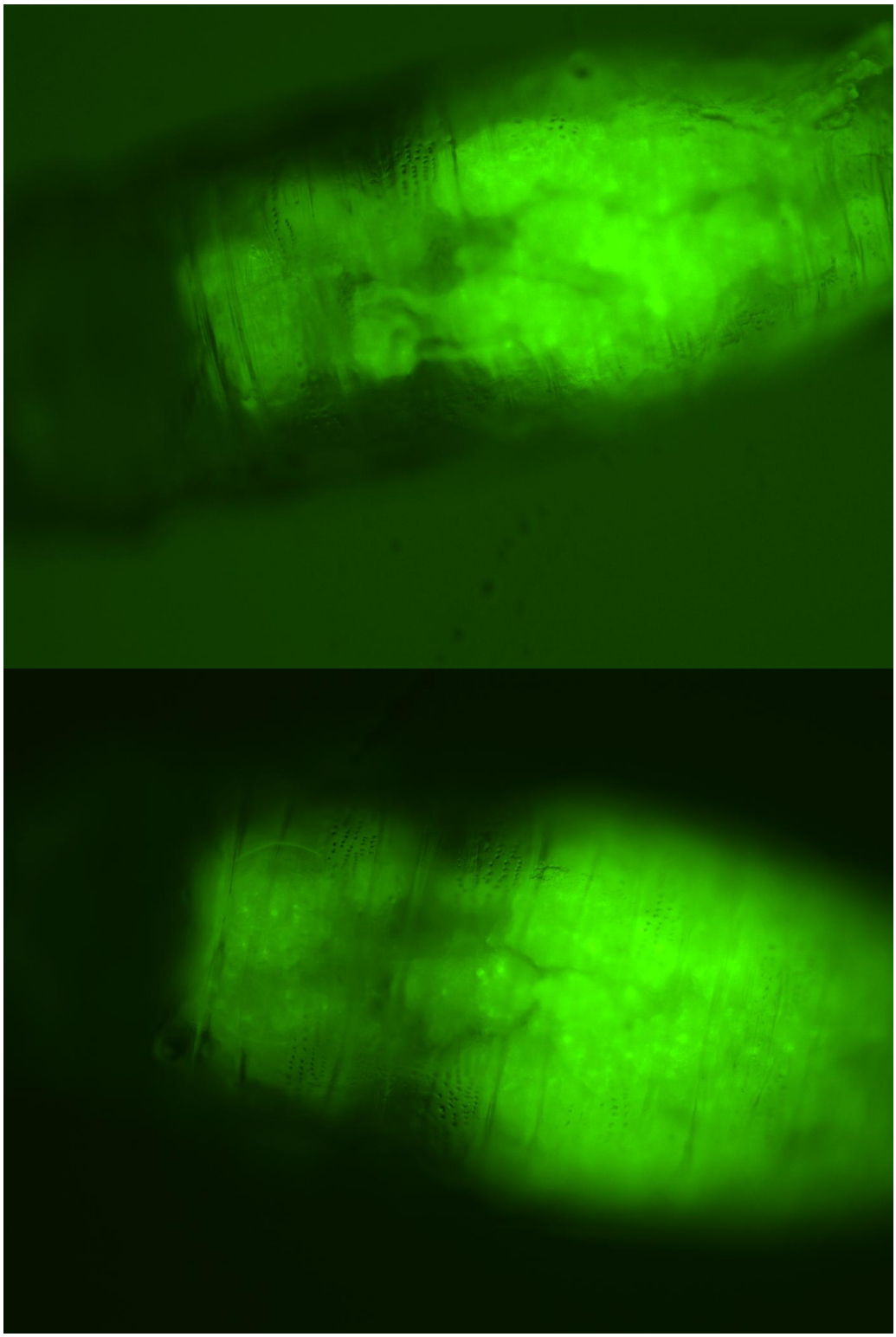

Figure 27. Fat body structure in *diap1 RNAi* animals at 12 hr APF.

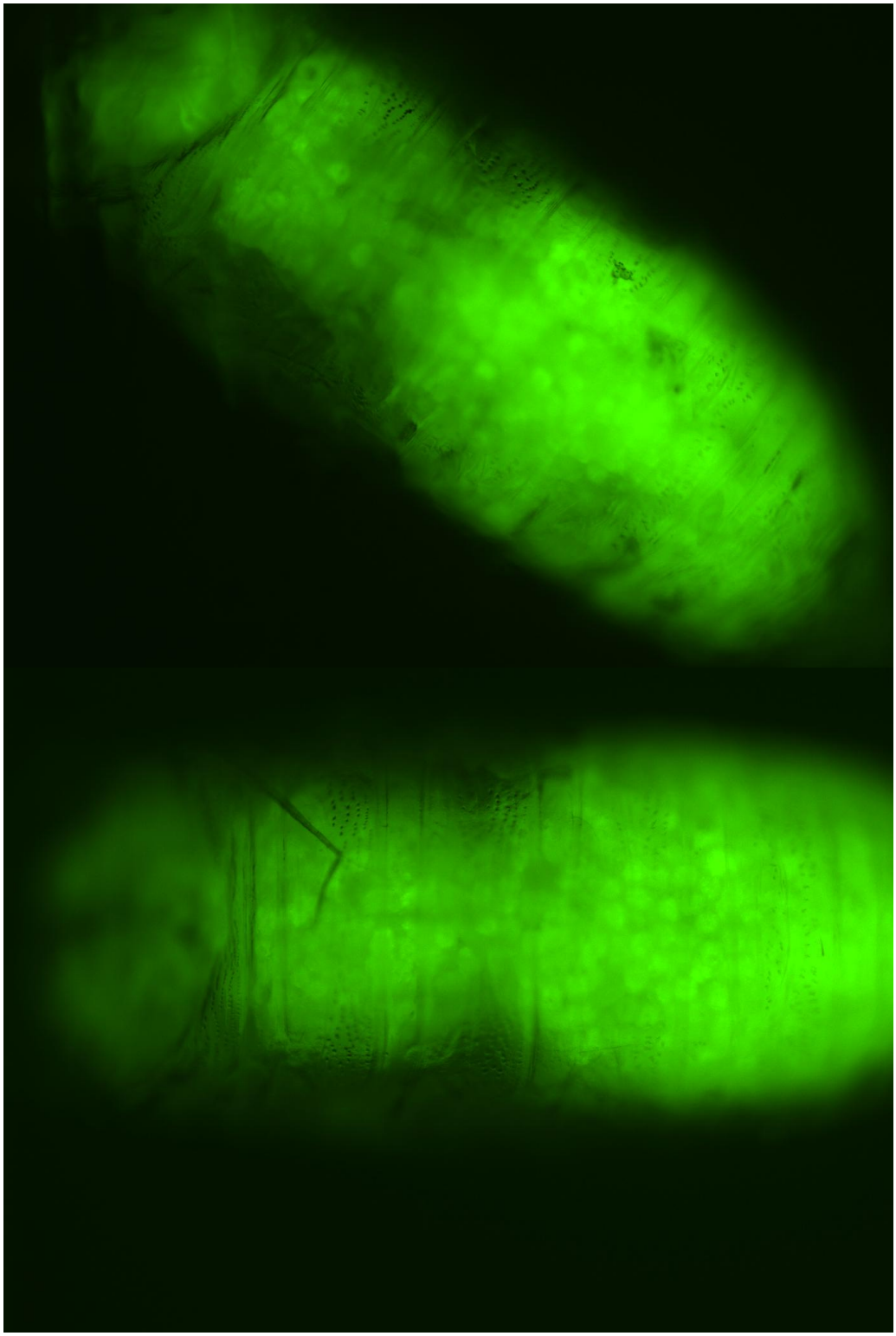

Figure 28. Fat body structure in *Lsp2-Gal4* animals at 14 hr APF.

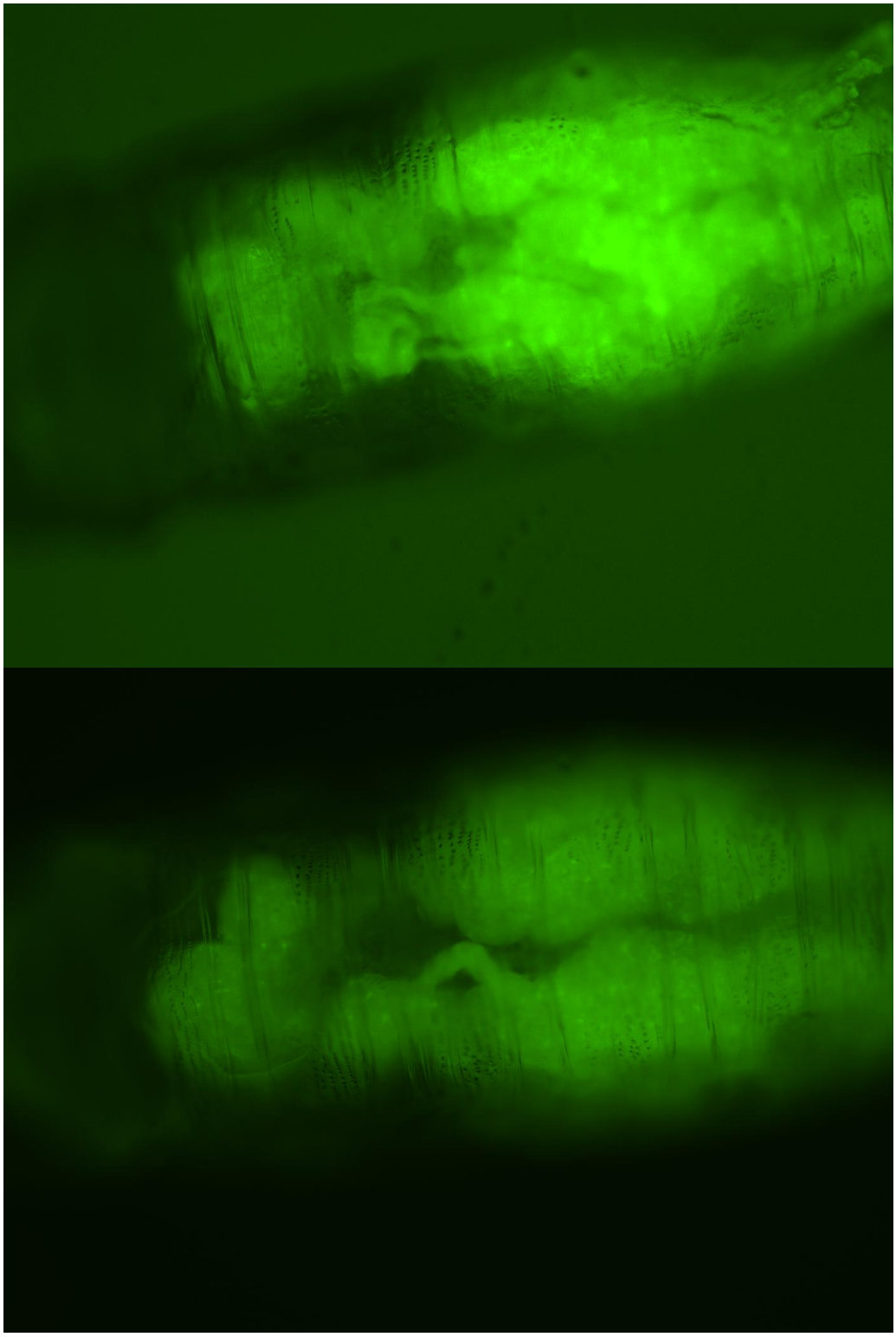

Figure 29. Fat body structure in *diap1 RNAi* animals at 14 hr APF.

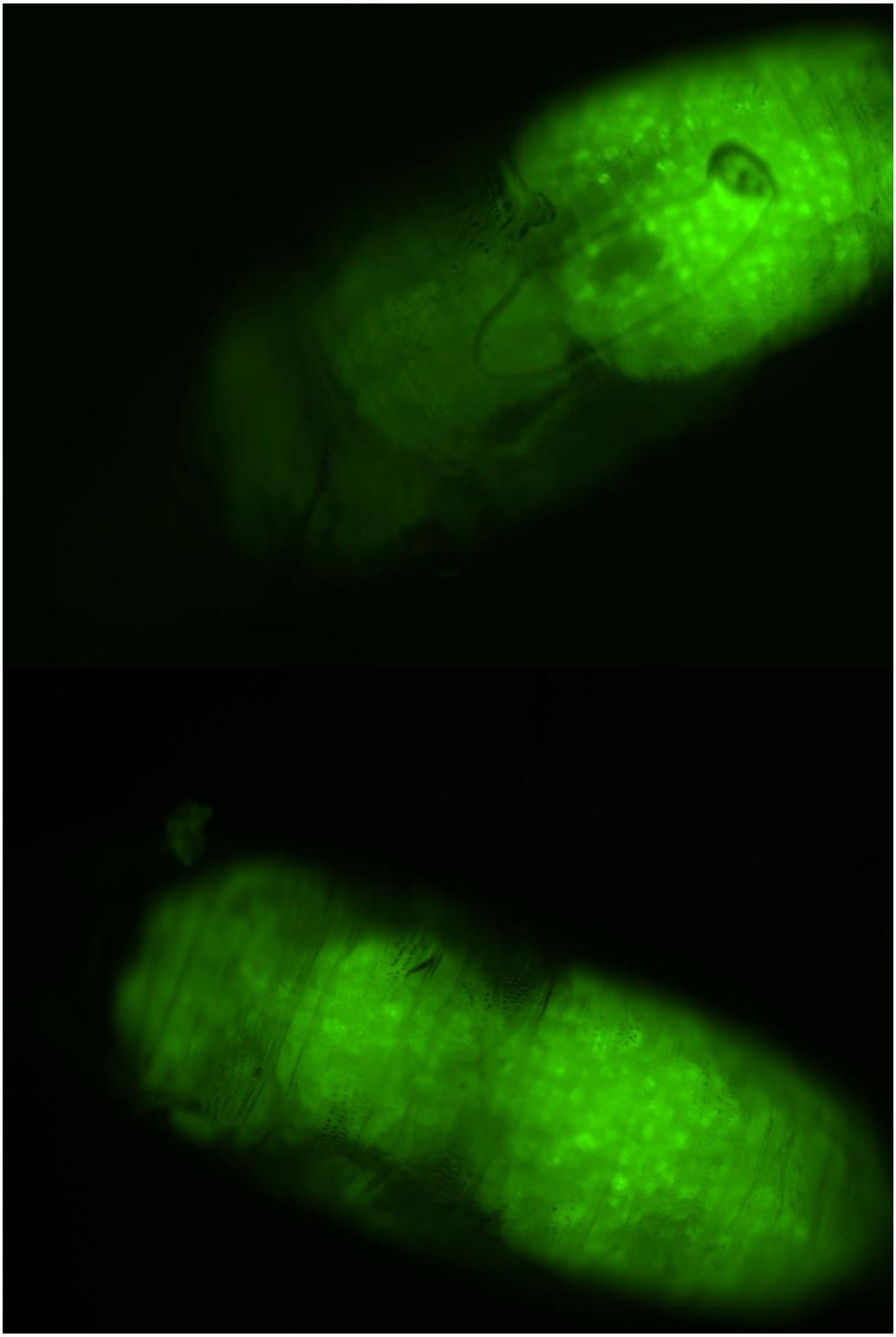

Figure 30. Fat body structure in *Lsp2-Gal4* animals at 20 hr APF.

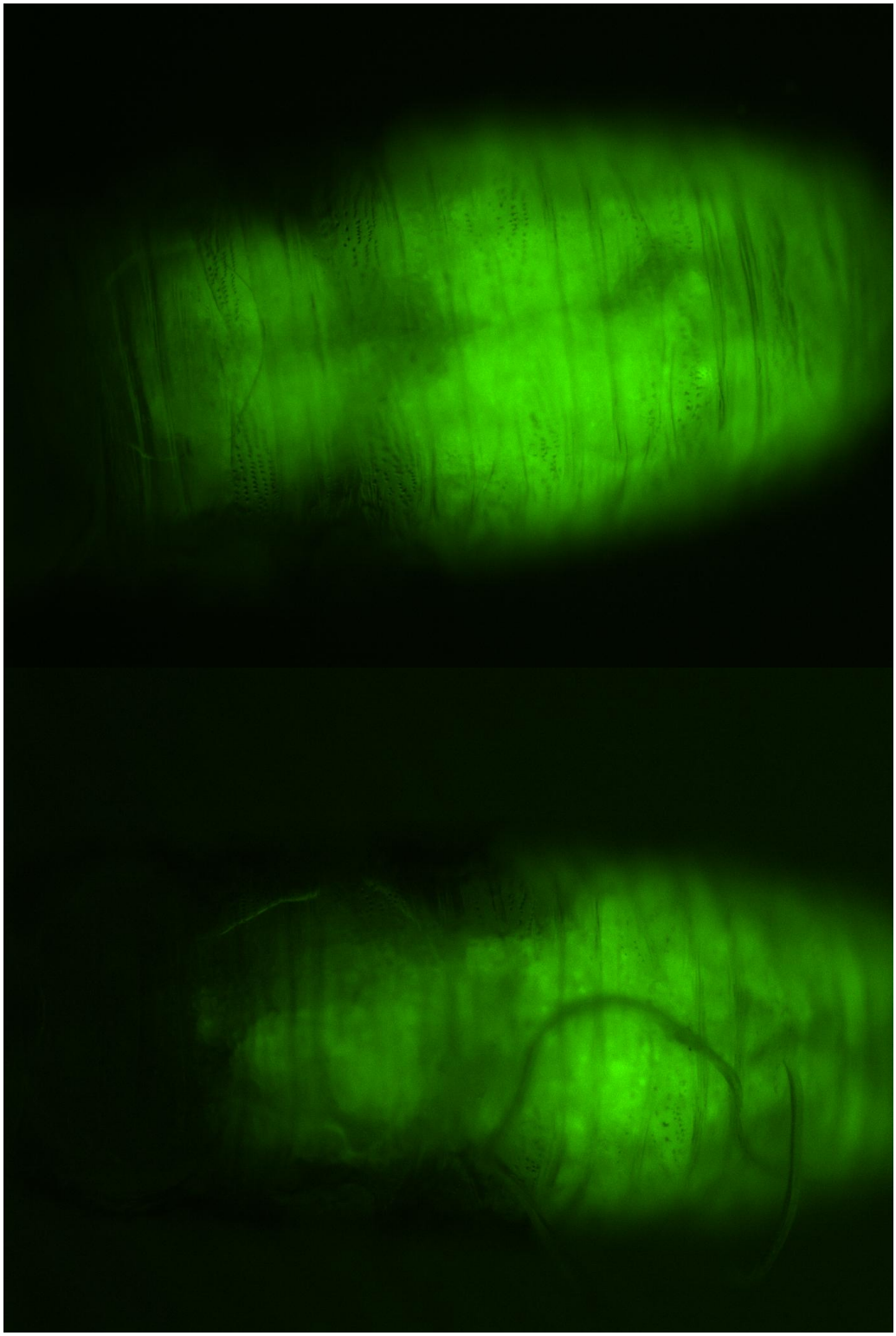

Figure 31. Fat body structure in *diap1 RNAi* animals at 20 hr APF.

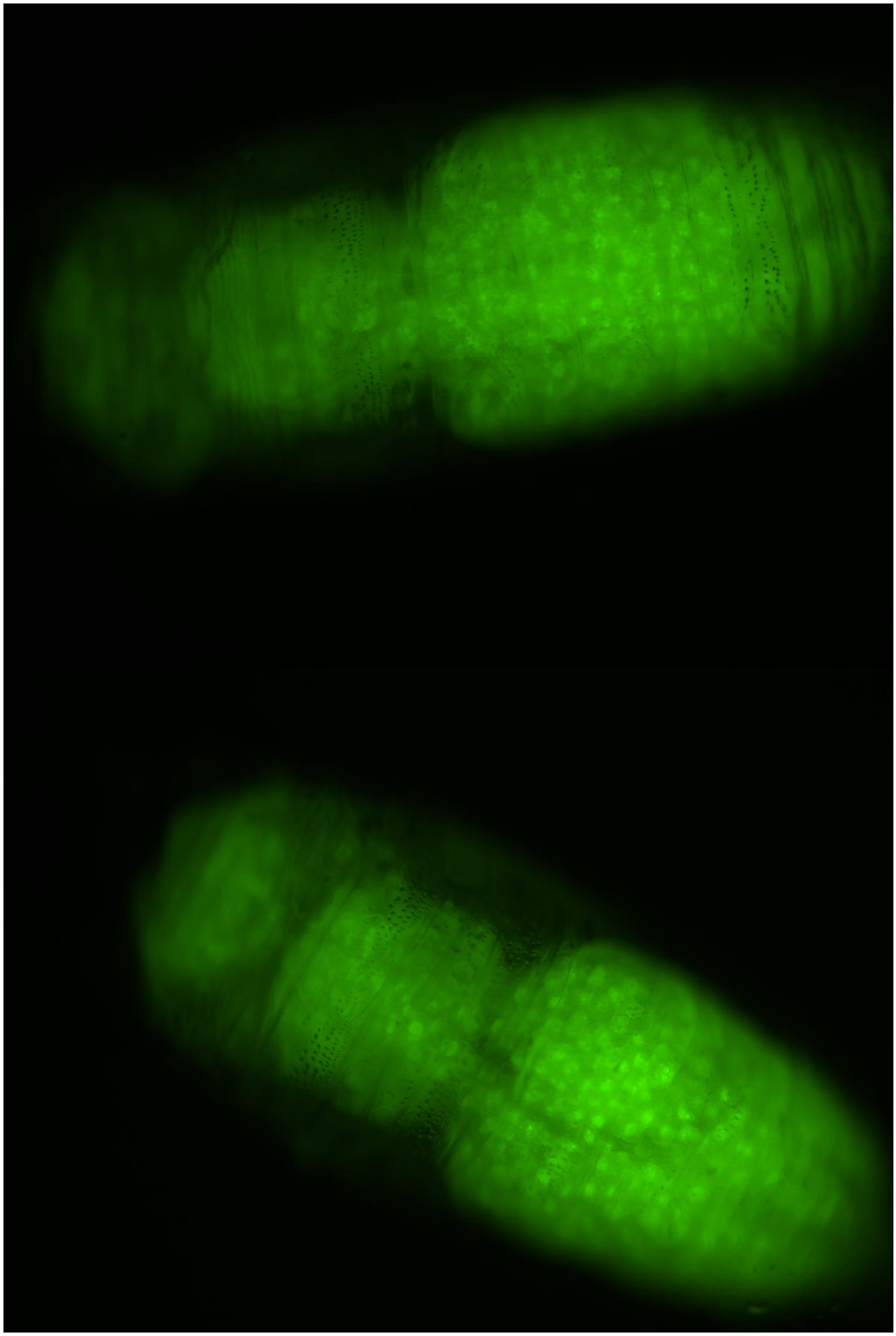

Figure 32. Fat body structure in *Lsp2-Gal4* animals at 24 hr APF.

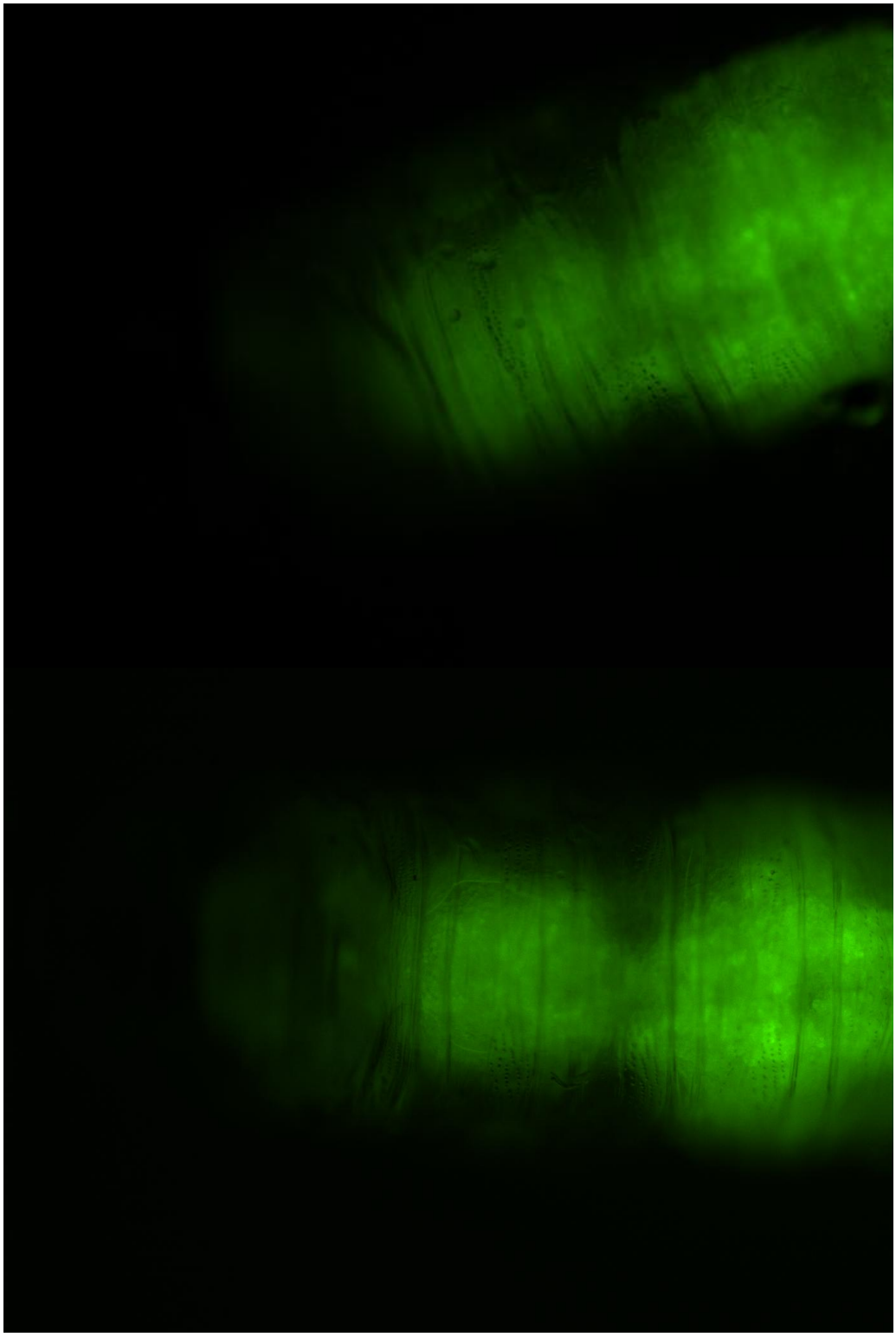

Figure 33. Fat body structure in *diap1 RNAi* animals at 24 hr APF.

Agarose Electrophoresis

The expression of *diap*1 in prepupal and early pupal development was qualitatively analyzed by gel electrophoresis. PCR was performed on RNA isolated from fat body, dissected at five time-points: L3, 0hr APF, 6 hr APF, 12 hr APF and 14 hr APF. Figure 35 illustrates that *diap1* is continuously expressed at each of these stages, as PCR amplicons of the expected size (147 bp) were detected at all time-points. There were no bands detected in the no RT control wells, demonstrating that non-specific amplification of genomic DNA was eliminated.

The removal of genomic DNA from PCR samples in this study was a persistent problem that was addressed in multiple ways. Elimination of contaminating DNA was crucial for qPCR experiments to quantify *diap1* expression. SYBR Green® binds to any double-stranded DNA in a PCR reaction and thus contaminated samples produce irreproducible results.

All cDNA syntheses were performed with nuclease free tips with fresh nuclease free water. New primer sets for both the target *diap1* and the endogenous control *actin 5C* were ordered. Additionally, only new SuperStrand® Reverse Transcriptase reagents were used. All lab equipment was cleaned with RNaseZap® Decontamination wipes from Ambion. Then, two rounds of DNAse treatment were performed instead of one. After these measures were taken, there still were residual bands in the no RT wells.

Genomic DNA elimination eventually succeeded when the preparatory work was moved to the Stranford lab in order to avoid cross-contamination from shared benches in the Woodard lab. The gel in Figure 35 was prepared with complete nuclease free equipment: pipeters, tubes, filter tips and reagents.

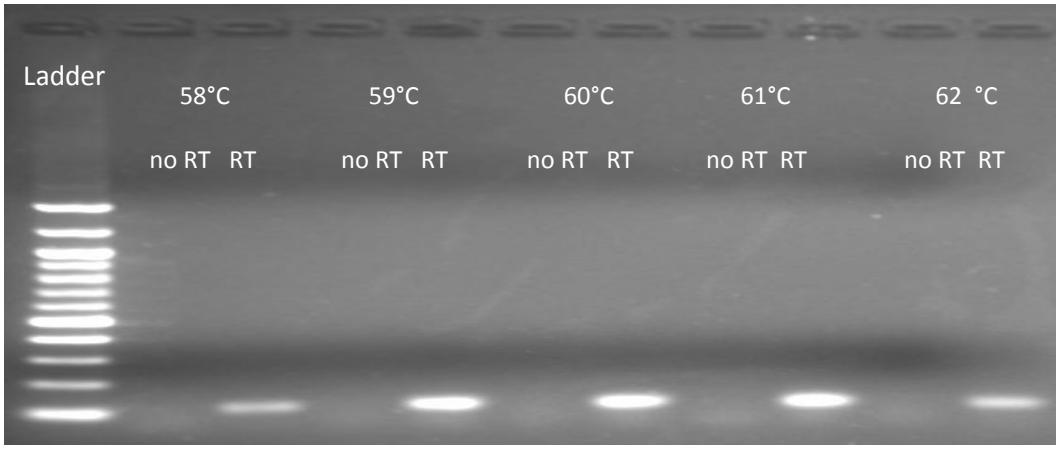

Figure 34. ***diap2*** **annealing temperature primer optimization.** Results suggesting that 59, 60 and 61°C were the optimal annealing temperatures for this primer set. Optimal efficiency is indicated by the band brightness in the RT wells. These values were in agreement with the IDT melting temperature of 60°C and it was selected for qPCR experiments.

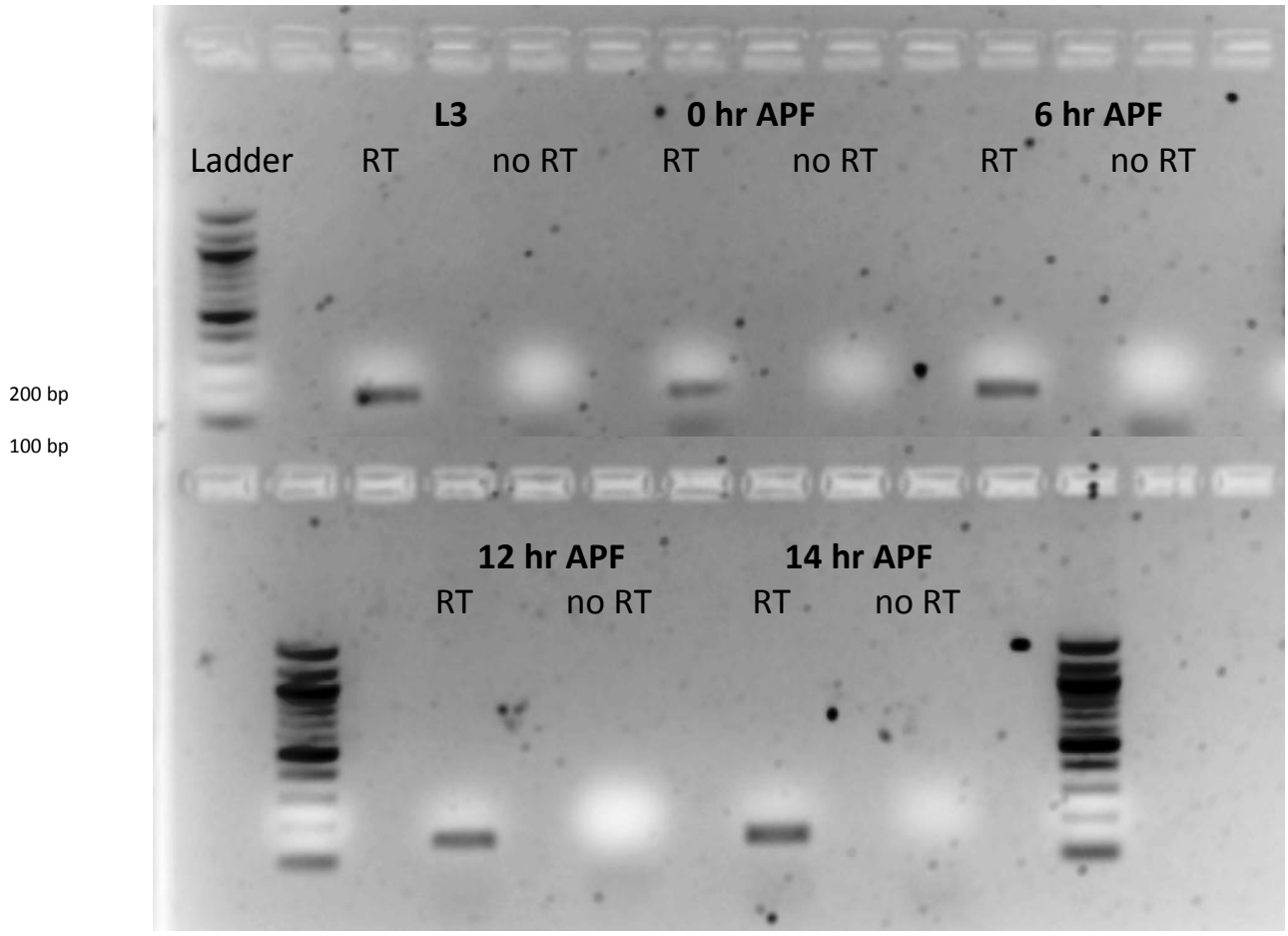

Figure 35. Confirmation of *diap1* expression in fat body isolated from wildtype (*Canton S*) flies. The animals were aged to the stages displayed on the gel, prior to RNA isolation. All PCR amplicons had the expected size of 147 bp. The absence of bands in the no RT wells confirms the elimination of genomic DNA. The faint bands that can be seen the *diap1* amplicons were attributed to primer dimer. The amount of primer dimer was later quantified via qPCR and deemed negligible.

Primer Optimization

At the onset of this study, a set of *diap2* primers was optimized for qPCR experiments with the intention of quantifying *diap2* expression in fat body during metamorphosis. The optimal concentrations of forward and reverse primers were determined to be both 500 nM, as qPCR reactions with these primers yielded the lowest C_t value of 14.

The optimal annealing temperature was determined by performing RT-PCR reactions on a temperature gradient of 58-62°C. The annealing temperature specified by IDT was 60°C. The amplification efficiency on the gradient was determined based on the brightness of PCR amplicons visualized on a gel (Figure 34). Since the brightest bands were detected at 59, 60 and 61°C, qPCR experiments were performed at 60°C annealing temperature. However, after identifying *diap2*'s secondary role in PCD regulation, no further quantification of *diap2* expression was performed. Additionally, due to the persistent contamination problem described above, the results of *diap2* qPCR experiments were not reproducible.

The following primer optimization experiments were performed at the IDT annealing temperatures for *diap1* and *actin 5C*. Following two rounds of DNase treatment, no amplification was detected in the no reverse transcriptase control wells. The optimal *diap1* primers were 100 nM forward

and 500 nM reverse (at C_t=23). The *actin 5C* primers were optimized at 500 nM forward and 300 nM reverse (at Ct=15). These concentrations were used to construct the standard curves below.

Amplification efficiency

To ensure that the selected primer sets amplified cDNA at a high efficiency, standard curves were constructed using 2-fold dilutions of fat body cDNA. C_t values were removed as outliers to construct a straight line for *diap1* and *actin 5C*. As seen from Figure 36, the standard curves obtained had slopes of -3.485 and -3.078 for *diap1* and *actin 5C*, respectively. These slopes indicate amplification efficiencies of 94 % and 111%. The elevated *actin 5C* value was assumed to be the product of minor pipetting error and was deemed acceptable for this experiment. In delta-delta analysis, a range of 90-110% is considered acceptable. Ideally, the amplification efficiency values of the target and the endogenous gene must be within 5% of each other. Using the Pfaffl method, standard curves are constructed for every qPCR experimental plate to normalize for inter-assay variation and to make an adequate comparison of gene expression levels.

a)

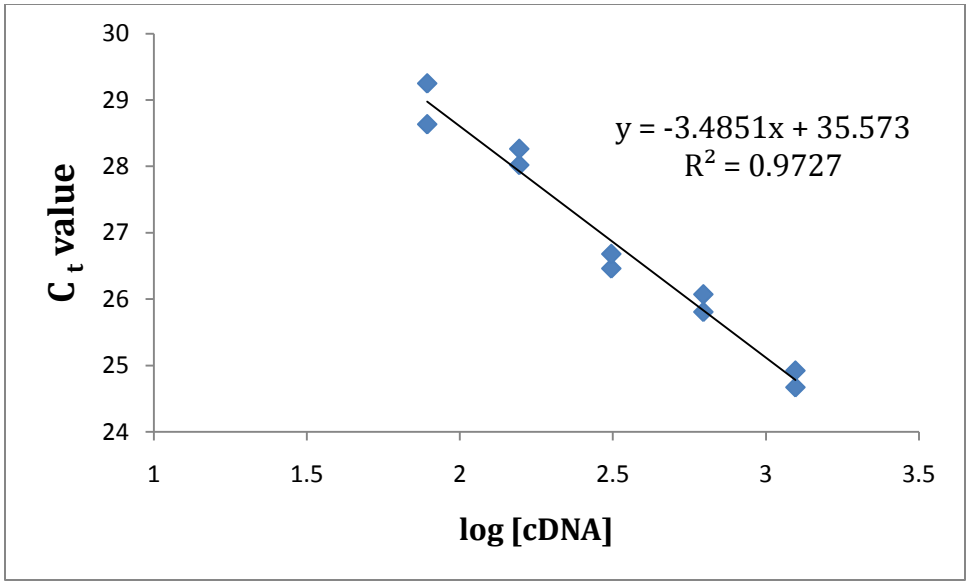

b)

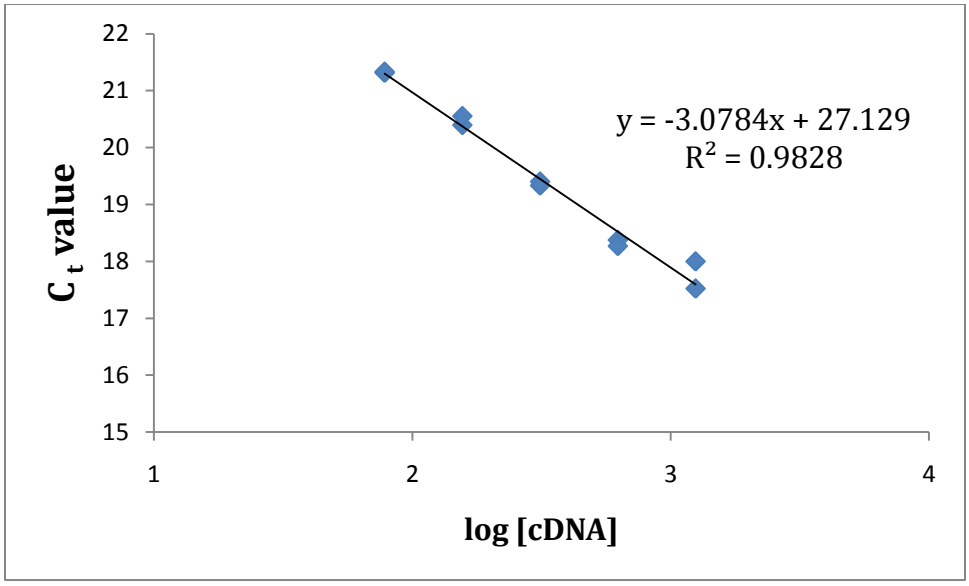

Figure 36. Standard curves confirming primer efficiency over a range of concentrations for a) *diap1* and b) *actin 5C*. A standard (normal) curve is generated by plotting C_t values vs. the log of [cDNA] dilutions. The slope of the curve indicates the primer efficiency, where -3.32 corresponds to 100% amplification. The normal curves were obtained using twofold dilutions of cDNA from whole wildtype 12 hr prepupae. The slopes of – 3.485 and -3.078 correspond to primer amplification efficiencies of 94% and 111%, respectively.

Experimental qPCR

The relative expression (RE) ratio of *diap1* under constant *actin 5C* reference gene expression was calculated by the Pfaffl RE formula, included in the Materials and Methods section. Figure 37 illustrates the results of evaluating the RE ratio at five time-points relative to puparium formation. The baseline in the graph below corresponds to an RE value of 1, which would indicate identical expression levels for the target and the reference gene. An RE ratio greater than 1 indicates upregulation of the target gene, and conversely, RE less than 1 means the target gene is downregulated.

Overall, *diap1* in the fat body was upregulated throughout prepupal and early pupal development. In third instar larvae, *diap1* was 7.4-fold upregulated with respect to *actin 5C*. At puparium formation*, Inhibitor of Apoptosis* was upregulated 3.3-fold. An increase in *diap1* expression resulted in 7.7-fold upregulation 6 hours APF. From 12 to 14 hours APF, during the destruction of the neighboring salivary glands, *diap*1 expression continuously increased. Thus, at 12 hr APF the target gene was upregulated 3.4-fold while at 14 hr APF it was 13.8-fold upregulated with respect to the reference.

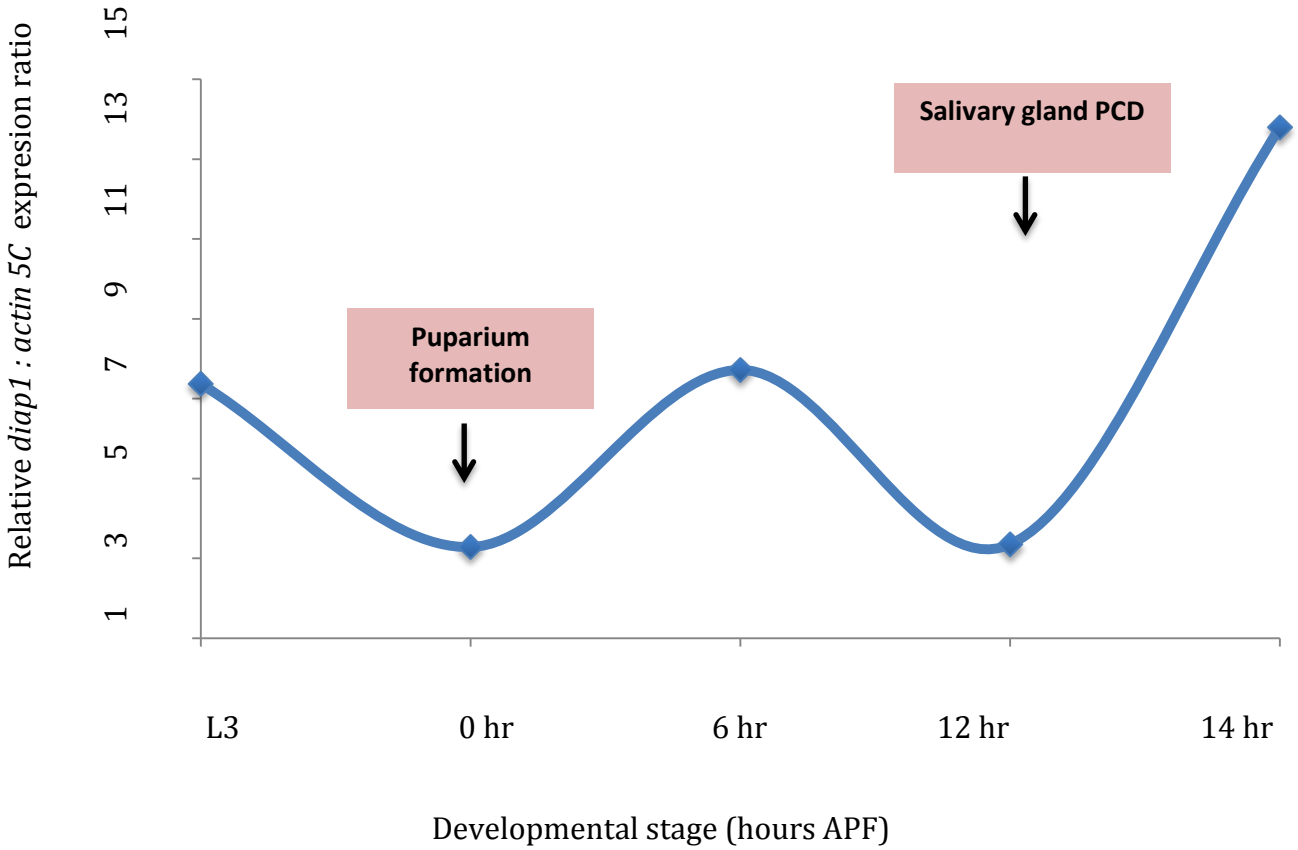

Figure 37. Relative expression ratio of *diap1* to *actin 5C* in wildtype prepupal and early pupal development of the fat body. The baseline in this figure corresponds to identical expression of target and reference gene (RE = 1). At each of the time-points shown, *diap1* was upregulated with respect to the *actin 5C* reference. The graph was constructed based on the amplification of wildtype fat body cDNA. The Real Time qPCR upregulation ratio was calculated to be: 7.4 –fold at L3; 3.3-fold at 0 hr APF; 7.7-fold at 6 hr APF; 3.4-fold at 12 hr APF and 13.8-fold at 14 hr APF.

DISCUSSION

Fat Body Remodeling in Tissue-Specific *diap1* Loss-of-Function Mutants

The fluorescence microscopy component of my project sought to identify the role of *diap1* expression in fat body remodeling by tissue-selective knock down. Based on previous studies by Wang et al. (1999) and Yin and Thummel (2004), we predicted that *diap1* is indispensable for fat body survival. Thus, we expected to observe PCD rather than remodeling in the loss-of-function mutants. Our results, however, led us to the following conclusions:

1. Tissue-specific *diap1* gene knockout in fat body did not induce (microscopically resolved) tissue cell death during prepupal and early pupal development. If RNA interference was successful, *diap1* expression is dispensable for fat body survival at this stage.

RNAi, or post-transcriptional gene silencing via direct introduction of ds RNA, is a technique with variable potency. The apparent absence of programmed cell death in *diap1 RNAi* prepupae may have been the result of a failure in the RNAi system. For RNAi initiation to occur, input *diap1* dsRNA must be digested into 21-23 nucleotide small interfering RNAs (siRNAs) by the enzyme Dicer (Viney and Thompson, 2008). It is possible that the input *diap1* dsRNA has failed to trigger Dicer. If the dsRNA did

not cleave, a *diap1* homolog may have been introduced to suppress PCD. Another component of the RNAi system, which could fail is the sequence specificity of the siRNAs (Ambion®, 2002). The effectiveness of siRNAs varies: the most potent siRNAs result in >90% reduction in target RNA and protein levels. The siRNAs, produced in this experiment, may not be as effective, due to single base pair mismatches between the siRNA and the *diap1* target mRNA. Single base pair mismatches can dramatically reduce *diap1* silencing (Ambion®, 2002).

If RNA interference was successful, *diap1* expression appears non-essential for fat body cell survival. Several antiapoptotic genes, candidates for compensating for *diap1* activity, are proposed in the discussion of wildtype *diap1* expression. Examples include *diap2* and *dBRUCE*. Here, an alternative explanation of our observations should be considered.

Aguila et al. (2007) propose that histolysis of larval tissues, including the fat body, occurs by two PCD modes: apoptotic and autophagic. *Inhibitor of Apoptosis 1* has been implicated in the final apoptotic destruction of the larval fat body in the young adult. Therefore, *diap1* post-transcriptional silencing may accelerate apoptosis at this stage. However, several molecular pathways can suppress fat body autophagy, resulting in the delay in remodeling we observed. Two such pathways are

the class I phosphoinositide (PI) 3-kinase (PI3K) and Target of Rapamycin (Tor). Rusten et al. (2004) suggest that ecdysone-induced autophagy can be suppressed by Tor and its upstream regulator PI3K. During the non-feeding stage, Tor suppresses autophagy, resulting in reduced developmental rate and survival. The delay in fat body remodeling and the developmental arrest we observed may be attributed to upregulation of the Tor pathway.

2. *diap1* appears essential for normal timing of fat body remodeling.

The RNAi reduction of *diap1* function in larval salivary glands and midguts results in premature destruction of these tissues (Yin and Thummel, 2004). As seen from my fluorescence images, *diap*1 RNAi appears to perturb the normal timing of fat body remodeling as well. There are several mechanisms, by which *diap*1 may be involved in temporal regulation of fat body reorganization.

Firstly, *diap1* may interact with *Fork head*, which has been implicated as a control of *hid* and *rpr* time-specific activation in salivary glands (Thummel, 2007). In salivary glands, *Fork head* has a similar role to *diap1*, as it blocks the death response, maintaining normal salivary gland function. At the onset of metamorphosis, however, *fkh* down-regulation provides competence for salivary gland cell death, allowing the death cascade to be triggered by the subsequent prepupal pulse of ecdysone (Cao et al., 2007). Since fat body

remodeling is also directed by ecdysone and mediated by *rpr* and *hid* (Aguila et al., 2007), it is possible that *fkh* interacts with *diap1* to orchestrate timely reorganization of this tissue.

Secondly, the timing of fat body remodeling may be regulated by *E93*, which can induce PCD by both apoptosis and autophagy (Lee and Baehrecke, 2001). *E93* has been shown to interact with the H99 genetic interval, which contains the *rpr, hid* and *grim* proapoptotic genes. *E93* activates the cell death genes to induce time-specific salivary gland autophagy at 14 hr APF. E93 suppresses baculovirus caspase inhibitors such as *p35* and *diap2* with varying efficiency (Lee and Baehrecke, 2001). If the normal fat body remodeling occurs by autophagy (Rusten et al., 2004) and *diap1* expression has been reduced by RNAi, it is possible that *E93* interaction with the aforementioned proapoptotic and antiapoptotic genes influences the temporal regulation of the remodeling.

3. Wildtype *diap1* expression is required for late pupal viability.

The premature death of late (36 hr APF) *diap RNAi* pupae occurred by overall necrosis, as these animals exhibited black necrotic patches all over their cuticles. The effect was observed in ~50% of the transgenic progeny, while control *Lsp2-Gal4* animals displayed no signs of premature cell death. A similar *diap1* RNAi experiment performed by Yin and Thummel (2004) used heat-shock induced *diap1* dsRNA expression, which also resulted in partial or

gross necrosis. The necrotic effect of *diap1* knock out reported by these authors, was more pronounced (76% of the transgenic animals), but the heat shock-initiated RNA interference was not tissue-specific. Thus, the overall endogenous *diap1* mRNA levels were significantly reduced in comparison to our study. Yet, we obtained similar results. Yin and Thummel report that although the remaining animals formed morphologically normal prepupae, they all underwent massive death before head eversion, leaving only an empty pupal case. In this project, the pupae that failed to eclose had everted their heads and also appeared morphologically normal. Assuming that only the fat body had died by autophagy raises the question why we observed whole-body necrosis. I propose that the *diap1 RNAi* animals died of starvation. During the non-feeding pupal stage, the fat body is a source of polypeptides for the re-architecture of the animal into its adult form (Haunerland, 1996). The possible premature death of the fat body may have deprived the transgenic progeny from the energy resource needed to complete metamorphosis.

qPCR Optimization Methodology

Previous research in the Woodard lab used the delta-delta C_t method for quantification of relative gene expression. In contrast, my project employed a new approach, the Pfaffl normalization method (Pfaffl, 2001). To

assess the accuracy and reproducibility of my results, my methodology choice must be clarified.

Before primer optimization, I analyzed *diap1* and *diap2* expression in wildtype fat body by agarose electrophoresis. This is not a precise method of determining optimal expression efficiency, but an estimation can be made based on the bands' brightness. I addressed two issues via electrophoresis: 1) size-specific amplification of the *diap* target sequences and 2) removal of genomic DNA. Figure 34 illustrates that all *diap1* products have the predicted size of 147 bp. Genomic DNA was successfully removed to avoid interference with the target and reference transcript in qPCR. Performing two rounds of DNase treatment with nuclease-free reagents and supplies was the key step in successful RNA purification for *diap1* PCR.

While the *diap2* primer set was temperature- and concentration-optimized, it was not used in qCPR experiments. The persistent genomic DNA contamination prevented construction of an accurate standard curve for this gene. The results in Figure 33 suggested that the optimal annealing temperatures were in the 59-61°C range. The temperature reported by IDT, 60°C, was selected to avoid non-specific primer annealing and extension by DNA polymerase. The primer concentrations I optimized at 60°C can be used in the future provided that genomic DNA is removed as described above.

The *diap1* and *actin 5C* primer concentrations were optimized at IDT melting temperatures. The same *actin 5C* primer set had been previously optimized at 58°C (Gorski, 2010). However, the reported concentrations (300 nM forward and 100 nM reverse) did not produce acceptable standard curves at the *diap1* annealing temperature (55.4°C). Amplification efficiency was significantly lowered to 60-70% (data not shown). After optimization at 55.4°C, I selected 500 nM forward and 300 nM reverse *actin 5C* concentrations to construct the standard curve in Figure 35. These values produced improved amplification efficiency (111 %). To prevent pipetting errors, twofold cDNA dilutions were used rather than tenfold dilutions as in previous work (Gorski, 2010; Ayerh, 2008).

The temporal *diap1* expression profile in Figure 36 was created based on a single qPCR experiment. The assay was not replicated because of a malfunction in the Applied Biosciences 7300 Real Time PCR System. I constructed the *diap1* profile under the assumption that the difference in target and reference gene efficiencies (94% and 111%), was normalized by Pfaffl standardization (Pfaffl, 2001). I eliminated variations in RNA integrity and input concentrations by purification and optimization. The Pfaffl equation was expected to compensate for additional background interferences, such as enzyme inhibitors and cDNA synthesis efficiency.

Regulation of *diap1* Expression in Wildtype Fat Body

The preliminary qPCR results support my hypothesis that *Inhibitor of Apoptosis* is upregulated to prevent fat body programmed cell death at the time of larval salivary gland histolysis. At this time, a model for *diap1* regulation during fat body remodeling cannot be proposed, since the qPCR experiment must be repeated in wildtype animals to validate my findings. The two maxima in *diap1* expression, at 6 hr APF (7.7-fold) and at 14 hr APF (13.8-fold), precisely follow the two peaks in ecdysone titer during metamorphosis. A comparison between Figure 12 and Figure 36 reveals a striking contrast in *diap1* regulation of the salivary gland and the fat body. While salivary gland *diap1* is downregulated to establish PCD competence, I observed a 4.4-fold increase in *diap1* expression. As *diap1* is completely shut down in salivary glands to initiate caspase activation, its expression is further elevated in the fat body to block caspases.

To analyze quantitatively the tissue-specific *diap1* regulation with my experimental design, an identical Pfaffl assay on salivary gland cDNA is necessary. A relative expression ratio of *diap1* to *actin 5C* should be generated for wildtype salivary glands at the time-points listed above. The resulting temporal profiles must be constructed after multiple trials, in order to test the reliability of the Pfaffl model.

Additionally, it is important to determine the specific role of *diap1* suppression of fat body PCD, among other antiapoptotic genes. As noted by

Yin and Thummel (2004), *diap2* expression in salivary glands parallels that of *diap1* during late larval and prepupal development. Although in this tissue RNAi knockout of *diap2* had no effect on PCD regulation, no *diap2* RNAi studies have been done on fat body. DIAP2 directly regulates drICE and contributes to the overall caspase activity threshold in living cells (Orme and Meier, 2009). A Pfaffl assay quantifying *diap2* expression in wildtype fat cells will help determine if *diap1* is indeed the major antiapoptotic gene responsible for the unique developmental fate of the fat body.

Besides DIAP1 and DIAP2, the *Drosophila* genome encodes other BIR-containing proteins, such as Deterin and dBRUCE (*Drosophila* BIR repeat containing ubiquitin-conjugating enzyme) (Orme and Meier, 2009). Deterin and dBRUCE have only one BIR domain and lack a RING domain. Although dBRUCE does not bind caspases, it blocks ectopic cell death (Vernooy et al., 2002). Consistent with the notion that it functions as modulator of cell death, mutation of endogenous dBRUCE enhances cell death induced by expression of pro-apoptotic proteins. Finally, Deterin, which is related to the mammalian Survivin, inhibits apoptosis when overexpressed (Jones et al., 2000) . Therefore, endogenous Deterin may be involved in PCD regulation in a physiological setting. It would be interesting to investigate these two genes for a potential role in programmed cell death and tissue remodeling during metamorphosis.

CONCLUSION AND FUTURE DIRECTIONS

The aim of this project was to examine the role and regulation of *Inhibitor of Apoptosis 1* (*diap1*) in the development of *Drosophila melanogaster* larval fat body. We became interested in this tissue, as it has critical importance for the full body plan reorganization of the fruit fly during metamorphosis. The fat body serves as an energy resource that fuels the transition of the fly from a stationary, non-feeding larva into to a fully developed adult. Research by Agulia et al. (2007) had indicated that unlike other larval tissues, such as the salivary gland and midgut, the larval fat body persists in the young adult. The larval fat cells are an efficient nutrient source, which protects the animal from starvation during its initial inactive state. The resistance of the fat body to destruction by histolysis has been shown to be *diap1*-dependent (Aguila et al., 2007). My thesis employed Quantitative Real Time PCR and fluorescence microscopy to detect the *diap1* effects on remodeling on the molecular and morphological level. My preliminary qPCR experiments supported our hypothesis that *diap1* is upregulated in the wildtype fat tissue while the larval salivary gland is destroyed by autophagy. At 14 hours after puparium formation, *diap1* was upregulated 13.8-fold relative to the housekeeping gene *actin 5C*. My microscopy work on tissue-specific *diap1* loss-of-function mutants revealed

that *diap1* is not critical for the survival of prepupal fat body, but essential for the accurate timing of the remodeling process. My research used a qPCR analysis approach, novel to our lab, referred to as the Pfaffl standardization method (Pfaffl, 2001).

In future research, I wish to perform more qPCR experiments on *diap1*, to be able to construct a valid model for this gene's regulation during metamorphosis. Furthermore, I would like to statistically evaluate the significance of fold change observed in *diap1* expression using Student T-tests. Last, but not least, I plan to investigate the success of *diap1* RNA interference in the fat body by a qPCR assay of *diap*1 expression in the loss-of-function mutant animals. The fold change will be calculated using the Pfaffl normalization method and related to wildtype *diap1* regulation.

APPENDIX

List of abbreviations used

ADGFs = adenosine-deaminease-related growth factors

AF = activation function domain

APF = after puparium formation

BIR = Baculovirus IAP Repeat domain

bp = base pair

CARD = caspase recruitment domain

CBP = CREB binding protein

DBD = DNA binding domain

DED = death effector domain

E2 = ubiquitin-conjugating enzyme

EcR = Ecdysone receptor

FXR = farsenoid X receptor

GFP = green fluorescent protein

JH = juvenile hormone

IDGFs = imaginal disc growth factors

L3 = third-instar larva

LBD = ligand-binding and dimerization domain

NTC = no template control

RING = Really Interesting New Gene domain

RNAi = RNA interference

RT = reverse transcriptase

RXR =retinoid X receptor

PCD = programmed cell death

PCR = polymerase chain reaction

PI3K = class I phosphoinositide 3-kinase

PTTH = prothoracicotropic hormone

qPCR = quantitative Real Time Polymerase Chain Reaction

RE = relative expression ratio

TAE = tris-acetate EDTA

TOR = Target of Rapamycin

UBR = ubiquitin recruitment

USP = Ultraspiracle

Table 6. Sample 96-well plate layout for primer concentration optimization.
Ratios are final concentrations of forward primer to reverse primer (in nM) in each 25 μL reaction.

	1	2	3	4	5	6	7	8	9	10	11	12
A	500 : 500				500 : 300				500 : 100			
B			300 : 500				300 : 300				300 : 100	
C	100 : 500				100 : 300				100 : 100			
D			500 : 500 No RT				500 : 300 No RT				500 : 100 No RT	
E	300 : 500 No RT				300 : 300 No RT				300 : 100 No RT			
F			100 : 500 No RT				100 : 300 No RT				100 : 100 No RT	
G	500 : 500 NTC		500 : 300 NTC		500 : 100 NTC		300 : 500 NTC		300 : 300 NTC		300 : 100 NTC	
H	100 : 500 NTC				100 : 300 NTC				100 : 100 NTC			

Table 7. Sample 96-well plate layout for a qPCR gene expression experiment. Standard curves were constructed using five twofold dilutions of whole 12 h APF animals (A and D). The expression of target (*diap1*) and reference (*actin 5C*) was measured using fat body cDNA samples from the following stages: L3, 0 hr APF, 6 hr APF, 12 hr APF and 14 hr APF.

	1	2	3	4	5	6	7	8	9	10	11	12
A	2^0 cDNA, *actin 5C*		2^{-1} cDNA, *actin 5C*		2^{-2} cDNA, *actin 5C*		2^{-3} cDNA, *actin 5C*		2^{-4} cDNA, *actin 5C*		NTC, *actin 5C*	
B	L3, *actin 5C*				0 hr APF, *actin 5C*				6 hr APF, *actin 5C*			
C			12 hr APF, *actin 5C*				14 hr APF, *actin 5C*					
D	2^0 cDNA, *diap1*		2^{-1} cDNA, *diap1*		2^{-2} cDNA, *diap1*		2^{-3} cDNA, *diap1*		2^{-4}cDNA, *diap1*		NTC, *diap1*	
E	L3, *diap1*				0 hr APF, *diap1*				6 hr APF, *diap1*			
F			12 hr APF, *diap1*				14 hr APF, *diap1*					
G	2^0 cDNA, *actin 5C*, No RT		L3, *actin 5C*, No RT		0 hr APF, *actin 5C,* No RT		6 hr APF, *actin 5C,* No RT		12 hr APF, *actin 5C,* No RT		14 hr APF, *actin 5C,* No RT	
H	2^0 cDNA, *diap1,* No RT		L3, *diap1,* No RT		0 hr APF, *diap1,* No RT		6 hr APF, *diap1,* No RT		12 hr APF, *diap1,* No RT		14 hr APF, *diap1,* No RT	

LITERATURE CITED

Aguila, J.R., Suszko, J., Gibbs, A.G. and D.K. Hoshizaki. 2007. The role of larval fat cells in adult *Drosophila melanogaster*. *Journal of Experimental Biology* **210**:956-963.

Ambion (Applied Biosystems). 2002. RNA Interference and Gene Silencing: History and Overview [online]. http://www.biocompare.com/Articles/ApplicationNote/1074/RNA-Interference-And-Gene-Silencing-History-And-Overview.html (Accessed April 5, 2011).

Applied Biosystems. Real-time PCR vs. traditional PCR [online]. http://www6.appliedbiosystems.com/support/tutorials/pdf/rtpcr_vs_tradpcr.pdf (Accessed March 3, 2011).

Applied Biosystems. Real-time PCR: Understanding C_t. http://www3.appliedbiosystems.com/cms/groups/mcb_marketing/documents/generaldocuments/cms_053906.pdf (Accessed March 7, 2011)

Ashburner, M. 1972. Patterns of puffing activity in the salivary gland chromosomes of *Drosophila*. VI. Induction by ecdysone in salivary glands of *D. melanogaster* cultured in vitro. *Chromosoma* **38**, 255-281.

Ashburner, M. 1974. Sequential gene activation by ecdysone in polytene chromosomes of *Drosophila melanogaster*. II. Effects of inhibitors of protein synthesis. *Developmental Biology* **39**: 141-157.

Ayerh, M. 2008. The role of β-FTZ F1 in fat body remodeling during pupal development of *Drosophila melanogaster.* Mount Holyoke College Library Archives.

Baehrecke, E. H. and C.S Thummel. 1995. The *Drosophila E93* gene from the 93F early puff displays stage- an d tissue-specific regulation by 20-hydroxyecdysone. *Dev. Biol*. **171**, 85-97.

Baehrecke, E. H. 2003. Autophagic programmed cell death in *Drosophila*. *Cell Death and Differentiation* **10**, 940–945

Billig H., Furata, I. and A. J. W. Hsueh. 1993. Estrogens inhibit and androgens enhance ovarian granulosa cell apoptosis*. Endocrinology* **133**, 2204-2212.

Bodenstein, D. 1943. Hormones and tissue competence in the development of *Drosophila*. *Biol. Bull. Mar. Biol. Lab. Woods Hole* **84**, 34-58.

Buszczak, M. and W. A. Segraves. 2000. Insect metamorphosis: Out with the old, in with the new. *Curr. Biol.* 2000, **10**, 830–833.

Butterworth, F.M. and E.C. Forrest. 1984. Ultrastructure of the preparative phase of cell death in the larval fat body of *Drosophila melanogaster. Tissue Cell* **16***,* 237-250*.*

Cagan, R.L. and D.F. Ready. 1989. Notch is required for successive cell decisions in the developing *Drosophila* retina. *Genes Dev.* **3**: 1099--1112

Cao, C., Liu, Y. and M. Lehmann. 2007. Fork head controls the timing and tissue selectivity of steroid-induced developmental cell death. *J. Cell Biol.* **176**:843–852

Chen, P., Nordstrom, W., Gish, B., and J.M Abrams. 1996. *grim*, a novel cell death gene in *Drosophila. Genes Dev.* **10**: 1773–1782.

Cherbas, L., Hu, X., Zhimulev, I., Belyaeva, E. and P. Cherbas. 2003. *EcR* isoforms in *Drosophila*: Testing tissue-specific requirements by targeted blockade and rescue. *Development* **130** : 271-284.

Clarke, P. G. H. 1990. Developmental cell death: morphological diversity and multiple mechanisms. *Anat. Embryol.* **181**, 195-213.

Dean, R.L., Locke, M., and J.V. Collins. 1985. Structure of the fat body. *Comprehensive Insect Physiology Biochemistry and Pharmacology* **3**. Pergamon, Oxford, UK, 155.

Dorstyn, L., Colussi, P.A., Quinn, L.M., Richardson, H., and S. Kumar.1999. DRONC, an ecdysone-inducible Drosophila caspase. *Proc. Natl. Acad. Sci. USA* **96**, 4307–4312.

Duffy, J.B. 2002. GAL4 system in *Drosophila*: a fly geneticist's Swiss army knife. *Genesis* **34**:1–15

Evans-Storms, R. B. and J.A. Cidlowski. 1995. Regulation of apoptosis by steroid hormones. *J.Steroid Biochem. Molec. Biol*. **54** (1-6), 1-8.

Finlayson, L. H. 1956. Normal and induced degeneration of abdominal muscles during metamorphosis in the Lepidoptera. *Quart. J. micr. Sci.,* **97**, 215-234.

Fraser, A.G. and G.I. Evan. 1997. Identification of a *Drosophila melanogaster* ICE/CED-3-related protease, drICE. *EMBO J*. **16**, 2805–2813.

Friedman, J.R. and K.H. Kaestner. 2006. The Fox: a family of transcription factors in development and metabolism. *Cell. Mol. Life Sci.* **63**:2317–2328.

Fristrom, D.K. and J. W. Fristrom. 1993. The metamorphic development of the adult epidermis. *Bate, Martinez Arias* : 843--897

Giniger E., Varnum S.M. and M. Ptashne. 1985. Specific DNA binding of GAL4, a positive regulatory protein of yeast. *Cell* **40**:767–774.

Gorski, K. 2010. Genetic regulation of fat body remodeling in *Drosophila melanogaster.* Mount Holyoke College Library Archives, p.44.

Haining, W.N., Carboy-Newcomb, C., Wei, C.L, Steller, H., Brand, A.H. and N. Perrimon. 1999. The proapoptotic function of *Drosophila Hid* is conserved in a means of altering cell fates and generating dominant phenotypes. *Proc. Natl. Acad. Sci*. *USA* **96**, 4936–4941.

Hannon, G.J. 2002. RNA interference. *Nature* **418**, 244-251.

Hartenstein, V. and Y. N. Jan. 1992. Studying *Drosophila* embryogenesis with P-*lacZ* enhancer-trap lines. Wilhelm Roux's Arch. *Dev. Biol*. 201, 194-220.

Harteinstein, V. 1993. Atlas of *Drosophila* development. Cold Spring Harbor Laboratory Press, p. 16-17.

Harvie, P. D., Filippova, M. and P.J. Bryant. 1998. Genes expressed in the ring gland, the major endocrine organ of *Drosophila melanogaster*. *Genetics* **149**(1): 217-231.

Haunerland, N.H. 1996. Insect storage proteins: gene families and receptors. *Insect Biochem. Mol. Biol*. **26**, 755–765.

Hay, B.A., Wassarman, D.A., and G. M. Rubin. 1995. *Drosophila* homologs of baculovirus inhibitor of apoptosis proteins function to block cell death. *Cell* **83**, 1253–1262.

Hengartner, M.O. and H.R. Horvitz. 1994. *C. elegans* gene that encodes two *ets*-related Cell gene *ced-9* encodes a functional homolog of the mammalian proto-oncogene *bcl-2*. *Cell* **76**, 665–676.

Hoshizaki D.K., Blackburn, T., Price, C., Ghosh, M., Miles, K, Ragucci, M. and R. Sweis. 1994**.** Embryonic fat-cell lineage in *Drosophila melanogaster. Development* **120**, 2489-2499.

Hoshizaki, D. K. 2005. Fat-Cell Development . *Comprehensive Insect Molecular Sciences, Biochemistry, Pharmacology and Molecular Biology.*

Hu, X., Cherbas, L. and P. Cherbas. 2003. Transcription activation by the ecdysone receptor (EcR/USP): identification of activation functions*. Mol. Endocrinol.* **17**, 716–731.

Huh, J.R, Foe, I., Muro, I., Hong Chen, C., Seol, J.H., Yoo, S.J., Guo, M. , Park, J.M., and B.A Hay. 2006. The *Drosophila* Inhibitor of Apoptosis (IAP) DIAP2 Is Dispensable for Cell Survival, Required for the Innate Immune Response to Gram-negative Bacterial Infection, and Can Be Negatively Regulated by the Reaper/Hid/Grim Family of IAP-binding Apoptosis Inducers. *J. Biol. Chem*. **282 (3):** 2056-2068.

Igaki, T., Kanuka, H., Inohara, N., Sawamoto, K., Nunez, G., Okano, and M. Miura. 2000. Drob-1, a *Drosophila* member of the Bcl-2/CED-9 family that promotes cell death. *Proc. Natl. Acad. Sci. USA*, **97**, 662–667.

Jacobson M.D., Well M. and M.C. Raff. 1997. Programmed cell death in animal development. *Cell* **88**:347-349.

Jiang, C., Baehrecke, E. H. and C. S. Thummel. 1997. Steroid regulated programmed cell death during *Drosophila* metamorphosis. *Development* **124**, 4673-4683.

Johnson, P. and H. Rees. 1977. The mechanism of C-20 hydroxylation of alpha-ecdysone in the desert locus, *Schistocerca gregaria. J. Biochem.* **168** (3): 513-520.

Jones, G., Jones, D., Zhou, L., Steller, H. and Y. Chu. 2000. Deterin, a new inhibitor of apoptosis from *Drosophila melanogaster*. *J Biol Chem* **275**:22157–22165.

Kanuka, H., Sawamoto, K., Inohara, N., Matsuno, K., Okano, H., and M. Miura. 1999. Control of the cell death pathway by Dapaf-1, a *Drosophila* Apaf-1/CED-4-related caspase activator. *Mol. Cell* **4**, 757–769.

Kawamura, K., Shibata, T., Saget, O., Peel, D. and P.J. Bryant. 1999. A new family of growth factors produced by the fat body and active on *Drosophila* imaginal disc cells. *Development* **126**, 211–219.

Kerr, J. F., Wyllie, A. H. and A. R. Currie. 1972. Apoptosis: a basic biological phenomenon with wide-ranging implications in tissue kinetics. *Br. J. Cancer* **26**, 239-257.

King-Jones, K. and C. Thummel. 2005. Nuclear receptors-a perspective from *Drosophila*. *Nature* **6**, 311-323.

Kiriishi, S., Rountree, D. B., Sakurai, S. and L. I. Gilbert. 1990. Prothoracic gland synthesis of 3-dehydroecdysone and its hemolymph 3ß-reductase mediated conversion to ecdysone in representative insects. *Experientia* **46**, 716 -721.

Lee, C.Y., Simon, C.R., Woodard, C.T. and E.H. Baehrecke. 2002. Genetic mechanism for the stage- and tissue-specific regulation of steroid triggered programmed cell death in *Drosophila*. *Dev. Biol*. **252**:138 –148.

Lee, C.-Y. and E. H. Baehrecke. 2001. Steroid regulation of autophagic programmed cell death during development. *Development* **128**, 1443-1455.

Lee, C.-Y., Wendel, D. P., Reid, P., Lam, G., Thummel, C. S. and E. H. Baehrecke. 2000. *E93* directs steroid-triggered programmed cell death in *Drosophila. Mol. Cell* **6**, 433-443.

Leulier, F., Rodriguez, A., Khush R.S, Abrams, J.M. and B. Lemaitre. 2000. The *Drosophila* caspase Dredd is required to resist Gram-negative bacterial infection. *EMBO Rep*. **1**:353-358.

Leulier F., Ribeiro P. S. , Palmer E., Tenev T., Takahashi K., Robertson D. , Zachariou A., Pichaud F., Ueda R. and P. Meier. 2006. Systematic in vivo RNAi

analysis of putative components of the *Drosophila* cell death machinery. *Cell death and differentiation* **13**, 1663-1674.

Li, P., Nijhawan, D., Budihardjo, I., Srinivasula, S.M., Ahmad, M., Alnemri, E.S. and X. Wang . 1997.Cytochrome c and dATP-dependent formation of Apaf-1/caspase-9 complex initiates an apoptotic protease cascade. *Cell*. **91**(4), 479-489.

Li, T. and M. A. Bender. 2000. Conditional rescue system reveals essential functions for the ecdysone receptor (*EcR*) gene during molting and metamorphosis in *Drosophila. Development* **127**, 2897–2905.

Locke, M. and J.V. Collins. 1968. Protein uptake into multi- vesicular bodies and storage granules in the fat body of an insect. *J. Cell Biol*. **36**, 453–483.

Lockshin, R. A. and C. M Williams. 1964. Programmed cell death. II: Endocrine potentiation of the breakdown of the intersegmental muscles of silkmoths. *J. Insect Physiol.* **10**, 643-649.

Lockshin, R. A. and C. M. Williams. 1965. Programmed cell death: I. Cytology of degeneration in the intersegmental muscles of the pernyi silkmoth. *J. Insect Physiol*. **11**, 123-133.

Lockshin, R. A. and Z. Zakeri. 1991. Programmed cell death and apoptosis. In Apoptosis: The Molecular Basis Of Cell Death, vol.3, pp. 47-60. Cold Spring Harbor, New York: Cold Spring Harbor Laboratory Press.

Martin, J.F., Hersperger, E., Simcox, A. and A. Shearn. 2000. *Minidiscs* encodes a putative amino acid transporter subunit required non-autonomously for imaginal cell proliferation. *Mech. Devel*. **92**, 155–167.

McCarthy, J.C. and V.M. Dixit. 1998. Apoptosis induced by *Drosophila Reaper* and *Grim* in a human system. *J. Biol. Chem*. **273**, 24009-24015.

McClure, K.D. and Schubiger, G. 2005. Developmental analysis and squamous morphogenesis of the peripodial epithelium in *Drosophila* imaginal discs. *Development* **132**:5033-5042.

Miller, J.M., Oligino, T., Pazdera, M., Lopez, A.J., and D.K. Hoshizaki. 2002. Identification of fat-cell enhancer regions in *Drosophila melanogaster. Insect Mol. Biol*. **11**, 67–77.

National Human Genome Research Institute Website. 2010. Polymerase Chain Reaction. Accessed on April 19, 2011.

Nelliot, A., Bond, N. and D.K. Hoshizaki. 2006. Fat-body remodeling in *Drosophila melanogaster. Genesis* **44**: 396-400.

O'Kane, C.J. and W. J. Gehring. 1987. Detection in situ of genomic regulatory elements in *Drosophila Proc. Natl. Acad. Sci. USA* **84,** 9123-9127.

Orme, M and P. Meier. 2009. Inhibitor of apoptosis proteins in *Drosophila*: gatekeepers of death. Apoptosis **14**:950–960.

Pffafl, M.W. 2001. A new mathematical model for relative quantification in real-time RT-PCR. *Nucleic Acids Research*, **29**(9): 2002-2007.

Rahman, I. 2008. The relative quantification of *Drosophila Broad Complex* expression in βFTZ-F1 loss-of-function mutants during metamorphosis. Mount Holyoke College Library Archives.

Riddiford, L. M. 1993. The Development of *Drosophila melanogaster,* 899–939 Cold Spring Harbor Laboratory Press.

Riddiford, L. M., Cherbas, P. and J.W. Truman. 2000. Ecdysone receptors and their biological actions. *Vitam. Horm*. **60**, 1–73.

Riechmann, V., Rehorn, K.P., Reuter, R. and M. Leptin.1998. The genetic control of the distinction between fat body and gonadal mesoderm in *Drosophila. Development* **125**, 713–723.

Renault, N., King-Jones, K. and M. Lehmann. 2001. Downregulation of the tissue-specific transcription factor Fork head by Broad-Complex mediates a stage-specific hormone response. *Development* **128:**3729–3737.

Robinow, S., Talbot, W. S., Hogness, D. S. and J. W. Truman. 1993. Programmed cell death in the *Drosophila* CNS is ecdysone-regulated and coupled with a specific ecdysone receptor isoform. *Development* **119**, 1251-1259.

Rodriguez, A., Oliver, H., Zou, H., Chen, P., Wang, X., and J.M Abrams. 1999. Dark is a *Drosophila* homologue of Apaf-1/CED-4 and functions in an evolutionarily conserved death pathway. *Nat. Cell Biol*. **1**, 272–279.

Rusten, T.E. , Lindmo, K., Juha, Sass, G., Seglen, P., Brech, A. and H. Stenmark. 2004. Programmed Autophagy in the Drosophila Fat Body Is Induced by Ecdysone through Regulation of the PI3K Pathway. *Developmental Cell* **7**, 179–192.

Salvesen G.S and J.M. Abrams. 2004. Caspase activation – stepping on the gas or releasing the brakes? Lessons from humans and flies. *Oncogene* **23**: 2774–2784.

Schwartz, L.M. and J.W. Truman. 1982. Peptide and Steroid Regulation of Muscle Degeneration in an Insect. *Science* **215**: 1420-1421.

Schwartz L. M. 1992. Insect muscle as a model for programmed cell death. *J. Neurobiol.* **23**, 1312-1326.

Schwartzman, R. A. and J. A. Cidlowski. 1993. Apoptosis: the biochemistry and molecular biology of programmed cell death. *Endocrine Rev*. **14**: 133-151.

Schweichel, J.U. and H.J. Merker.1973. The morphology of various types of cell death in prenatal tissues. *Teratology* **7**, 253-266.

Scott. R.C., Schuldiner, O. and T.P. Neufeld. 2004. Role and regulation of starvation-induced autophagy in *Drosophila* fat body. *Developmental Cell* **7**: 167-176.

Shipston, R.J. and F.A. Antoni. 1992. Early glucocorticoid induction of calmodulin and its suppression by corticotropin-releasing factor in pituitary corticotrope tumor (AtT20) cells. *Biochem. Biophys. Res. Commun*. **189**: 1382-1388.

Song, Z., McCall, K. and H. Steller. 1997. DCP-1, a *Drosophila* cell death protease essential for development. *Science* **275**: 536–540.

Steller, H. 1995. Mechanisms and genes of cellular suicide. *Science* **267** (5203): 1445-1449.

Stocker, H. and E. Hafen. 2000. Genetic control of cell size. *Curr. Opin. Genet. Devel*. **10**: 529–535.

Talbot, W.S., Swyryd, E.A., Hogness, D.S. 1993. *Drosophila* tissues with different metamorphic responses to ecdysone express different ecdysone receptor isoforms. *Cell* **73**(7): 1323--1337.

Taylor, B. J. and J.W. Truman. 1992. Commitment of abdominal neuroblasts in *Drosophila* to a male or female fate is dependent on genes of the sex-determining hierarchy. *Development* **114**, 625–642.

Tenniswood M. P., Guenette R. S., Lakins J., Mooibroek M., Wong P. and J. E. Welsh .1992. Active cell death in hormone dependent tissues. *Cancer Met. Rev.* **11**: 197-220.

Thompson, C. B. 1995. Apoptosis in the pathogenesis and treatment of disease. *Science* **267**:1456-1462.

Thummel, C. S. 1996. Flies on steroids – *Drosophila* metamorphosis and the mechanisms of steroid hormone action. *Trends Genet* **12**, 306-310.

Thummel, C. S. 2007. To die or not to die—a role for Fork head. *J Cell Biol* **176** (6): 737-739.

Tweedie, S., Ashburner, M., Falls, K., Leyland, P., McQuilton, P., Marygold, S., Millburn, G., Osumi-Sutherland, D., Schroeder, A. , Seal, R., Zhang, H. and The FlyBase Consortium. 2009. FlyBase: enhancing *Drosophila* Gene Ontology annotations.*Nucleic Acids Research* **37**: D555-D559;doi:10.1093/nar/gkn788.

Uckun, F. M., Tuel-Ahlgren, L., Song, C. W., Waddick, K., Myers, D. E., Kirihara J., Ledbette, J. A. and G. L. Schieven. 1992. Ionizing radiation stimulates unidentified tyrosine-specific protein kinases in human B-lymphocyte precursors, triggering apoptosis and clonogenic cell death. *Proc. Natn. Acad. Sci.* **89**:9005-9009.

Untergasser, A., Nijveen, H., Rao, X., Bisseling, T., Geurts, R., and J. Leunissen. 2007. Primer3Plus, an enhanced web interface to Primer3. *Nucleic Acids Res* **35**:71-74.

Uren, A.G., Coulson, E.J. and D. L.Vaux. 1998. Conservation of baculovirus inhibitor of apoptosis repeat proteins (BIRPs) in viruses, nematodes, vertebrates and yeasts. *Trends Biochem. Sci*. **23**, 159–162.

Vaux, D.L., Weissman, I.L. and S.K. Kim.1992. Prevention of programmed cell death in *Caenorhabditis elegans* by human *bcl-2*. *Science* **258**, 1955–1957.

Vernooy, S.Y., Chow, V., Su J., Verbrugghe, K., Yang J., Cole, S., Olson, M.R. and B.A. Hay. 2002. *Drosophila* Bruce can potently suppress Rpr- and Grim-dependent but not Hid-dependent cell death. *Curr Biol* **12**:1164–1168.

Viney, M.E. and F.J. Thompson. 2008. Two hypotheses to explain why RNA interference does not work in animal parasitic nematodes. *International Journal for Parasitology* **38**: 43-47.

Vucic, D., Kaiser, W., Harvey, A. and L. Miller.1997. Inhibition of Reaper-induced apoptosis by interaction with inhibitor of apoptosis proteins (IAPs). *Proc. Natl. Acad. Sci. USA* **94**, 10183–10188.

Wagner, J. 1997. The logic of molecular approaches to biological problems. Cornell University Medical College Website. Accessed on April 20, 2011.

Wang, S., Hawkins, C., Yoo, S.J., Müller, H.A., and B.A.Hay. 1999. The *Drosophila* Caspase Inhibitor DIAP1 Is Essential for Cell Survival and Is Negatively Regulated by HID. Cell **98**, 453–463.

Weeks, J. C. and J. W. Truman. 1985. Independent steroid control of the fates of motoneuronsand their muscles during insect metamorphosis. *J . Neurosci.* **5**, 2290-2300.

White, K. P., Hurban, P., Watanabe, T. and D. S. Hogness. 1997. Coordination of *Drosophila* metamorphosis by two ecdysone-induced nuclear receptors. *Science* **276**, 114-117.

Wing J.P., Zhou , L., Schwartz L.M. and J.R. Nambu. 1998. Distinct cell killing properties of the *Drosophila reaper*, *head involution defective*, and *grim* genes. *Cell Death Differ* **5**:930–939.

Wolff, T. and D.F Ready. 1991. Cell death in normal and rough eye mutants of *Drosophila*. *Development* **113**(3): 825-839.

Woodard, C.T., Baehrecke, E.H. and C.S. Thummel. 1994. A molecular mechanism for the stage specificity of the *Drosophila* prepupal genetic response to ecdysone. *Cell* 79, 607-615.

Yuan, J.S., Reed, A., Chen, F. and C. N. Stewart. 2006. Statistical analysis of real-time PCR data. *BMC Bioinformatics*. **7**: 85-97.

Yin, V., Thummel, C.S. and A. Bashirullah. 2007. Down-regulation of *Inhibitor of apoptosis* levels provides competence for steroid-triggered cell death. *J Cell Biol* **178** (1): 85-92.

Yin V.P. and C. S. Thummel. 2004. A balance between *the diap1* death inhibitor and *reaper* and *hid* death inducers controls steroid-triggered cell death in *Drosophila*. *PNAS* **101** (21): 8022–8027.

Zachariou, A., Tenev, T., Goyal, L., Agapite, J., Steller, H. and P. Meier. 2003. IAP-antagonists exhibit non-redundant modes of action through differential DIAP1 binding. *EMBO J* **22**:6642–6652.

Zhou, L., Song, Z., Tittel, J. and H. Steller.1999. HAC-1, a *Drosophila* homolog of APAF-1, abd CED-4 functions in developmental and radiation-induced apoptosis. *Mol. Cell* **4**:745-755.

Zhou X., Zhou, B., Truman, J.W. and L.M. Riddiford. 2004. Overexpression of broad: a new insight into its role in the *Drosophila* prothoracic gland cells. *J. Exp.Biol.* **207**, 1151-1161.

Zinke, I., Kirchner, C., Chao, L. Tetzlaff, M. and M.J.Pankratz. 1999. Suppression of food intake and growth by amino acids in *Drosophila*: the role of *pumpless*, a fat body expressed gene with homology to vertebrate glycine cleavage system. *Development* **126**: 5275-5284.

Zou, H., Henzel, W.J., Liu, X., Lutschg, A. and X. Wang. 1997. Apaf-1, a human protein homologous to *C. elegans* CED-4, participates in cytochrome c-dependent activation of caspase-3. *Cell* **90**, 405–413.

Zurovec, M., Dolezal, T., Gazi, M., Pavlova, E. and P.J Bryant . 2002. Adenosine deaminase-related growth factors stimulate cell proliferation in *Drosophila* by depleting extracellular adenosine. *PNAS* **99**(7): 4403-4408.